Electrochemical versus Chemical Oxidation of Bulky Phenols: 2,6-diphenylphenol and 2,2-dihydroxybiphenol

A Thesis Submitted to the Committee of Graduate Studies in Partial Fulfillment of the Requirements for the Degree of Master of Science in the Faculty of Art and Science

TRENT UNIVERSITY

Peterborough, Ontario, Canada

Environmental and Life Sciences M.Sc. Graduate Program

January 2023

Abstract

Electrochemical versus Chemical Oxidation of Bulky Phenols: 2,6-diphenylphenol and 2,2-dihydroxybiphenol

Stephanie Gao

Phenolic compounds are used in industry, such as agriculture and biotechnology, and inevitably end up in our environment. These compounds may serve as a phenolic precursor to produce raw materials for a wide range of applications. Chemical oxidation has been the common synthetic pathway to oxidize phenols and related compounds. However, traditional chemical approaches suffer from use of harsh chemicals, waste generation, and lack of reaction selectivity. Electrochemical synthesis has emerged as an alternative method to mitigate common challenges associated with organic synthesis. Herein, electrochemical oxidation of 2,6-diphenylphenol (DPP) and 2,2-dihydroxybiphenol (DHBP) was carried out and compared to traditional chemical oxidation. Contrasted with chemical oxidation, cyclic voltammetry of DPP resulted in a range of products based on the specific potential ranges used, whereas chemical oxidation of DHBP yield a dark-coloured polymeric product. The electrooxidation and chemical oxidation of DPP and DHBP resulted in a solution colour change, indicative of the formation of new, but different products monitored by UV-vis, and characterized by nuclear magnetic spectroscopy (NMR), X-ray single crystal diffraction, IR spectroscopy, transmission electron microscopy (TEM), and gas chromatography-mass spectrometry (GC-MS). The data indicate that the synthetic outcomes are dependent on the synthetic

methodology employed, and that electrooxidation and chemical oxidation can form products unique to the pathway utilized.

Keywords: Cyclic voltammetry, electrooxidation, phenols, electrocatalysis, polymerization, C-C coupling

Abbreviations

DPP	2,6-diphenylphenol
2,6-DPPQ	2,6-diphenyl-*p*-benzo-quinone
ACN	acetonitrile
BDD	boron-doped diamond
BSF	bisphenol F
CD_3CN	deuterated acetonitrile
$CDCl_3$	deuterated chloroform
CV	cyclic voltammetry
DHBP	2,2-dihydroxybiphenol
DTBP	2,6-di-*tert*-butylphenol
FTIR	Fourier-transform infrared
GCE	glassy carbon electrode
GC-MS	gas chromatography-mass spectrometry
HFIP	hexafluoroisopropanol
NMR	nuclear magnetic resonance
Pt	platinum
$TBACF_3SO_3$	tetrabutylammonium trifluoromethanesulfonate
TBAP	tetrabutylammonium perchlorate
TEM	transmission electron microscopy
TPBD	3,3',5,5'-tetraphenyl-biphenyl-4,4'-diol
TPDQ	3,3',5,5'-tetraphenyldiphenoquinone

UV-vis	ultraviolet-visible
XRD	x-ray diffraction

Acknowledgements

I would like to express my deepest appreciation for my supervisor, Dr. Martic, who supported me at every stage these last two years. Her willingness to help me grow as a writer and critical thinker has changed my perspective in research. I am glad I made my choice to stick with her these two years. It takes a lot of mental power and beyond to do research as a woman in STEM. Huge credits to Dr. Martic!

I am thankful for past and present lab members who have provided the most amazing feedback at our fun lab meetings. They are a fun and intelligent group of people and I hope the best for them! Josephine has played a huge role for my transition into the Martic Lab and provided great support inside and outside of the lab. Without her tips and tricks, I doubt things would have gone as well as I hoped. I like to further extend my thanks to Dr. Eric Keske and Lori Van Belle for helping me with the GC-MS and NMR. I also would like to thank my committee members, Dr. Naomi Stock and Dr. Shegufta Shetranjiwalla-Merchant for all their input and support these last two years.

These last two years would not have sailed as smoothly if it wasn't for my family, who supported me from the very beginning. The moral support and love I have received has pushed me through tiring times. Lastly, I would like to thank my lovely partner, who lifted me up when things got bad, and stress took a toll on me. The support you provided has uplifted me, and hence, the completion of this thesis!!

This thesis is dedicated to everyone who I encountered since 2020. The support and love from everyone lead to the completion of my degree and I am very thankful.

Table of Contents

ABSTRACT II

ABBREVIATIONS IV

ACKNOWLEDGEMENTS VI

LIST OF FIGURES X

LIST OF TABLES XV

CHAPTER 1 – INTRODUCTION TO PHENOLS AND CHEMICAL/ELECTRO-OXIDATION METHODS 1

1.1. Phenols, phenolics and their applications 1

1.2. Chemical oxidation of phenols 2

1.3. Electrooxidation of phenols 5

1.3.1. Types of electrode materials 11

1.3.2. Effect of solvent type 19

1.3.3. Effect of supporting electrolyte 21

1.3.4. Effect of pH 23

1.3.5. Green electrosynthesis 24

1.4. Characterization techniques used to monitor phenol oxidation and characterize product formation 24

1.5. Thesis research 27

CHAPTER 2 – ELECTROCHEMICAL VS CHEMICAL OXIDATION OF 2,6-DIPHENYLPHENOL 28

2.1. Introduction 28

2.2. Experimental Section 29

2.2.1. Materials and Reagents 29

2.2.2. Electrochemical Measurements 30

2.2.3. UV-vis Spectroscopy 30

2.2.4. Fourier-transform infrared spectroscopy (FT-IR) 30

2.2.5. Gas chromatography-mass spectrometry (GC-MS) 30

2.2.6. Nuclear magnetic resonance (NMR) 31

2.2.7. Chemical oxidation and reduction 31

2.2.8. X-ray single-crystal diffraction 31

2.3. Results and Discussion 31

2.3.1. Electrochemical Characterization of DPP 31

2.3.2. Spectroscopic Characterization of DPP Electrooxidation 35

2.4. Conclusions 56

CHAPTER 3 – ELECTROCHEMICAL VERSUS CHEMICAL OXIDATION OF 2,2-DIHYDROXYBIPHENOL 58

3.1. Introduction 58

3.2. Materials and Reagents 59

3.3. Electrochemical Measurements 59

3.4. Results and Discussion 61

3.4.1. Electrochemical characterization of DHBP 61

3.4.2. Spectroscopic Characterization of DHBP Electrooxidation.....64

3.4.3. Chemical Oxidation of DHBP.....68

3.5. Conclusion.....79

CHAPTER 4 – CONCLUSIONS AND FUTURE WORK..... 80

4.1. Conclusions 80

4.2. Future Research Directions 83

REFERENCES 86

APPENDICES 104

Appendix II 104

Appendix III 142

List of Figures

Figure 1.1. Structure of phenol and common phenolic pollutants. 2

Figure 1.2. Resonance structures of 2,4,6- tri-*tert*-butylphenol radical obtained from oxidation of 2,4,6- tri-*tert*-butylphenol (top) and products generated from reaction of radicals with nitrogen dioxide and bromine (bottom)..... 3

Figure 1.3. Schematic of standard 3-electrode electrochemical cell (left) general cyclic voltammogram (right). 6

Figure 1.4. General schematic of phenolic electrooxidation. a) desired reaction to form product, b) side reaction. 7

Figure 1.5. Electrochemical oxidation of phenol to hydroquinone..... 7

Figure 1.6. Proposed mechanism of benzotriole electrochemical oxidation to form radical via two-electron, one proton processes, in aprotic solvent and basic conditions..... 8

Figure 1.7. Cyclic voltammograms of 1 mM UV327 with 0.2 M n- Bu4NPF6 at a scan rate of 0.1 V/s; (Black line); UV327 (Red line) – prepared by adding an equimolar amount of n-Bu4NOH; (Blue line) Further oxidation of the phenoxyl radicals UV327●.. 9

Figure 1.8. One-electron oxidation and deprotonation of tri-tert-butyl phenols to form phenoxyl radical (top) and oxidation dimerization of phenoxyl radical for dimer formation (bottom). 10

Figure 1.9. Major oxidation products of DTBP. 11

Figure 1.10. Electrochemical oxidation of 2,4-dimethylphenol to form 2’2-biphenol analogue. 12

Figure 1.11. (a) undivided cell (b) divided cell..... 13

Figure 1.12. Anodic phenol–arene cross-coupling reaction and the potential mechanism. 15

Figure 1.13. Solvent effects on the potential windo..... 19

Figure 1.14. Electrode and supporting electrolyte combinations at its effect on potential windows (vs Fc/Fc^{+}). 23

Figure 1.15. Chromatogram (GC-MS) obtained from the anodic oxidation of key pharmaceuticals..... 25

Figure 2.1. Cyclic voltammograms of DPP at (A) initial CV scan, and (B) 1 CV (10 scans) ([DPP] = 10 mM, [TBAP] = 0.1 M, ACN, 10 scans per CV)..... 33

Figure 2.2. (A) Absorbance of 10 mM DPP as a function of CV cycling (B) Triplicate analysis of DPP at 1, 5, 10, 15, 20 CV with standard deviation (C) UV plot of 10 mM DPP as a function of concentration. 20 CV performed for each concentration. (D) Triplicate analysis of DPP at 0.5, 1, 5, 10, and 20 mM with standard deviation..... 35

Figure 2.3. 20 CV of various potential ranges (200 scans = 20 CV) (A) 3 to 0 V (B) corresponding UV-vis spectra of non-diluted DPP post electrochemical reaction at positive range. (C) -3 to 0 V (D) corresponding UV-vis at -3 to 0 V range (1) Non-diluted DPP post electrochemical reaction (2) non-diluted post electrochemical reaction after 48 hours..... 39

Figure 2.4. (A) Time-dependent analysis using UV-vis spectroscopy of the chemical oxidation of DPP with copper perchlorate. [DPP] 10 mM, $[Cu(ClO_4)_2]$ = 10 mM in 3 mL ACN. Inset: time-dependent UV measurements performed using a 100x dilution. (B) single molecule XRD of 3,3',5,5'-tetraphenyldiphenoquinone (i) Ball-stick form of blue-green reflective crystal obtained from the chemical oxidation of DPP using single-crystal

x-ray diffraction (ii) Bond lengths in ellipsoid (iii) view of packing along c-axis in capped sticks form (iv) View observed from the top of the c-axis in capped sticks form. 40

Figure 2.5. 1 CV, [DPP] = 10 mM, [TBAP] = 0.1 M, -3 to 3 potential range (A) Working: GCE, counter: GCE, reference: $Ag/AgNO_3$ (B) corresponding UV-vis using Pt/Pt pair (C) working: Pt wire, counter: Pt wire, reference: $Ag/AgNO_3$ (D) corresponding UV-vis using GCE/GCE pair. 43

Figure 2.6. 1 CV, [DPP] = 10 mM, [TBAP] = 0.1 M, working: GCE, counter: GCE, reference: $Ag/AgNO_3$. (A) 0 to 3 V, (B) corresponding UV-vis at 0 to 3 V range (c) -3 to 0 V, (D) corresponding UV-vis at -3 to 0 V range. 44

Figure 2.7. 1 CV, [DPP] = 10 mM, [TBAP] = 0.1 M, Working: GCE, counter: GCE, reference: $Ag/AgNO_3$ (A) 0 to 3 V; (B) corresponding UV-vis at 0 to 3 V range (C) -3 to 0 V (D) corresponding UV-vis at -3 to 0 V range. 45

Figure 2.8. GC-MS of DPP only, chemical oxidation, electrooxidation with a -3 to 0 V and 3 to 0 V range after 20 CV (200 scans), and electrochemical oxidation after 80 CV at a -3 to 3 V range (800 scans) using working: GCE, counter: Pt. 48

Figure 2.9. Proposed 2,6-disubstituted phenol oxidation pathways. 49

Figure 2.10. Proposed DPP radical formation, resonance contributors and oxidative dimerization pathway of DPP radical to produce a homodimer. 50

Figure 2.11. Structure of DPP and the proposed DPP-based C-C dimers and other products. 56

Figure 3.1. Scheme of the chemical polymerization of DHBP[15]. 59

Figure 3.2. Cyclic voltammograms of DHBP as a function of CV ([DPP] = 20 mM, [TBAP] = 0.1 M, ACN, 10 scans per CV). (A) Initial scan at 1st CV (1 CV) overlaid with ACN blank with TBAP only (green-dotted) and (B) all 1-20 CVs. 61

Figure 3.3. Scheme of the electrooxidation of PDHBP[15]..... 62

Figure 3.4. (A) UV-vis of CV-dependent analysis of DHBP using electrooxidation at 0, 1, 5, 10, 15 and 20 CVs. [DHBP] = 10 mM, [TBAP] = 0.1 M TBAP, 3 mL ACN (B) triplicates of CV-dependent analysis with standard deviation (C) UV-vis spectra of concentration-dependent analysis of DHBP, [DHBP] = 0.5, 1, 5, 10, 20 mM, [TBAP] = 0.1 M, 3 mL ACN at 20 CVs (D) triplicates of concentration-dependent analysis with standard deviation. 65

Figure 3.5. 20 CV of 10 mM DHBP and 0.1 M TBAP in ACN at various potential ranges (200 scans = 20 CV) (A) 3 - 0 V (B) UV-vis spectra of non-diluted DHBP post electrochemical reaction at positive range. (C) -3 to 0 V (D) respective UV-vis spectra. 66

Figure 3.6. TEM image of insoluble film at GCE surface provided by Dr. Ruby Sullan Lab at the University of Toronto Scarborough. 68

Figure 3.7. UV-vis spectra of the chemical oxidation of 10 mM DHBP and 10 mM copper perchlorate in ACN. Solid line: 100x dilution of the solution, dotted line: 24h after addition of copper perchlorate (measurement of liquid sample only). Inset: Formation of amorphous material after 24 h. 69

Figure 3.8. FT-IR spectrum of brown precipitate from chemical oxidation DHBP with copper perchlorate in acetonitrile..... 71

Figure 3.9. FT-IR spectrum of DHBP..... 72

Figure 3.10. Superimposed FTIR spectra of: DHBP (black); brown precipitate obtained from chemical oxidation of DHBP (red)..... 72

Figure 3.11. Stacked GC-MS spectra of various solutions: DHBP only, electrooxidation (0 to 3 V range), electrooxidation (-3 to 0 V range), electrooxidation (full range) and chemical oxidation of DHBP. 75

List of Tables

Table 2.1. TPDQ yield was generated from various electrode combinations, [DPP] = 10 mM, [TBAP] = 0.1 M in ACN (after 1 CV = 10 0.min reaction time).....46

Table 3.1. Solubility of brown product using various solvents (~ 0.2mg in ~3 mL solvent).....77

Chapter 1 – Introduction to phenols and chemical/electro-oxidation methods

1.1. Phenols, phenolics and their applications

Phenols are aromatic compounds containing at least one hydroxyl group substituent (Figure 1.1). They have a wide variety of applications in industry, such as pharmaceuticals and product syntheses. The most common compound, phenol, is generally used in the synthesis of plastics, phenolic resins and related materials[1]. Phenol-formaldehyde-polyethylene glycol polyether polyols (PF-PEGs) were synthesized using polymerization and etherification to obtain polyurethane (PU) films[2]. Other plastics and materials include plasticizers and epoxy resins.

Other common phenols include salicylic acid, is used in the synthesis of acetylsalicylic acid, which has been trademarked as the more commonly known pharmaceutical brand, Aspirin ©. Common routes to synthesizing aspirin include acetylation of salicylic acid. In addition to pharmaceutical use, phenols belong to a large group of varying bisphenols, such as bisphenol F (BSF). With two OH groups connecting to two aromatic rings, linked *via* methylene group, BSF is commonly used in the manufacturing of plastics and epoxy resins[3].

Polluting compounds such as phenol, various chlorophenols, -*p*-cresols and other phenolic compounds have been shown to have significant presence in soils and groundwaters from leaching[4]. Being structurally related to bisphenol F, bisphenol A (BPA) is a largely used precursor to produce daily plastics, epoxy resins, and other

materials (Figure 1.1). On average, 9 billion pounds of BPA are produced worldwide annually[5]. Discharge from industrial and domestic use of BPA has been a global concern regarding aquatic life, surface waters, ecosystems and many other environmental concerns[6]. Contaminated water with phenolics has a variety of health concerns associated, such as respiratory issues. Phenolics in the ecosystem is mainly due to production and degradation of pesticides, as well as production of materials such as dyes, polymers, and drug, and can be introduced into sewage systems[7]. BPA is present in plastics and metal products, and are also prominent in the air, drinking water, and other water sources[5].

Hence, developing mitigating strategies, such as degradation, oxidation, and modification, to recycle and reuse phenolic compounds is of interest both for environmental reasons as well as for greener industrial applications.

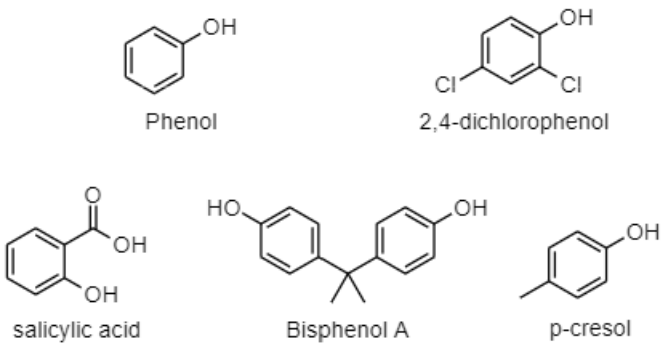

Figure 1.1. Structure of phenol and common phenolic pollutants.

1.2. Chemical oxidation of phenols

Phenol oxidation has been studied over many decades ago to understand the mechanism and electron transfer. The oxidation of hindered phenols, such as 2,4,6- tri-

tert-butylphenol to the 2,4,6-tri-*tert*-butylphenoxy radical (Figure 1.2) was previously done *via* one-electron oxidation using agents such as lead oxide and ferricyanide[8]. The 2,4,6- tri-*tert*-butylphenol radical (phenoxyl radical) formed in solution exhibited a cobalt blue colour that can generate up to 90-100% yield of the respective phenoxyl radical if alkaline ferricyanide was used as the oxidizing agent[8]. Further reaction of this radical with nitrogen dioxide and bromine yielded 2,4,6-tri-*t*-butyl-4-nitro-2,5-cyclohexadienone and 2,4,6-tri-*t*-butyl-4-bromo-2,5-cyclohexadienone respectively (Figure 1.2).

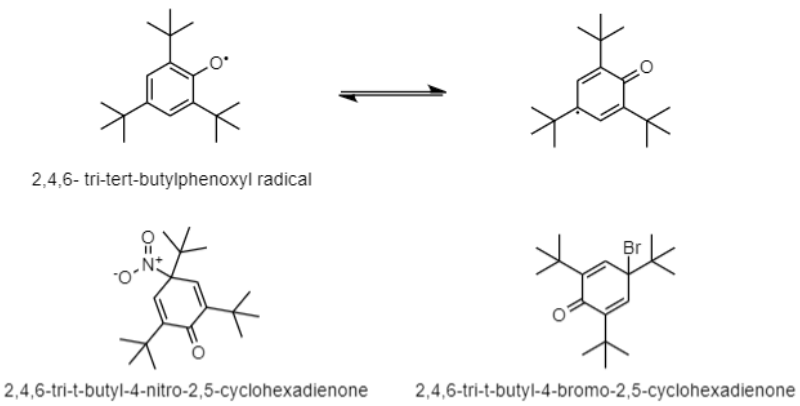

Figure 1.2. Resonance structures of 2,4,6- tri-*tert*-butylphenol radical obtained from oxidation of 2,4,6- tri-*tert*-butylphenol (top) and products generated from reaction of radicals with nitrogen dioxide and bromine (bottom)[8].

Coupling of 2,6-disubstituted phenols has been previously studied in the presence of oxygen and cuprous-pyridine catalyst to generate polymeric analogues and mixed dimers in aprotic solvents[9]. 2,6'-dimethylphenol and 2,6-diphenylphenol (DPP) underwent oxidative polymerization to high linear polymers. A few pathways were described to have potentially taken place, in which radical intermediates undergo

redistribution and rearrangement to form the mixed dimers. Rearrangement involves coupling of two radicals to yield a quinone ketal in which the oxygen of one radical attack the *para* position of the ring on the second radical, such that rearrangement of this new structure will yield a "new" ketal. Secondly, redistribution assumes that the quinone rapidly dissociates either to regenerate the same radicals or to produce two new radicals. Most importantly, the two pathways are involved in polymer coupling and their relative importance is dependent on the experimental conditions[9].

2,6-di-*tert*-butylphenol (DTBP) was chemically oxidized in ethanol as the solvent and base with added oxygen to form 3,3',5,5'-tetra-*t*-butyldiphenoquinone. Product formation was monitored at 420 nm (absorbance)[10]. DTBP oxidation with peroxy radicals yielded dimer products from C-C coupling in the *ortho* position due to sterically hindered *t*-butyl groups in the *para* position, preventing *para*-dimerization[11].

Ultimately, the general consensus for the oxidation of hindered phenols is primarily the formation of 1,4-benzoquinone, diphenoquinones (C-C homodimers), polymers, and redox-inactive analogues, depending on the reaction conditions employed[8,11–14]. Other phenolic compounds, such as 2,2-dihydroxybiphenol (DHBP), undergo similar reactions including polymerization due to the two hydroxyl groups. This was successfully characterized *via* methods such as infrared (IR) spectroscopy and NMR analyses[15]. Depending on the reaction conditions, the molecular polymer weight (g/mol) would differ substantially.

Some challenges associated with traditional chemical oxidation of phenols include the lack of selectivity, poor yields, need for harsh chemicals, and waste generation. Therefore, alternative methods are of interest, especially greener technologies.

1.3. Electrooxidation of phenols

As the demand for fossil fuels increase, the need for viable energy substitutes also increase. Currently, some new energy sources are being generated by using electrochemistry. Electrolysis to form H_2 gas has been one of the most heavily studied reactions in electrochemistry[16]. In general, water electrolysis can be split into two half-cell reactions: hydrogen evolution reaction (HER) and oxygen evolution reaction (OER). The HER reaction produces H_2 when water is reduced at the cathode, and the OER reaction produces O_2 when water is oxidized at the anode. On the other end, a greener alternative to chemical synthesis is also a growing interest. As a common industrial material and environmental pollutants, phenolic compounds are subject to investigation. The electrochemical oxidation of phenols has been explored, implementing techniques such as cyclic voltammetry (CV) to form new materials and products. CV involves applying an electric potential (V) to a redox active substrate in solution. Varying potentials can oxidize and reduce compounds by generating a current signal (A). These oxidative (anodic) and reductive (cathodic) peaks represent valuable information, such as redox-couples and mechanistic details. A standard 3-electrode setup consists of a working, counter, and reference electrode (Figure 1.3). The working electrode material consists of a durable and inert surface that can endure a vast range of chemical conditions and is where the reaction takes place. The counter electrode is also composed of an inert material and does actively participates in the reaction but supplies the electrochemical cell with current to complete the circuit. The reference electrode contains a stable redox solution that the measured current can be referenced to, but can also be a metal, such as a silver wire. During a CV measurement, potential (V) is supplied from a potentiostat to the

working electrode, if a redox-active species is in solution, the compound will undergo redox reactions at the working electrode surface. If oxidation is undergoing at the working electrode, a complementary reduction reaction is occurring at the counter electrode (by completing the electric circuit). Depending on the type of reference electrode employed, the signals may vary due to the differing redox potentials of redox species, such as Ag/AgCl, and $Ag/AgNO_3$.

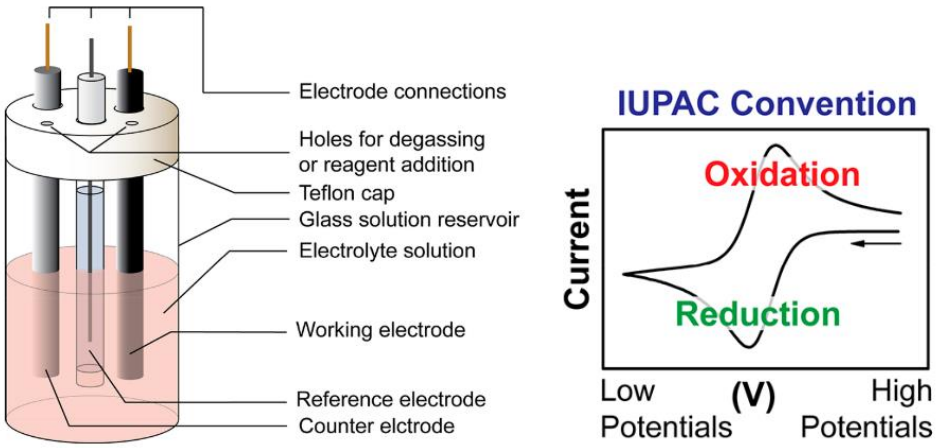

Figure 1.3. Schematic of standard 3-electrode electrochemical cell (left) general cyclic voltammogram (right)[17].

The common oxidation pathway of phenol-based compounds involves a phenoxyl radical formation (Figure 1.4) that will further react to form a desired product, or undergo a side reaction, i.e., polymerization, which may potentially redeposit onto the electrode surface in a process called fouling.

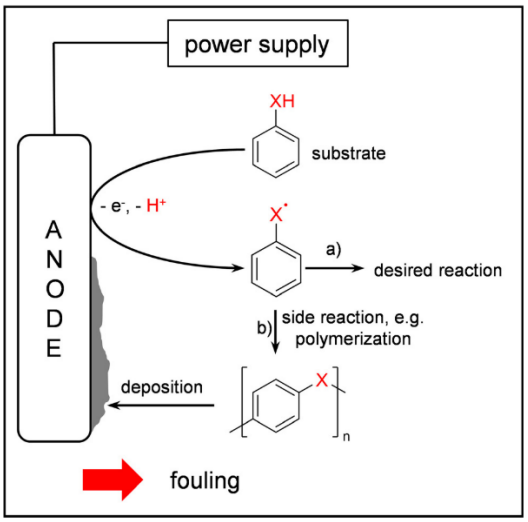

Figure 1.4. General schematic of phenolic electrooxidation. a) desired reaction to form product, b) side reaction[18].

Electrooxidation of phenol to form 1,4-hydroquinone was performed with high yield of 87% and selectivity[19] (Figure 1.5). Electrode stability, repeatability, and the type of product formed by the electrochemical oxidation of phenol have been investigated using CV and optimized for constant current electrolysis. The application of surface modified carbonaceous electrodes containing disordered graphene-like structures and oxygen functional groups were able to achieve high yield for the hydroquinone product.

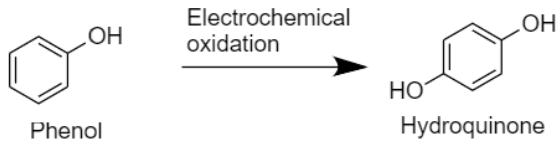

Figure 1.5. Electrochemical oxidation of phenol to hydroquinone.

Phenolic benzotriazoles in organic solvents have been electrochemically oxidized to form valuable intermediates[20]. Benzotriazoles (BZTs) are compounds containing a

phenolic functional group attached to the benzotriazole moiety with substituents (alkyl, aryl, or ester functional groups) at the *ortho*- and *para*-position). BZTs containing additional phenolic groups undergo enol-keto tautomerism to provide UV stabilization. To understand intermediate formation of benzotriazole groups, the oxidation mechanism for phenolic benzotriazoles: UV327 and UV234, in which both compounds absorb strongly at 327 nm and 234 nm respectively. They were investigated and found to likely undergo two-electron/one proton process to form a benzotriazole-substituted phenoxonium cation in neutral/acidic conditions. UV327 and UV234 differs in the substituents, specifically an isopropyl group and phenyl ring respectively. Under basic conditions, benzotriazole phenolics are deprotonated through a homogeneous chemical process to benzotriazole-substituted phenolates, which are then oxidized through a heterogeneous electron transfer to give a neutral benzotriazole-substituted phenoxyl radical, that undergoes reversible dimerization which exists in equilibrium with the radicals due to conjugation (Figure 1.6). Product formation is influenced by stability of intermediates formed; therefore, it is important to probe the potential mechanism, which affect yield and stability. In addition, dimer structure was not fully characterized.

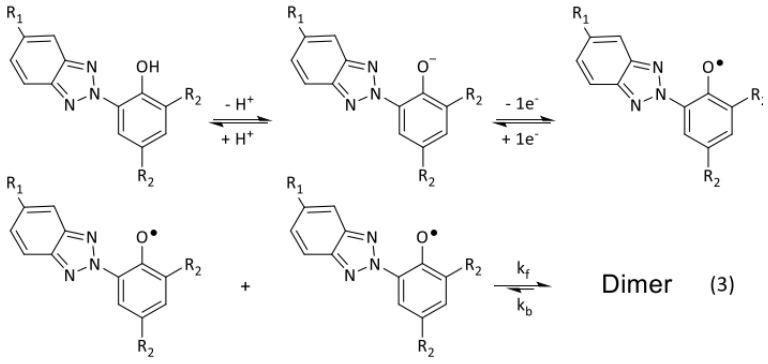

Figure 1.6. Proposed mechanism of benzotriazole electrochemical oxidation to form radical *via* two-electron, one proton processes, in aprotic solvent and basic conditions[20].

Cyclic voltammograms (CVs) of benzotriazole-based compounds exhibited chemically irreversible oxidation peaks; E_{pa} ~ 1.00 V vs. Fc/Fc^+ in CH_3CN, and ~ 1.20 V in CH_2Cl_2 solutions, and cathodic reduction peaks; E_{pc} at –2.10 V and –2.70 V indicating the reduction of the benzotriazole moiety (Figure 1.7). Irreversible oxidation is common in most phenolic compounds due to the formation of unstable oxidized species that quickly react to form secondary oxidized products, before being able to reduce back to the starting material[21,22]. To probe if a chemical additive will produce chemical reversibility, equimolar *n*-Bu_4NOH was added to solution (Figure 1.7) and a peak consistent with the phenolate anion was observed at ~-0.3 V[23,24]. Typically, this peak is observed as phenol is converted to its corresponding phenolate.

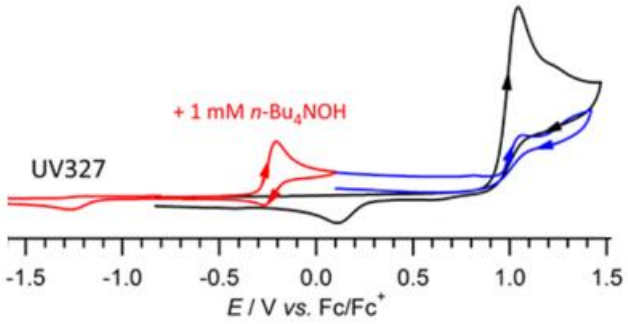

Figure 1.7. Cyclic voltammograms of 1 mM UV327 with 0.2 M n- Bu4NPF6 at a scan rate of 0.1 V/s (Black line); UV327 (Red line) – prepared by adding an equimolar amount of n-Bu4NOH; (Blue line) Further oxidation of the phenoxyl radicals UV327●[20].

More recent work on substituted phenols was focused on electrochemical oxidation of bulky phenols[22]. 2,6-di-*tert*-butylphenol, 2,4,6-tri-*tert*-butylphenol, 2-*tert*-butylphenol, and 4-*tert*-butylphenol were subjected to various oxidizing conditions. DTBP was the only compound that formed under electrooxidizing conditions and was

characterized using single-molecule x-ray diffraction (XRD) as 3,5,3′,5′-tetra-*ter*t butyl-4,4′-diphenoquinone, a dimer product that was expected to form based on previous work[14,25]. The compound was proposed to undergo one-electron oxidation and deprotonation to form a phenoxyl radical before dimerizing at the *para* site (Figure 1.8).

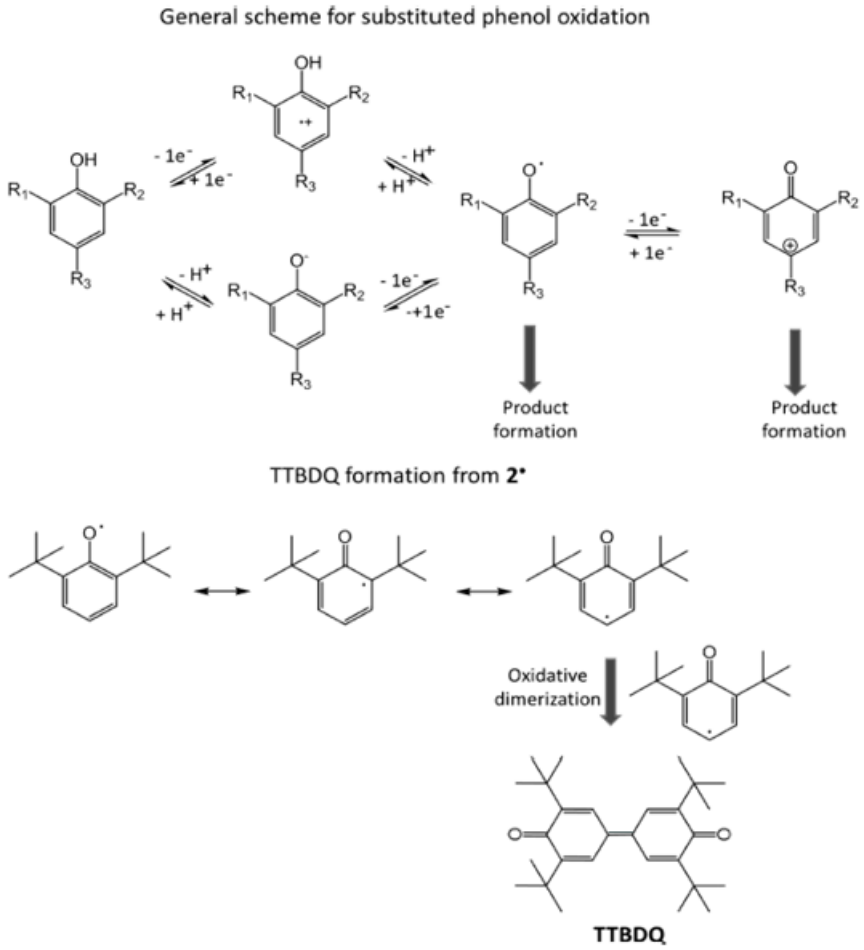

Figure 1.8. One-electron oxidation and deprotonation of tri-*tert*-butyl phenols to form a phenoxyl radical (top) and oxidation dimerization of the phenoxyl radical for dimer formation (bottom)[22].

However, it was observed that lack of dimer formation of other compounds was likely due to steric hindrance of the *tert*-butyl group at the *para* position, destabilizing the radical formed[12,22]. In addition, it has been shown that crude mixtures are rather common in major oxidation of DTBP, such as reduced analogues of the dimer product, and quinone analogues of DTBP (Figure 1.9).

Therefore, the number and position of substituents affects the stability of the radical formed, further influencing if a dimer product can be formed.

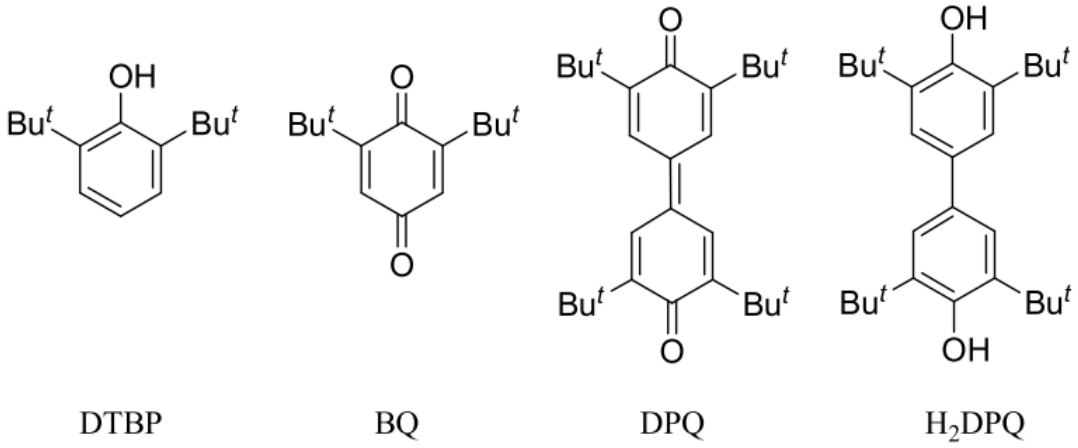

Figure 1.9. Major oxidation products of DTBP[26].

1.3.1. Types of electrode materials

The effect of anode material involved in electrooxidation is complex and versatile. Depending on the conditions of the electrode peroxidation, or anodic surface modifications, and experimental parameters, the reaction mechanism can include oxidative polymerization and dimerization, among others mechanisms.

1.3.1.2. Boron-doped diamond electrodes

The Waldvogel lab based in Germany has been known for their cross-coupling reactions using a multitude of electrooxidation mechanisms. Most of their work has been concentrated on using an non-divided electrolysis cell equipped with a boron-doped diamond electrode (BDD), nickel cathode, and hexafluoroisopropanol (HFIP) as selected solvent[27–29]. Most importantly, their work on BDD electrodes has shown high selectivity in product formation[30]. The *ortho*-coupling reaction of 2,4-dimethylphenol on the BDD has shown high chemoselectivity for 2'2-biphenol analogue under solvent-free conditions with additional water to enhance conductivity (Figure 1.10).

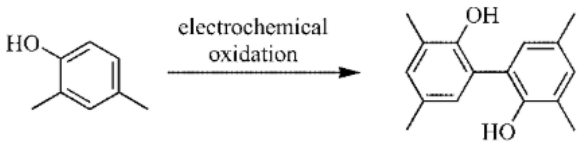

Figure 1.10. Electrochemical oxidation of 2,4-dimethylphenol to form 2'2-biphenol analogue[31].

Reaction pathways were shown to be dependent on the physical construction of the electrochemical cell[30]. Various cell setups can range from full submersion of electrodes in solution or divided into separate units (Figure 1.11A & B). Using a non-divided electrolysis cell equipped with a BDD anode and a nickel cathode, galvanostatic electrolysis with a current density of 10 mA/cm^2 was performed to ultimately yield a product ratio of 18:1 (2'2-biphenol analogue:by-products). The performance of the BDD

electrode exhibited far superior product outcome in contrast to the platinum anode, which formed a 1:17 a ratio, indicating low product selectivity.

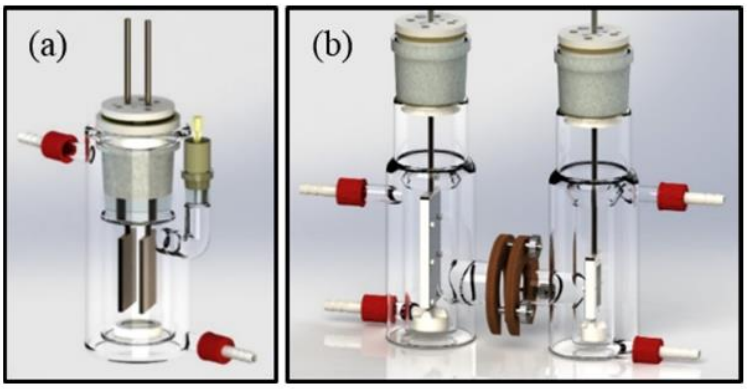

Figure 1.11. (a) undivided cell (b) divided cell[32].

Cross coupling reactions were observed with anodic oxidation to form direct phenol-arene bonds[33]. Furthermore, the direct cross-coupling of symmetric and non-symmetric *meta*-terphenyl-2,2’’-diols was electrochemically synthesized without leaving groups nor chemical oxidants[28]. With BDD as the anode, nickel as the cathode, and HFIP as the solvent - known for its stabilizing effect on the intermediate radicals[34] - two mechanistic pathways were determined. Forming a symmetrical species required four electron/four proton process, whereas non-symmetrical *meta*-terphenyl-2,2’’-diol required a -two electrode/two proton oxidation and deprotonation. Multiple substituted phenols were tested, such as 2,3,4-trimethoxyphenol, that resulted in the highest yield of 84% for a non-symmetrical species. In addition, phenolic precursors containing alkyl groups, such as methyl or *tert*-butyl, and electron-donating groups, such as methoxy

groups, in the 2- and 4-positions were exhibiting the highest efficiency in forming symmetrical *meta*-terphenyl-2,2''-diols[28].

The benefit of the BDD electrode has expanded to industrial and pharmaceutical applications, such as anodic oxidation of phenolic pharmaceutical compounds in wastewater[35]. Parameters such as flow rate in the electrochemical cell, current, initial compound concentration, and wastewater matrices versus simulated wastewater matrices were evaluated. The anodic oxidation reaction can be described as a pseudo first-order reaction. While flow rate influenced the compound degradation, the applied current in the reaction had a major impact on the degradation process. 0.9 A was the optimal current for significant degradation of all compounds tested.

Using fluorinated alcohols, *ortho*-selective phenol-coupling reactions were employed for the oxidation of 2'4-dimethylphenol[27]. Due to the BDD's ability to over-oxidize compounds, leading to limited product selectivity, efficiency for the anodic coupling processes of phenols on BDD electrodes were mediated by fluorinated alcohols. Mediators, such as HFIP and the fluorinated analogue of phenethyl alcohol provided the most comparable product yield of approximately ~45%. To evaluate optimization of product formation, various currents were tested. To optimize 2'2-biphenol formation, product formation can be improved *via* application of 1 F electric current per mole substrate. Chemoselectivity using the BDD electrode was further expanded into arene cross-coupling reactions in which anodic and selective phenol–arene cross-coupling reaction exhibited chemoselectivity *via* preferential formation of oxyl spin centers on BDD electrodes[36] (Figure 1.12).

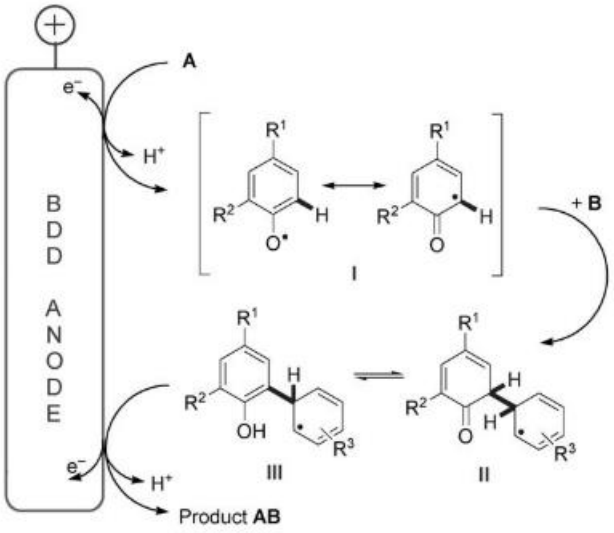

Figure 1.12. Anodic phenol–arene cross-coupling reaction and the potential mechanism[36].

The BDD electrode has been the most popular electrode choice due to the high overpotential for O_2 and hydrogen production (low oxygen and hydrogen evolution reaction), thus increasing efficiency for •OH production. A high current efficiency and poor product selectivity suggest that the oxidation of small organic molecules at diamond anodes happens through electrogenerated •OH radicals (intermediates)[37]. Early work analyzing the importance of hydroxyl radical formation implemented a spin trap system, utilizing 5,5- dimethyl-1-pyrroline-N-oxide as a trapping agent with salicylic acid[38]. Hydroxyl radicals were formed from water discharge at the anode surface, which further reacts with the trapping agent to form a stable radical adduct. Essentially, this allows direct detection and identification of radical formation using electron resonance. Furthermore, the hydroxylation of salicylic acid leads to the production of hydroxylated products: 2,3- and 2,5-dihydroxybenzoic acids, demonstrating that the oxidation process on BDD electrodes include generating •OH radicals as reaction intermediates[38]. Hydroxyl

radicals are able to exist at the surface as a free species, enabling them to further react with other small organic molecules[39]. Ultimately, the BDD electrode demonstrates as one of the best performing anode surfaces for oxidation of organic materials.

1.3.1.3. Platinum electrodes

Pt anodic materials has been widely used in electrochemical applications. As an inert metal, the Pt electrode can also be used as an auxiliary electrode due to non-reactivity with the substrate. However, extreme high potential can lead to metal degradation into respective Pt ions[40]. Normally noble metal electrode activity is short-lived due to electrode fouling; hence the oxidation of phenols and phenolic compounds decrease in current during cyclic voltammetry after the first scan. The rapid decrease can be observed as the quick passivation of material onto the electrode surface[41–43]. If oxidizing a phenol, then a formation of a film of Pt oxide/hydroxides will be deposited onto the electrode surface from electrochemical oxidation[43]. The magnitude of passivation, or electrode fouling is highly dependent on experimental conditions, such as substrate concentration and pH[42]. The presence of methanol in solution influences passivation on the electrode surface, specifically by forming a well-organized polymer film. In contrast, absence of methanol produced small black spots on the metal surface. The very distinct peaks on cyclic voltammograms show that in the presence of methanol at the surface of the Pt electrode, phenol oxidation occurs *via* a separate process[43].

1.3.1.4. Carbon and graphite-based electrodes

Finally, the glassy carbon electrode (GCE) is a popular electrode constructed of non-graphitized carbon that blends glassy and ceramic features with graphite qualities. The material is highly resistant to degradation and temperature, impermeable to gases and liquids, as well as having a flat homogeneous surface. Typically used for anodic oxidation, the GCE has been able to oxidize a wide variety of small organic molecules, including paracetamol, otherwise known as the brand Tylenol ©. Paracetamol contains both an amide and an alcohol functional group, where the latter can be oxidized using the modified GCE to a carbonyl bond[44].

Furthermore, electrochemical synthesis of 3,3′,5,5′-tetramethyl-2,2′-biphenol by dehydrogenative coupling has been reported using a flow cell consisting of the GCE anode, and a stainless steel cathode[31]. The typical flow cell allows the liquid sample to flow through a path in the presence of a supporting electrolyte and requires isolation and removal to obtain the final synthesized product. Hence, the need for efficient synthesis of the product is ideally in the absence of an electrolyte. The Waldvogel lab was able to successfully synthesize 3,3′,5,5′-tetramethyl-2,2′-biphenol by adding pyridine to HFIP, which can be easily evaporated and recovered from solution. Dependent on temperature and current applied, yields obtained reached as high as 61%. However, for scale production, productivity of the reaction must be improved. A 59% yield of 3,3′,5,5′-tetramethyl-2,2′-biphenol and a productivity of 9.60 g/h were reached with the scale-up into the narrow-gap of a 4 cm x 12 cm flow cell using the GCE. In contrast, the BDD electrode was only able to yield as much as 39% of product.

High regioselectivity of (*E*)-vinyl sulfones from the oxidation of cinnamic acids and sulfonate were achieved with high yields at room temperature[45]. A multitude of various anode/cathode combinations were tested such as, Pt/Pt, C/C, and C/Pt. The highest yield was achieved using the C/Pt electrode pair and acetonitrile/water solvent, ultimately producing a yield of 77%.

1.3.1.5. Mixed metal oxide electrodes

Mixed metal oxides (MMOs) are electrodes composed of a mixture of various metals. They are highly conductive and resistant to corrosion. Performance of MMOs vary amongst metal composition. For example, phenol was able to mineralize at the Ti/SnO_2-Sb anode, however, degradation was slower at the $TiRuO_2$ and Pt surface[46]. Furthermore, formation of coloured polymeric compounds were also observed using the $TiRuO_2$ electrode but not the Ti/SnO_2-Sb anode, suggesting that product formation and reaction pathway is heavily influenced by the anode material[46]. The removal rate of total organic carbon (TOC) was shown to be most efficient with the Ti/BDD electrode. The Ti/BDD anode cell had a TOC removal rate of 98%, whereas the Ti/SnO2-Sb/PbO2 and Ti/SnO2-Sb anode cells had just 34% and 25% TOC degradation rates, respectively.

Although the anode material plays a significant role in reaction outcome, the combination of experimental parameters as well as substrate identity strongly affects product yield.

1.3.2. Effect of solvent type

Depending on the oxidation and reduction potentials, the choice of solvent impacts the potential window in which the reaction can occur. Due to this, there is a selection of solvents to choose from. However, it is also important to consider the effect of the electrolyte as well as the electrode material as these factors all impact the potential window (Figure 1.13). Using a Pt electrode and select electrolyte, dimethylformamide (DMF) and dichloromethane (DCM) exhibits a similar potential window with a difference of 1 V. This information can be valuable if the redox-active species undergoes reactions in that range.

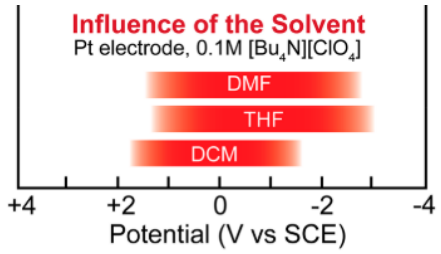

Figure 1.13. Solvent effects on the potential window[17].

An effective solvent depends on the dielectric constant, oxidation outside of applied potential window, as well as its electrical conductivity. A solvent with a wide potential window, such as acetonitrile (ACN) enables flexibility for the oxidation of a wide variety of compounds. ACN is an organic and inert solvent with small background current, compared to other solvents, such as tetrahydrofuran. A large ohmic drop was observed in tetrahydrofuran caused by its low permittivity, thus the extent of ion association from the electrolyte was high[47]. ACN has previously been tested with

potentials as high as 3 V[22,47]. ACN can polarize the electrode to potentials above 2 V for the removal of the formed polymer films on electrode surfaces. Dimethyl sulfoxide, dimethyl formamide and tetrahydrofuran have been shown to have potential for *in-situ* synthesis of polyphenol-based membranes[48]. Dimethyl sulfoxide and dimethyl formamide was shown to be effective in minimizing electrode fouling when electrooxidizing phenol. Unfortunately, the oxidation of dimethyl sulfoxide and phenol overlapped significantly at around 1.7 V, exhibiting no tangible data. Dimethyl formamide exhibited a large peak on the CV due to the overlapping oxidation of the phenols and solvent. The formation of polyphenol was indicated by anodic peaks at 1.7 V, followed by scans with lower current. This suggests that the formed product does not passivate as aggressively compared to other solvents. Therefore, the extent of electrode fouling, and passivation can be minimized by solvent choice.

HFIP was a common solvent utilized mainly by the Waldvogel lab. As a fluorinated alcohol, HFIP has shown exceptional qualities for the electrooxidation of phenols. For example, when HFIP and acetonitrile was used in the electrooxidation of catechol to 2,3,6,7,10,11-hexahydroxytriphenylene, the yields generated were 20% and 4% respectively[49]. Its wide potential window and ability to stabilize organic radicals was able to electrooxidize and perform C-C coupling of aryl compounds[50]. HFIP has been found to have an effect of on the lifetime of the phenoxyl radical as it is able to act as a hydrogen donor[27]. HFIP is also able to prevent overoxidation due to solvation and its combined usage with BDD electrode expands the potential window (-2 V to 4.5 V vs Ag/AgCl)[51,52]. The solvent has been ascribed to form polar and nonpolar micro heterogeneous phases, which can extend the life of cationic radicals, primarily due to the

hydrogen-donating ability[53,54]. This implies that the well-defined regions of polarity of HFIP can hold molecules, or even intermediates between them, based on polarity[27,54]. Further, co-mixing solvents have shown selectivity in product formation. MeOH/HFIP solvent mixture was shown to lower the oxidation potential of phenols and biphenols[55]. It was proposed the MeOH/HFIP clusters are formed, which may contain the phenolic compounds *via* hydrogen bond interactions, therefore facilitating phenol oxidation[55].

Hence, depending on the type of compound that will undergo electrooxidation, careful consideration of the solvent is required.

1.3.3. Effect of supporting electrolyte

In electrocatalysis, the addition of an electrolyte facilitates the electron transfer processes during oxidation and reduction reactions by improving conductivity between the solution and electrode surface. Higher concentration of electrolytes have a higher ion transfer number, electrochemical window, higher thermal stability, and low volatility[56]. Hence, a high electrolyte concentration is normally employed. In addition, the pH of the supporting electrolyte is crucial for reactions containing protons as a reactant or product, as the pH greatly influences the electrode–solution interface and, as a result, the kinetics of the charge transfer process. Popular electrolytes for electrocatalysis include tetrabutylammonium perchlorate (TBAP) and tetrabutylammonium hexafluorophosphate ($TBAPF_6$). The combination of electrode material and supporting electrolyte influences the potential window (Figure 1.14). For example, the Pt electrode with the TBAP electrolyte exhibits different potential ranges depending on the solvent choice. In acetone,

the range is limited to -2 to 1 V, however, in pyridine, the range increases greatly to -2 to 3 V.

The electrochemical oxidation of an aromatic, benzene tricarbonyl chromium, in dichloromethane (CH_2Cl_2) with selected electrolytes formed radical cations during the reaction and was shown to be more persistent depending on the supporting electrolyte selected[57]. TBAP, tetrabutylammonium trifluoromethanesulfonate ($TBACF_3SO_3$) and tetrabutylammonium tetrafluoroborate ($TBABF_4$) as selected electrolytes formed chemically irreversible oxidation at room temperature. However, it was shown that low temperatures (-90ºC) exhibited irreversibility regardless of the three electrolytes chosen. Room temperature reversibility of the reaction was sensitive to the small amounts of nucleophilic species in solution, ultimately destroying the reversibility. Electrolyte precipitation was also less likely with $TBABF_4$ and $TBACF_3SO_3$ compared to TBAP.

Hence, the selected supporting electrolyte requires consideration that is dependent on the temperature, pH, as well as concentration.

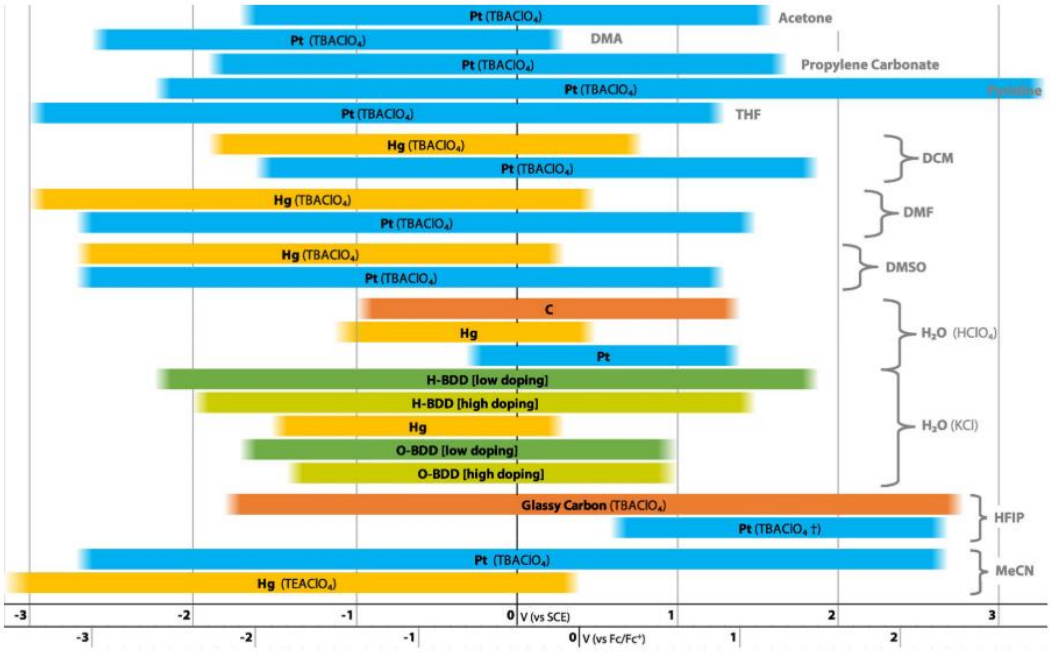

Figure 1.14. Electrode and supporting electrolyte combinations at its effect on potential windows (vs Fc/Fc^{+})[58].

1.3.4. Effect of pH

As concentration of H+ ions increase, the redox potential increases[59]. The current efficiency increases with decreasing pH[60,61]. Hence the effect of pH has been investigated. In the case for the oxidation of paracetamol, an acidic media (H_2SO_4) strongly influences the current observed in both anodic and cathodic peaks[44]. The increased reversibility with decreasing pH was reflected on the significant change in the difference of peak potential between anodic and cathodic peaks. The strongly acidic media was able to influence the reaction for further oxidation of paracetamol into quinone, a highly reversible compound[44]. The effect of pH can also shift the oxidation potentials of small organic molecules, such as phenol, which was observed to have shifted from 0.85 V (pH 6.5) to 1 V (pH 2.2)[62].

1.3.5. Green electrosynthesis

Electrochemical syntheses have shown numerous benefits, such as selectivity, scalability, and high yield[28,31,50,63]. The absence of strong oxidizing agents reduces the need for excess chemicals and reagents that would commonly be used in product syntheses and isolation. The process enables the user to gain more control of a reaction, in contrast to conventional chemical oxidation in which there is no stopping a reaction once it begins. Selective oxidation and reaction by varying currents and potential is possible with electrochemical syntheses that is not normally observed with conventional oxidation.

1.4. Characterization techniques used to monitor phenol oxidation and characterize product formation

Techniques such as gas chromatography-mass spectrometry (GC-MS) and nuclear magnetic resonance (NMR) spectroscopy are common instrumentation employed for structural analysis. The electropolymerization of phenol and chlorinated phenols were investigated using a Pt electrode and characterized using GC-MS[64]. Using GC-MS can allow for the analysis of monomers, polymers, as well as tetramers formed during the reaction. The reaction monitoring for the degradation of various pharmaceuticals were monitored using GC-MS, exhibiting clear signal depletion, indicating that the compounds were degrading over time[35] (Figure 1.15) However, the technique is limited by the detection of the mass analyzer and the low mobility of the large species in the column.

Hence, some understanding of the coupling mechanism can help distinguish between species formed.

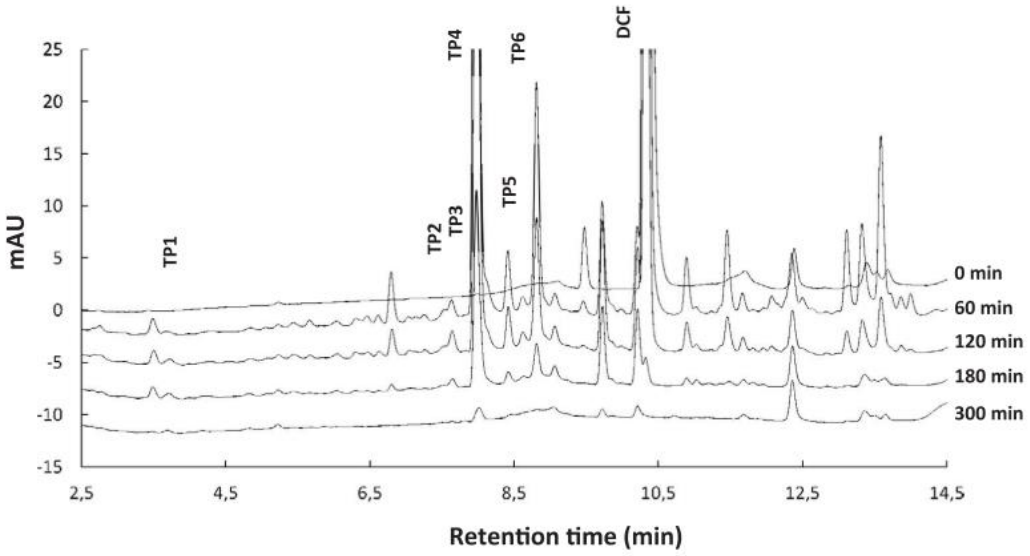

Figure 1.15. Chromatogram (GC-MS) obtained from the anodic oxidation of key pharmaceuticals[35].

If the product is isolated, then the reaction can be monitored using NMR analysis. Obtaining NMR spectra prior and after electrochemical synthesis enables monitoring of new C-C coupling interactions that can support reaction mechanisms[31]. The application of NMR allows more detailed information on the organic framework of the molecule, particularly if there is an interest in a specific compound generated. The anodic oxidation 2'6-dimethylphenol yielded products that were successfully characterized using NMR, single XRD, and GC-MS analyses[65].

To further add to structural analysis, IR spectroscopy enables functional group determination. The appearance and disappearance of vibrational bands observed in IR spectra serves as an effective indicator if a new product was formed. In the electropolymerization of different phenolic compounds, the formation of a C=O band at

1640-1660 cm^{-1} in the IR spectra indicated that the film formed during phenol and *m*-cresol oxidation was due to ketones from quinone moieties of the polymer[66]. The absence of the OH vibrational band at 3300 cm^{-1} after oxidation suggests that the polymer has been formed. Hence IR analysis can be beneficial in polymer studies.

Moreover, single molecule x-ray diffraction (XRD) enables precise calculation of individual atoms and placement. If there is interest in further crystal characterization, powder x-ray diffraction would be beneficial is the compounds exhibits crystal polymorphism. Additionally, powder XRD may serve useful for probing bond formation, solvent interactions, as well as relations with surface electrodes, as observed with HFIP's interaction with 1-phenyl-2,2,2-trifluoroethanol *via* hydrogen bonded aggregates[67].

Another method is UV-vis spectroscopy, in which compounds absorbing in the UV-vis range can be characterized. UV-vis characterization is generally used to monitor the formation of new compounds. Changes in the UV-vis profile is an indicator of new product formation. Isolated products, such as dimers and its analogues were able to provide a UV profile that was substantially different from its precursor material[68]. Phenol oxidation with Fenton reagents to form aromatic phenolics were also observed to form dark colors, in which color variation is dependent on the reaction intermediates generated[69]. Furthermore, UV-vis can also be used to monitor the synthesis of non-coordinated phenolate anions, in which obvious color changes in solutions were due to hydrogen bonding of the non-coordinated anion[24].

To understand the reaction mechanism, the formation of intermediates must be studied. Electron paramagnetic resonance (EPR)-spin trapping is generally used to monitor and identify free radicals formed. The effect of HFIP on phenoxyl radical

formation was investigated[34]. O-H bond dissociation enthalpy (BDE) found in phenols was lowered in the presence of HFIP as it favorably stabilizes the phenoxyl radicals formed. By comparing integrated signal intensity with a long-lived radical anion model created during the one-electron reduction of 7,7,8,8-tetracyanoquinodimethane, the radical quantity can be determined[70]. Hence, EPR-spin trapping experiments are effective for understanding the oxidation/reduction mechanism of phenolic compounds. Depending on what is being achieved in electrooxidation or chemical oxidation, the characterizing methods will vary. Hence, it is important to consider the nature of the products being formed.

1.5. Thesis research

This thesis will focus on the electrochemical oxidation and chemical oxidation of two distinct phenols: 2'6-diphenylphenol (DPP) (Chapter 2) and 2'2-dihydroxybiphenol (DHBP) (Chapter 3) followed by reaction monitoring and product characterization using various analytical methods, such as UV-vis spectroscopy, NMR spectroscopy, single-crystal XRD, GC-MS, and FTIR spectroscopy. The comparison studies of phenolic compounds, clearly illustrate the key differences in their reactivity under chemical and electrochemical processes. Reaction monitoring and product characterization allowed for greater understanding of the reaction mechanism, role of electrode material, and reaction selectivity during electrochemical oxidation.

Chapter 2 – Electrochemical vs chemical oxidation of 2,6-diphenylphenol

2.1. Introduction

Compared to traditional organic synthesis, electrosynthesis provides several advantages, such as lower use of hazardous and toxic reagents, lower waste and chemical pollutants generation[22,71,72]. Recent advances in the electrosynthesis towards small organic compounds *via* carbon-carbon or carbon-nitrogen bond formation have yielded efficient chemical transformations with high selectivity and yields[73,74]. Specifically, the biaryl (cross) coupling *via* C-C bond formation has been recently demonstrated *via* a direct anodic oxidation of 2,4-dimethylphenol (at constant current) to produce a homodimer *ortho*-*ortho*-coupled biphenol[33,65]. Using anodic oxidation of 2,4-dimethylphenol, several other products were also formed in addition to an ortho-coupled homodimer, and selectivity of the reaction was improved by using boron-doped diamond electrode or molybdenum-based anode[30,75]. This type of reaction produced predominantly C-C dimerization *via ortho* position of the phenol. Such chemistry was further expanded to include synthesis of non-symmetrical biphenol, cross-coupled phenol/naphthol, phenol/arene and phenol/thiophene products at constant current[33,50,76,77].

The electrooxidation of phenolics to produce *para* C-C coupling products are rare[78]. In addition, the electrooxidation of phenols at the constant potential (or varied potential) is less common than at constant current. The electrosynthesis of *para*, *para*-homodimer from *tert*-butyl substituted phenols, under varied potentials, has been

reported[22], with high selectivity for 2,6-di-*tert*-butylphenol due to the number and site of bulky substituents. In addition, the electrooxidation of bulky phenols was selective compared to chemical oxidation. The reactivity of other bulky phenols under an electro synthetic environment is far less understood but could provide alternative synthetic avenues towards new C-C coupled products.

Herein, the electrooxidation of 2,6-diphenylphenol (DPP), a common industrially relevant chemical, was carried under applied potential (varied or constant) and compared to traditional chemical oxidation. The reaction was monitored, and products were characterized by using electrochemistry, UV-vis spectroscopy, nuclear magnetic resonance spectroscopy, gas chromatography mass spectrometry, and single crystal X-ray diffraction. The reaction selectivity and yield were evaluated as a function of applied potential, solvent composition, and electrode type.

2.2. Experimental Section

2.2.1. Materials and Reagents

2,6-diphenylphenol (DPP) (>98%) from TCI America, tetrabutylammonium perchlorate (TBAP) from Alfa Aesar and Honeywell 99.9% purity, HPLC-grade acetonitrile (ACN) was standard for electrochemical experiments. The glassy carbon working electrode, silver wire reference, and platinum wire counter electrodes were obtained from CH Instruments (USA). Silver nitrate was from Fisher Scientific. Reducing agent used was tin (II) chloride (>98%) from Fisher Chemical. Copper (II) perchlorate was purchased from Alfa Aesar.

2.2.2. Electrochemical Measurements

Electrochemical measurements were performed using Autolab PGSTAT302N potentiostat by Metrohm AG. The solutions containing 10 mM DPP and 0.1 M TBAP in 3 mL acetonitrile were prepared for all reactions, unless stated otherwise. The working electrode was the glassy carbon, the reference electrode was an Ag/Ag^+ 10 mM silver nitrate ($Ag/AgNO_3$), and the counter was a platinum wire, unless otherwise mentioned. Cyclic voltammetry was performed at 100 mV/s scan rate, unless otherwise specified, and potential ranges: -3 to 3 V, -3 to 0 V, and 0 to 3 V. For each CV, 10 scans were performed.

2.2.3. UV-vis Spectroscopy

Spectroscopic measurements were performed using the Agilent Cary 60 UV-vis spectrophotometer, 1 cm quartz cuvette and 200 - 800 nm wavelength range.

2.2.4. Fourier-transform infrared spectroscopy (FT-IR)

The FT-IR instrument used was the ThermoScientific Nicolet 380 spectrophotometer.

2.2.5. Gas chromatography-mass spectrometry (GC-MS)

The Agilent 7890B GC with the HP-5MS UI column and a 5977A MSD was used for reaction monitoring. All solutions were filtered using silica gel obtained from Sigma Aldrich. Experimental parameters can be found in the Appendix (Appx II 2.34).

2.2.6. Nuclear magnetic resonance (NMR)

The Oxford AS500 NMR with a Varian Unit INOVA console and VnmrJ 4.2 software was employed for all NMR experiments. Solutions were prepared in deuterated acetonitrile (CD_3CN) and TPDQ was prepared in deuterated chloroform ($CDCl_3$).

2.2.7. Chemical oxidation and reduction

10 mM of DPP and 10 mM copper perchlorate in 3 mL acetonitrile was used for chemical oxidation. All UV-vis spectra were recorded before, during and after the reaction. Tin chloride dihydrate (~6.0 mM) was used as a reducing agent, to reduce TPDQ to TPBD.

2.2.8. X-ray single-crystal diffraction

Crystallized solid from the chemical oxidation reaction was analyzed using single-crystal X-ray diffraction, performed using the Apex2 Kappa CCD 4-Circle Kappa FR540C diffractometer from Brüker AXS (additional experimental parameters can be found in Appx II Table 2.2 – 2.6). Data processing was performed on crystal software called Mercury and CrystalExplorer.

2.3. Results and Discussion

2.3.1. Electrochemical Characterization of DPP

Using the undivided cell in the presence of GCE (WE), Pt (CE) and $Ag/AgNO_3$ (RE) and ACN/TBAP, the 2,6-di-*tert*-butylphenol was oxidized into a *para, para* homodimer using applied potential[22]. ACN was used due to the large potential window[22,47]. Similarly, herein, the starting point for electrooxidation of DPP into targeted

para, *para* homodimer was initiated under the identical experimental conditions. Cyclic voltammograms (CVs) of DPP were measured to characterize its oxidation/reduction potentials (Figure 2.1A). Up to 5 irreversible anodic peaks, E_{pa}, were observed at the initial CV scan (2.11±0.09 V, 1.46±0.05 V, -0.31±0.01 V, and 1.25±0.02 V, and -1.58±0.2 V) (Appx II Table 2.1). To determine that the listed peaks were not attributed to the electrolyte and solvent, a blank containing ACN and TBAP was obtained (Appx II 2.2). Without an electrolyte, no tangible oxidation/reduction peaks were observed (Appx II 2.1A). The respective UV-vis also exhibited no major peaks (Appx II 2.3). The irreversible anodic peaks were associated with one-electron oxidation of DPP, or its phenolate, which was similar to the electrooxidation of other phenols[22].

Drastic shifts in the anodic peaks in the first few scans (3 scans) indicate the loss of starting material and formation of new products (Figure 2.1B). The anodic peak at 2.11 V shifts left over continuous scans before stabilizing into the 2 V position. The single cathodic peak at -1.58 V shifts left after its first scan (Appx II 2.4A). The cathodic peak is likely the reduction of the species following oxidation of the redox active species. Specifically, changes in the current above 1.2 V indicate consumption of starting material, which correspond to a phenol oxidation[47]. Additional CV cycling from 5 to 20 CV did not exhibit any additional changes (Appx II 2.4B). The dramatic change in CV may be attributed to irreversible one one-electron oxidation of DPP at the hydroxyl group followed by a proton loss to generate a radical cation intermediate to form a phenoxyl radical[22]. Alternatively, if proton loss precedes the one-electron oxidation, a phenolate anion will form and subsequently get oxidized into phenoxyl radical. The two phenyl groups at the 2’ and 6’ position cause steric hindrance, preventing C-C coupling from all

sites except the *para* position[22]. Irreversible oxidation peaks observed with phenolic compounds are not uncommon due to the formation of the unstable oxidized species that react to form a variety of products, that cannot be converted back to the starting materials[21]. Cycling up to 20 CV (200 scans) did not produce additional electrochemical changes and indicated no polymerization of DPP.

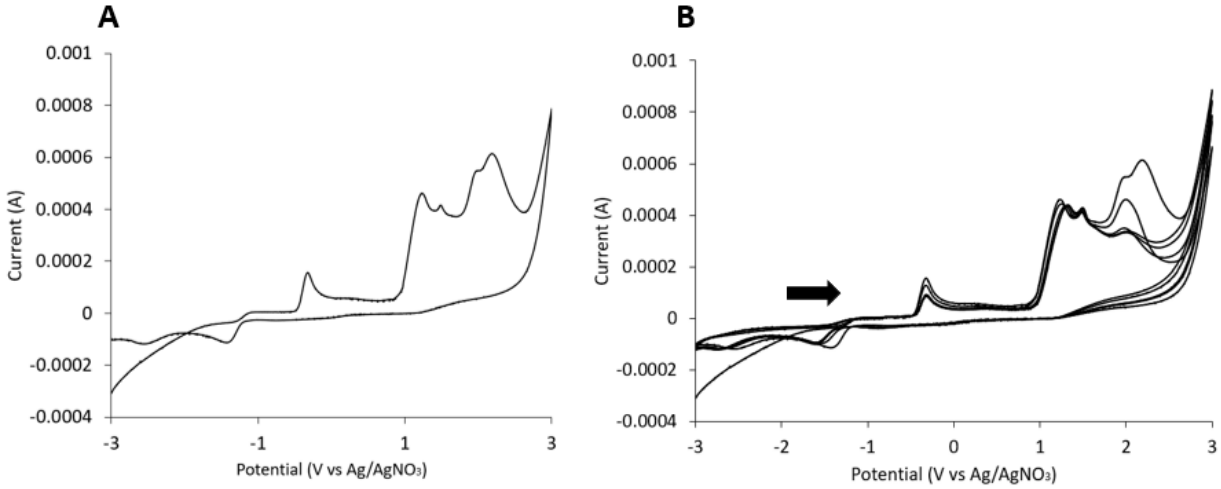

Figure 2.1. Cyclic voltammograms of DPP at (A) initial CV scan, and (B) 1 CV (10 scans) ([DPP] = 10 mM, [TBAP] = 0.1 M, ACN, 10 scans per CV). Scan direction indicated by arrow.

Next, the CV scan rate, *v*, dependent analysis of DPP has shown an increase in peak current as *v* increased, which is a common trend[79]. The thicker the diffusion layer, the slower the scan rate, and the slower the mass transport of the species in the bulk solution[80]. Thickness of the diffusion layer is affected by the irreversibility of the reaction, the more irreversible the reaction the smaller the diffusion layer[80]. For the slowest *v*, the CV shows the E_{pa} at 1.26 V, 1.47 V, -0.27 V and E_{pc} at -1.68 V were

present except for the peak at 2.11 V. As the potential is scanned at a higher *v*, there is a formation of a new E_{pc} peak at -0.92 V (200 mV/s). As *v* gradually increases (increments of 100 mV/s), the new E_{pc} shifts to -1.29 V/s (at 1 V/s) and E_{pa} at -1.68 V disappears.

Upon scan rate-dependent experiments, the linear dependence of current versus square root of scan rate is related to diffusion controlled-processes (where the redox probe is in solution) and is observed by its correlation coefficient (Appx II 2.5). The Randles-Sevcik equation (Appx II Eq. 2.1) was used to describe the relationship between the peak current (i_p) and the square root of the scan rate (V s^{-1}), where *n* is the number of electrons transferred in the reaction, A (cm^{-1}) is the surface area of the working electrode, C^o is the concentration of the bulk analyte in solution and D_o is the diffusion coefficient of the oxidized species. By utilizing the scan rate data, the Randles-Sevcik plot, dictated by the Randles-Sevcik equation can be generated to describe the effect of the scan rate on the peak potential[81]. Generally, the observed peak current increases linearly with the square root of the scan rate in an electrochemically reversible electron transfer process involving a freely diffusing redox species. The shift of E_{pa} peaks to a positive potential value with an increase in scan rate and an increase in current peak density confirms an irreversible oxidation process. According to the Randles-Sevcik equation, deviation from linearity is an indication of irreversible electron transfer processes. Irreversible behaviour for this process results in shifts in peak potentials due to slow electron transfer and an extreme potential is required for the electron transfer to occur.

2.3.2. Spectroscopic Characterization of DPP Electrooxidation

During CV measurements of DPP, the solution colour changed from clear and colourless to dark yellow within a few hours (Figure 2.2A). The electrooxidation reaction and the formation of a coloured product was monitored using the UV-vis spectroscopy.

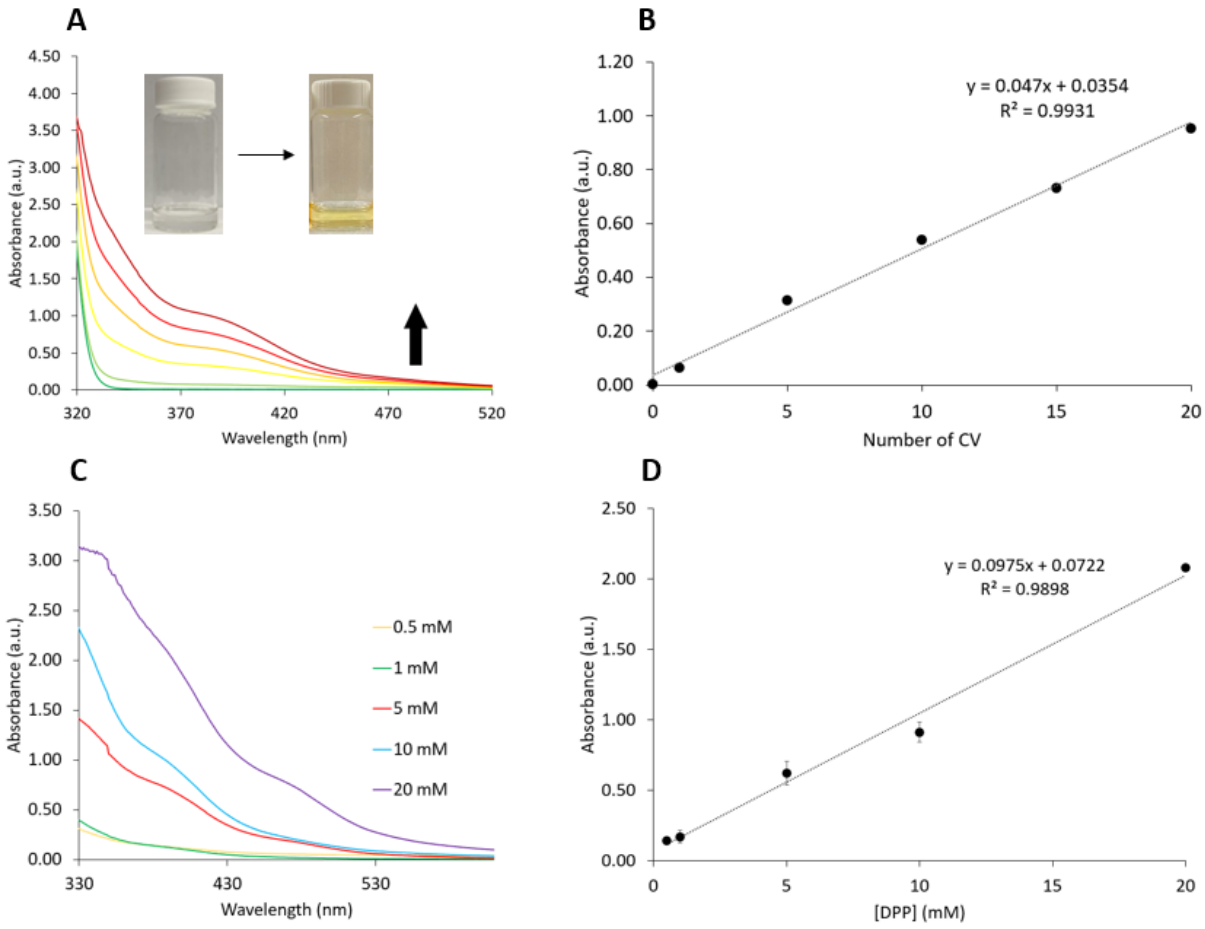

Figure 2.2. (A) Absorbance of 10 mM DPP as a function of CV cycling. Arrow indicates increase in absorbance (B) Triplicate analysis of DPP at 1, 5, 10, 15, 20 CV with standard deviation (C) UV plot of 10 mM DPP as a function of concentration. 20 CV performed for each concentration (D) Triplicate analysis of DPP at 0.5, 1, 5, 10, and 20 mM with standard deviation.

In the 320 - 520 nm range, DPP did not absorb. After 5 CVs (reaction time = ~50 min), the formation of a new product resulted in a new absorbance band at 390 nm (~0.5 a.u.) which was reflected in the solution colour change. The greatest absorbance observed was after 20 CVs (reaction time = 6.5 h). To increase reaction yield, up to 80 CVs (reaction time = 26 h) were performed which resulted in a dark yellow solution. The increase in absorbance was proportional to an increase in CV scanning, indicating that product formation was dependent on duration of electrochemical measurements in the applied potential range (-3 to 3 V). This resulted in a linear relationship observed between the number of CVs and absorbance (Figure 2.2B).

DPP concentration-dependent electrochemical experiments have displayed a similar pattern to that of CV-dependent measurements (Figure 2.2C) (Appx II 2.4C). The concentration of starting material (DPP) was tested at 0.5, 1, 5, 10, and 20 mM at 20 CVs. The CV profile differed slightly at various concentrations (Appx II 2.4C) UV-vis spectroscopy was also used to monitor electrooxidation reaction. At 5 mM concentration, the maximum absorbance was ~0.8 a.u. at 390 nm. The more starting material was used, the darker the solution colour after CV scanning. At a 20 mM DPP, the absorbance doubled to that of 10 mM DPP, indicating that twice the amount of product was being formed. Up to 40 mM DPP was electrooxidized which resulted in a rich yellow solution with high absorbance. Hence, a linear dependence between DPP concentration and absorbance was observed (Figure 2.2D). Similarly, this behavior was also observed in the electrooxidation of 2,6-di-*tert*-butylphenol in which a linear dependence was observed in both CV-dependent and concentration-dependent UV-vis analyses[22].

When using the GCE, Pt, and $Ag/AgNO_3$ undivided cell, the coloured product formation was taking place at the working GCE during positive CV cycling, while noticeable coloured product formed on Pt CE during the scan in the negative direction. Hence, the product(s) formed during the large applied potential window were highly dependent on the sign of the potential applied, and reaction site was switching from GCE (initial scan in a positive potential direction) to Pt (reverse scan toward negative potential direction). To investigate the effect of the specific potential range on the electrooxidation of DPP and subsequent product formation, two potential ranges were applied: -3 to 0 V (negative) and 0 to 3 V (positive range). This would allow probing two types of reactions. Typical irreversible phenol oxidation takes place at positive potentials (higher than 0 V) hence, by conducting electrooxidation in the 0 to 3 V, solely phenol oxidation may be taking place. By contrast, when the phenolate is oxidized, the redox potential is separated away from the phenol oxidation. In the -3 to 0 V potential range, the phenol oxidation is negligible, rather phenolate oxidation predominates. Figure 2.3A shows clear irreversible oxidation of DPP at a positive potential and a dramatic change in CV profile with additional scanning, clearly indicating DPP consumption during reaction. A single scan CV can be found in the appendix (Appx II 2.1A) After applying 20 CV (reaction time = 3.5 h), the absorbance at 390 nm reached ~1 a.u., which was like the electrooxidation in the full potential window. At the positive potential range, the solution changed from colourless to yellow, as monitored by UV-vis. At this stage, the yellow product was formed from GCE WE surface only. No reaction was observed stemming from the Pt CE. Irreversible oxidation at ~-0.5 V was ascribed to phenolate oxidation[23]. In the negative potential range (-3 to 0 V), the solution changed from colourless to bright orange (Figure

2.3C). At a negative potential, an absorbance band at 480 nm was obtained after 20 CVs (reaction time = 3.5 h) (Figure 2.3). Clearly products at 390 and 480 nm were formed selectively, depending on the applied potential. Hence, chronoamperometry measurements were made for 3.5 h and held at -2 V, yielding a 480 nm band at ~0.5 a.u. (Appx II 2.6). Chronoamperometry is a technique in which a selected potential is held constant. Noticeably, after 48 h, the 480 nm absorbance disappeared and a new band at 390 nm was formed alongside a solution colour change from orange to yellow, indicating conversion of product (at 480 nm) in the new product (at 390 nm).

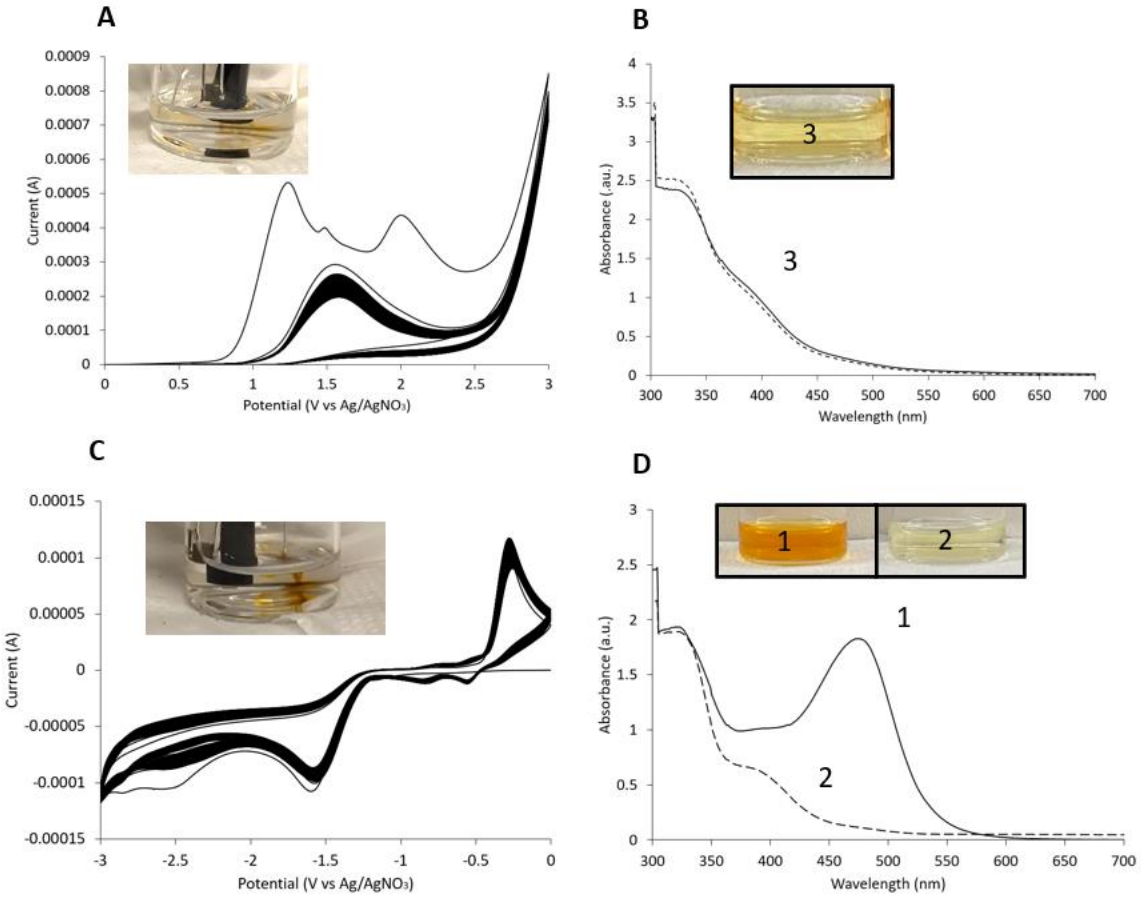

Figure 2.3. 20 CV of various potential ranges (200 scans = 20 CV); (A) 0 to 3 V; (B) corresponding UV-vis spectra of non-diluted DPP post electrochemical reaction at positive range; (C) -3 to 0 V; (D) corresponding UV-vis at -3 to 0 V range (1) Non-diluted DPP post electrochemical reaction (2) non-diluted post electrochemical reaction after 48 hours.

Similar absorbance at 480 nm was observed when DPP was chemically oxidized by lead oxide with acetic acid to form *para, para* homodimer[13]. In this work, the chemical oxidation of DPP was achieved by using the copper perchlorate (1:1 equimolar ratio of copper perchlorate to DPP). This allowed for a direct comparison of reaction selective and product identification between electrooxidation vs traditional chemical oxidation of DPP. The chemical oxidation of DPP yielded an absorbance band at 480 nm (Figure 2.4A). The colour change from colourless to dark orange was immediate with the highest absorbance seen within the first 15 minutes of reaction. However, the absorbance decreased after 5 hours of reaction time due to the crystallization of the blue-green reflective solid product. Through electrooxidation, 2,6-di-*tert*-butylphenol was oxidized to yield brown crystals that were determined to be 3,5,3′,5′-tetra-*tert*-butyl-4,4′-diphenoquinone[22]. Hence, depending on the oxidation pathway taken (either

electrooxidation or chemical oxidation), the formation of the major product differs.

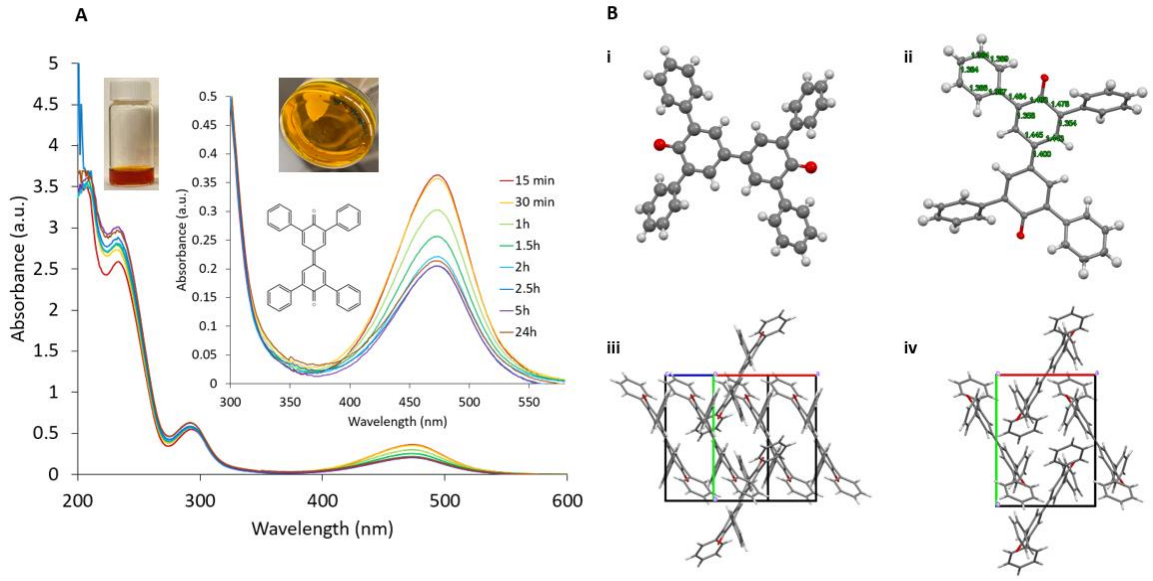

Figure 2.4. (A) Time-dependent analysis using UV-vis spectroscopy of the chemical oxidation of DPP with copper perchlorate. [DPP] 10 mM, [$Cu(ClO_4)_2$] = 10 mM in 3 mL ACN. Inset: time-dependent UV measurements performed using a 100x dilution; (B) single molecule XRD of 3,3',5,5'-tetraphenyldiphenoquinone (i) Ball-stick form of blue-green reflective crystal obtained from the chemical oxidation of DPP using single-crystal x-ray diffraction (ii) Bond lengths in ellipsoid (iii) view of packing along c-axis in capped sticks form (iv) View observed from the top of the c-axis in capped sticks form.

The solution containing the solid exhibited no shift in wavelength and change in absorbance after 24 h, indicating that the product was stable under oxidizing conditions. Of note is that the negative potential range resulted in an identical 480 nm band. The spectroscopic data indicated that the electrooxidation of DPP in -3 to 0 V range, and the chemical oxidation of DPP produced the same product which absorbed at 480 nm. Due to

the successful crystallization of the product from chemical oxidation, a single-crystal XRD was performed. The XRD analysis identified the product as 3,3',5,5'-tetraphenyldiphenoquinone (TPDQ) (Figure 2.4B), a quinone-based dimer proposed from a reaction mechanism from a previous study[22]. The Hirschfeld surface indicates that are some aromatic π-π stacking interactions present in the structure (Appx II 2.7 & 2.8). XRD parameters can be found in supplementary information (Appx II Table 2.2-6). Similarly, previously recorded absorbance bands for chemically synthesized TPDQ include the main absorbance peak at ~ 480 nm[68]. TPDQ was further characterized by ^{1}H NMR, ^{13}C NMR, COSY NMR and IR spectroscopy (Appx II 2.10-14). ^{1}H NMR, COSY NMR, and IR spectra of DPP has also been obtained for comparative purposes (Appx II 2.10-14). NMR and IR of DPP can also be found in the appendix (Appx II 2.15-17) TPDQ spectral data was also contrasted with NMR data of electrochemical oxidation of DPP in the -3 to 3 V range (Appx II 2.18 & 2.19). NMR analysis of reaction post electrochemical oxidation reveals formation of multiple products. IR analysis of solid DPP and TDPQ revealed the loss of an OH band at 3519.89 cm^{-1} and appearance of C=O functional group at 1583.09 cm^{-1} indicating successful conversion of DPP to TPDQ. The % yield of TPDQ for chemical synthesis was ~20% (combined mass of product absorbance and solution absorbance).

Upon chemical oxidation of DPP to form TPDQ, the orange-coloured solution remained, indicating products were stable and conversion to by-products was minimal. This is due to the presence of an oxidant in the solution, providing a continuous oxidizing environment for TPDQ. To further probe the stability of TPDQ, tin chloride, a reducing agent, was added to TPDQ solution. If TPDQ is reduced by tin chloride, then the non-

quinone (tetraphenyl analogue) product would be formed with hydroxyl groups. This compound is 3,3',5,5'-tetraphenyl-biphenyl-4,4'-diol (TPBD). Immediately after adding excess tin chloride, the orange-coloured solution gradually transformed into light yellow colour (Appx II 2.6). The UV-vis spectra displayed a new band at 390 nm, indicating a hypsochromic shift. Hence, the reduction of TPDQ to TPBD in the negative potential range, the 480 nm band was indicative of the formation of TPDQ which was like the chemical oxidation reaction. However, under electrochemical conditions, the TPDQ was slowly reduced to TPBD (after 48 h), which resulted in the hypsochromic shift from 480 to 390 nm.

In the initial stages of the reaction, it is visually observed that the orange product was diffusing around the Pt wire and eventually dispersed into the solution. Therefore, when the GCE and Pt wire were used in the cell, the reaction site was on the Pt surface when the negative potential was applied. To further investigate the role of the electrode surface, the electrooxidation of DPP was carried out using a GCE/GCE pair and a Pt/Pt pair. The product absorbing at 480 nm was formed when a) -3 to 3 V using the GCE/GCE pair (Figure 2.5C), b) -3 to 0 V using the Pt/Pt pair (Figure 2.6C) c) -3 to 0 V using the GCE/GCE pair (Figure 2.7C), d) 0 to 3 V using GCE/GCE pair (Figure 2.7A), e) -3 to 0 V using GCE/Pt pair (Figure 2.3C). Hence, the product at 480 nm was formed in the absence of using Pt. The negative potential favoured the formation of the product at 480 nm, regardless of the type of electrode surface. When a negative potential was applied, the electrooxidation of DPP took place at the surface of the counter electrode, regardless of the surface type.

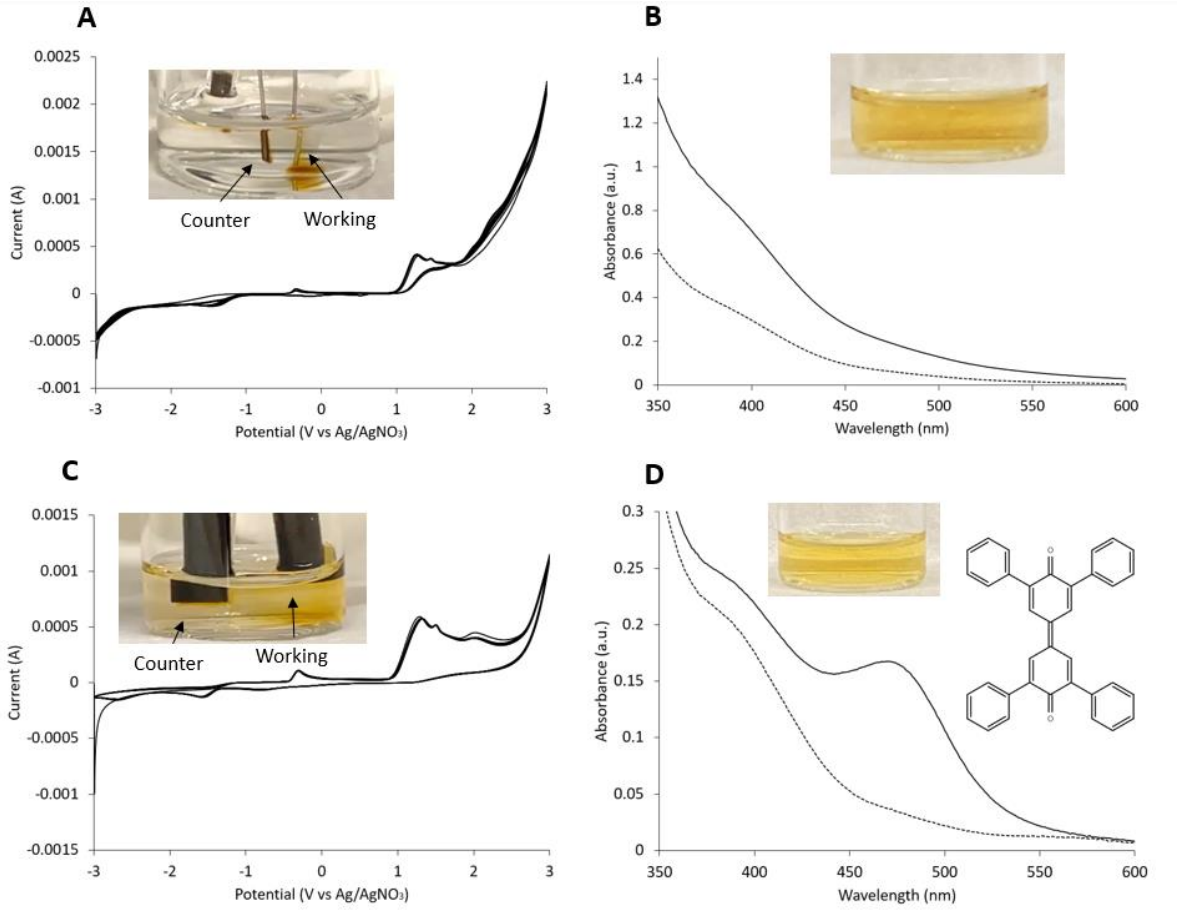

Figure 2.5. 1 CV, [DPP] = 10 mM, [TBAP] = 0.1 M, -3 to 3 V potential range; (A) Working: GCE, counter: GCE, reference: $Ag/AgNO_3$; (B) corresponding UV-vis using Pt/Pt pair; (C) working: Pt wire, counter: Pt wire, reference: $Ag/AgNO_3$; (D) corresponding UV-vis using GCE/GCE pair.

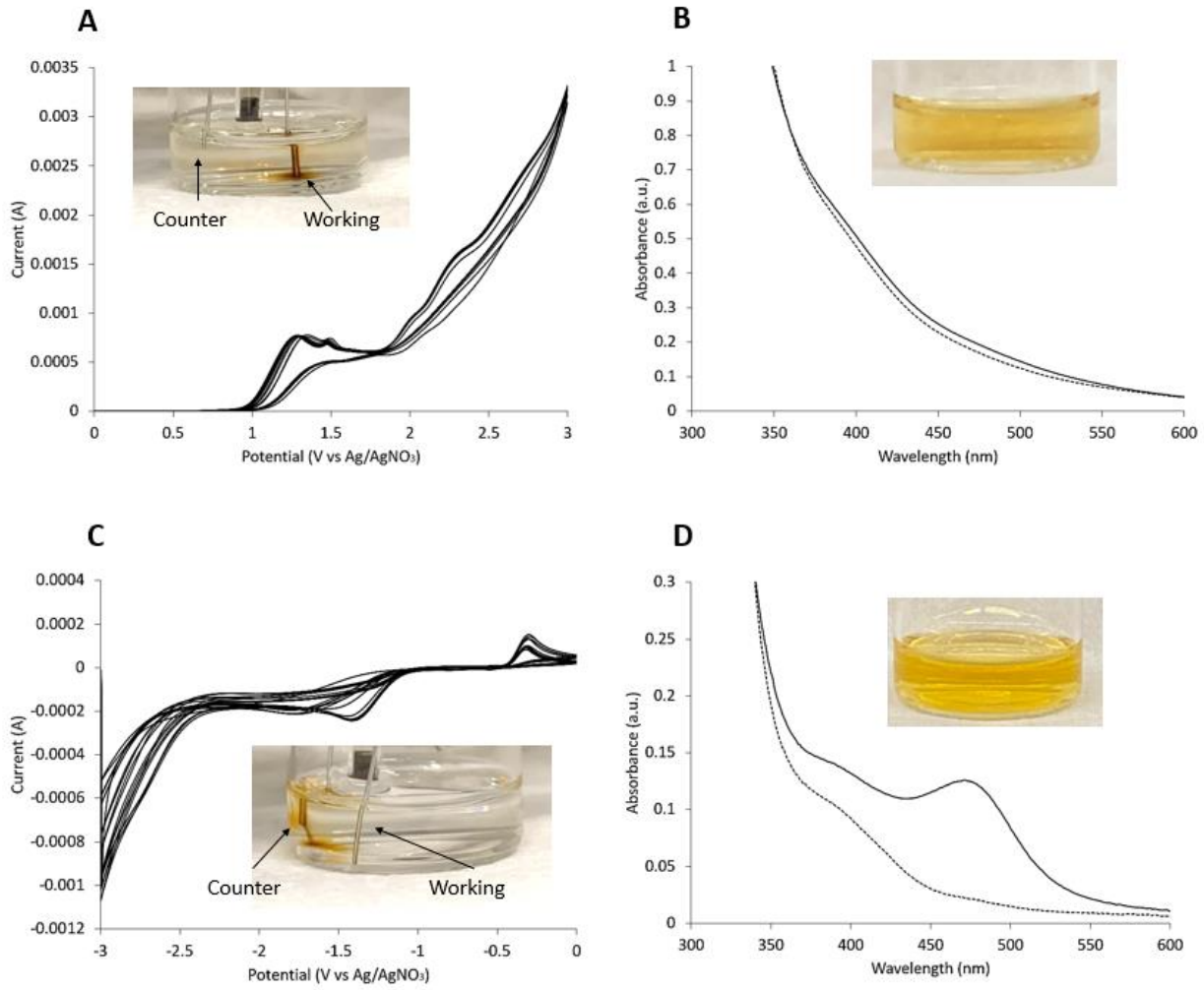

Figure 2.6. 1 CV, [DPP] = 10 mM, [TBAP] = 0.1 M, working: GCE, counter: GCE, reference: $Ag/AgNO_3$. (A) 0 to 3 V; (B) corresponding UV-vis at 0 to 3 V range; (C) -3 to 0 V; (D) corresponding UV-vis at -3 to 0 V range.

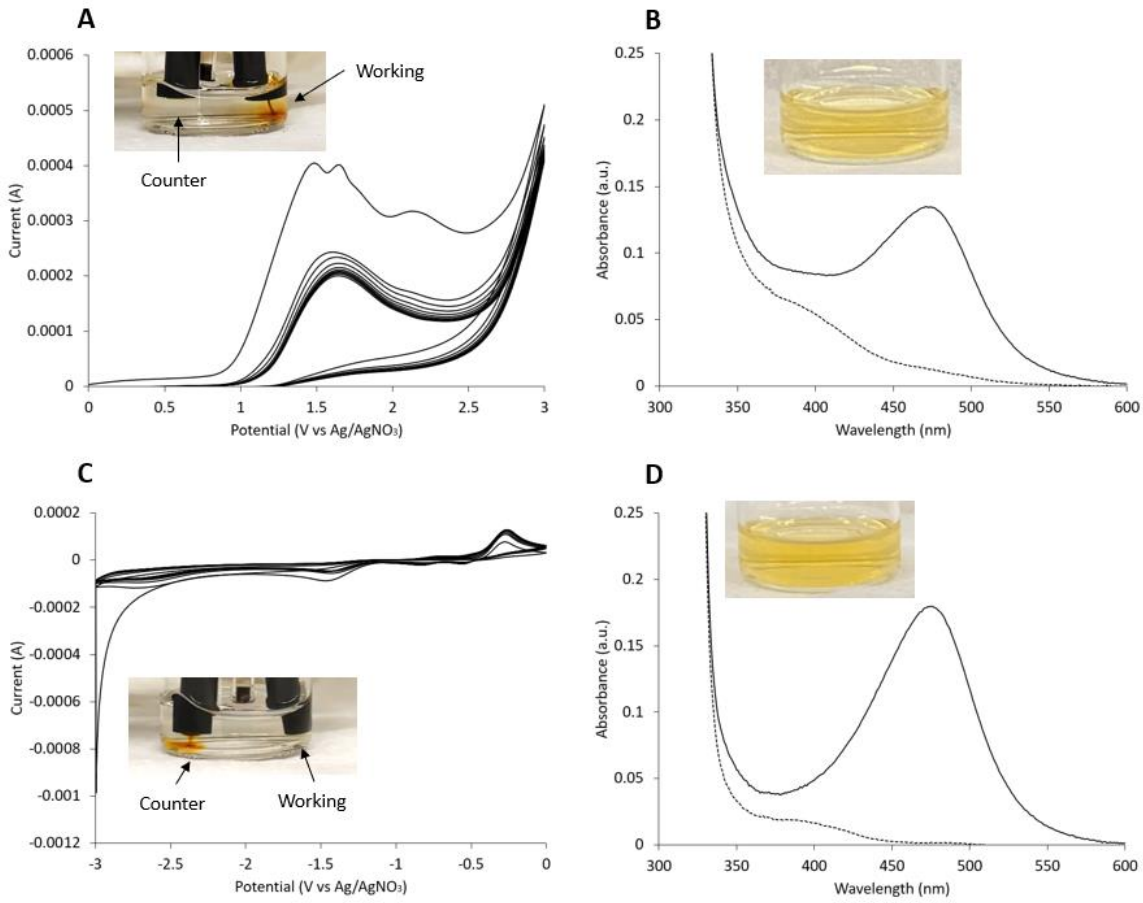

Figure 2.7. 1 CV, [DPP] = 10 mM, [TBAP] = 0.1 M, Working: GCE, counter: GCE, reference: $Ag/AgNO_3$ (A) 0 to 3 V; (B) corresponding UV-vis at 0 to 3 V range; (C) -3 to 0 V; (D) corresponding UV-vis at -3 to 0 V range.

Hence the formation of product absorbing at 480 nm was clearly observed under controlled potential and specific electrode types.

The TDPQ and its absorbance at 480 nm were used to determine the extinction coefficient which was used alongside Beer-Lambert Law to determine the % yield of the reaction. The absorbance of TPDQ as a standard in a co-mixture of acetonitrile and chloroform was used (95/5%) (Appx II 2.20). The various synthetic conditions were

tested initially using short reaction times (<30 min) to quickly screen experimental conditions. Table 2.1 illustrated that the % yield was in 0.01 - 0.09% range when 1 CV was used (10–20-minute reaction time). However, yield was improved with longer CVs (3.5 h) of reaction time to obtain the yield of ~1% for the GCE/Pt electrode combination (Figure 2.3). Out of all electrode combinations, the GCE/GCE pair at a negative potential was able to achieve the highest yield. It should be noted that under electrochemical conditions, once TPDQ is formed it underwent other reactions, effectively reducing absorbance at 480 nm, and reducing the apparent yield. It is suspected that the yields are greater than what was estimated by UV-vis spectroscopy.

Table 2.1. TPDQ yield was generated from various electrode combinations, [DPP] = 10 mM, [TBAP] = 0.1 M in ACN (after 1 CV = 5-10 min reaction time).

	Working Electrode	Counter Electrode	Potential (V)	TPDQ Abs (λ = 480 nm)	TPDQ Yield (mM) (%)
Cyclic Voltammetry	GCE	Pt	-3 to 3 V	---	---
			-3 to 0 V	0.02936	0.00071 (0.0142%)
			0 to 3 V	---	---
	Pt	Pt	-3 to 3 V	---	----
			-3 to 0 V	0.1251	0.0032 (0.0640%)
			0 to 3 V	----	----
	GCE	GCE	-3 to 3 V	0.1654	0.00401 (0.0802%)
			-3 to 0 V	0.1795	0.00435 (0.087%)
			0 to 3 V	0.1348	0.00326 (0.0652%)

When TPDQ was first synthesized in 1900 with PbO_2 *via* chemical oxidation, the minor product formed was 2,6-diphenyl-*p*-benzo-quinone (2,6-DPPQ)[68,82]. To confirm if 2,6-DPPQ was formed during chemical or electrochemical oxidation of DPP, the reactions were also monitored by GC-MS (Appx II 2.21-33). In addition to the major

TPDQ product, the minor chemical oxidation product, 2,6-DPPQ, was also observed by GC-MS (Figure 2.8). Notably, a significant amount of unreacted DPP was still present. Hence, the chemical oxidation of DPP yielded the *para, para* homodimer (TPDQ), major product, and the corresponding 2,6-DPPQ, minor product. Similarly, the GC-MS monitoring of electrochemical oxidation reaction (after 80 CV) (-3 to 3 V) yielded a significant amount of unreacted DPP and the formation of DPPQ, and no formation of TPDQ (due to lack of absorbance at 480 nm). Previously recorded electrochemically generated quinone analogues and derivatives absorbed in the 337-381 nm range[83]. Similarly, tyrosinase-catalyzed quinone oxidation with H_2O_2 addition yield an absorbance at 385 nm was associated with the generation of quinone derivatives[84]. Authors reported that the quinone derivatives are associated with the 350-400 nm range. However, in the -3 to 0 V range, the major product was the TPDQ (due to the presence of the absorbance band at 480 nm). According to the UV-vis data, it can be speculated that 2,6-DPPQ was generated regardless of the potential range used except at the positive potential range using the GCE/Pt pair. The products from the electrochemical oxidation of DPP were TPDQ (from radical dimerization), and 2,6-DPPQ (from solvolysis of the phenoxy-cation)[85]. The reaction selectivity observed with electrooxidation was dependent on the potential applied, as well as electrode material used. This was not possible with chemical oxidation.

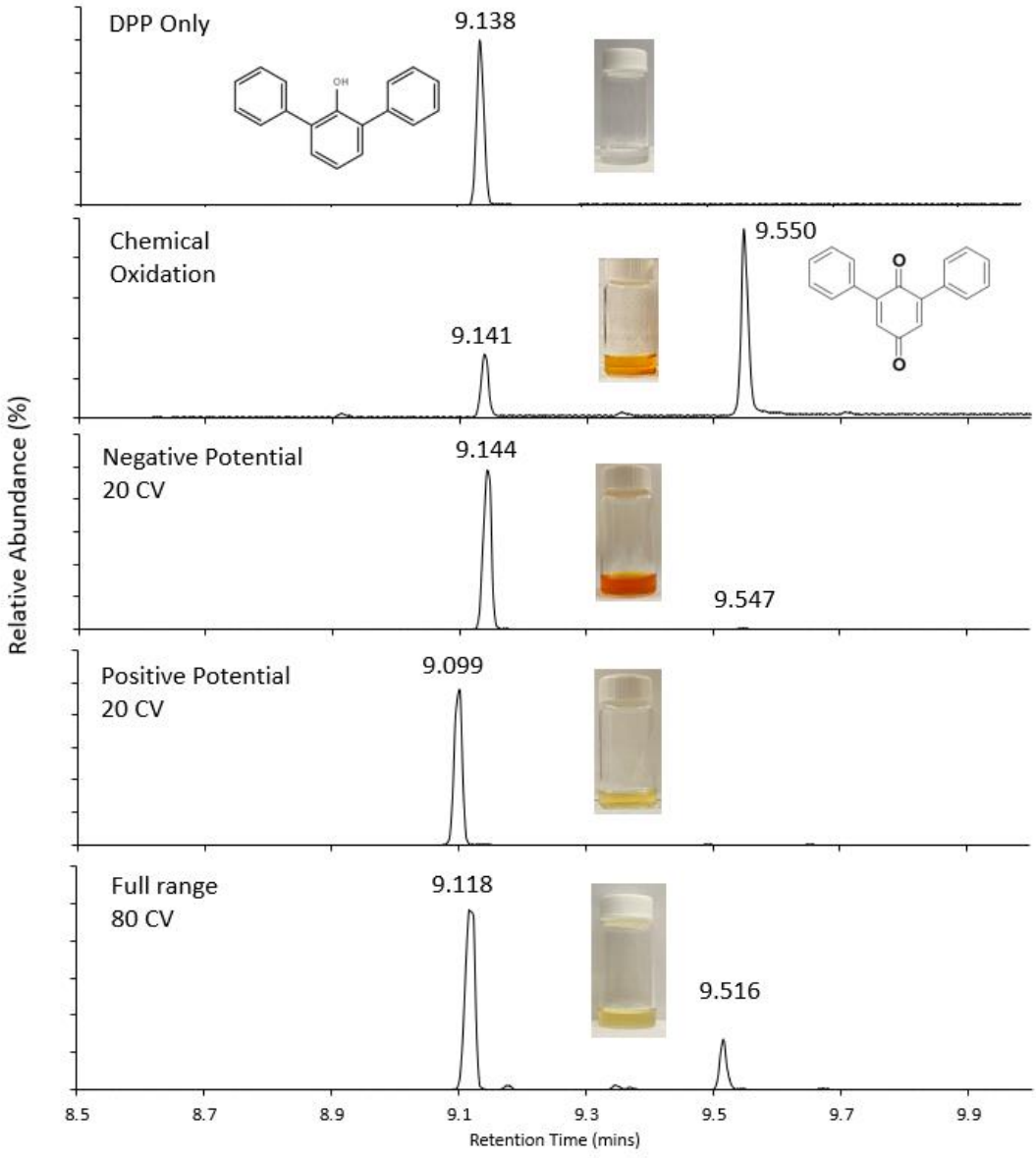

Figure 2.8. Normalized GC-MS of DPP only, chemical oxidation, electrooxidation with a -3 to 0 V and 0 to 3 V range after 20 CV (200 scans), and electrochemical oxidation after 80 CV at a -3 to 3 V range (800 scans) in ACN using working: GCE, counter: Pt, reference: $Ag/AgNO_3$.

The oxidation of phenols involves a one-electron oxidation to form a radical cation intermediate, followed by deprotonation to form a phenoxyl radical (Figure 2.9). It

is also likely that the proton loss to form a phenolate anion precedes one-electron oxidation to form a phenoxyl radical[22]. Once formed, the phenoxyl radical may undergo a variety of reactions depending on the number or type of substituents around the phenol ring. One type of reaction of interest is the dimerization of phenoxyl radicals and cations to produce a new C-C bond. 2,6-disubstituted phenols have been shown to have both the capability of polymerization and dimer formation[86]. 2,6-dimethylphenol with potassium ferricyanide and Cu(I) amine complex as a catalyst was shown to yield poly(2,6-dimethyl-1,4-phenyleneoxide) and poly(2,6-dimethyl-1,4-phenylene oxide)[87].

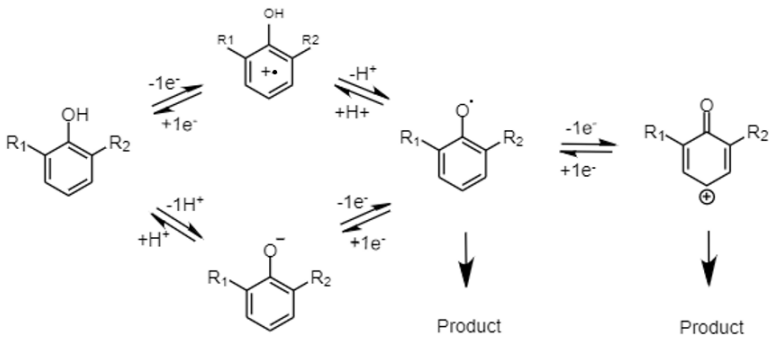

Figure 2.9. Proposed 2,6-disubstituted phenol oxidation pathways[22].

Upon oxidation of DPP, phenoxyl radicals may be formed which can undergo resonance and yield a radical at the *para* position. When formed, this radical can then react with another to form a new carbon-carbon bond within a homodimer. The homodimerization would lead to the formation of the dimer product (Figure 2.10) which may exist in a quinone or phenol form. The chemical oxidation of DPP into the dimer

product has been previously reported, however the equivalent electrochemical transformation has not been demonstrated yet[9,87].

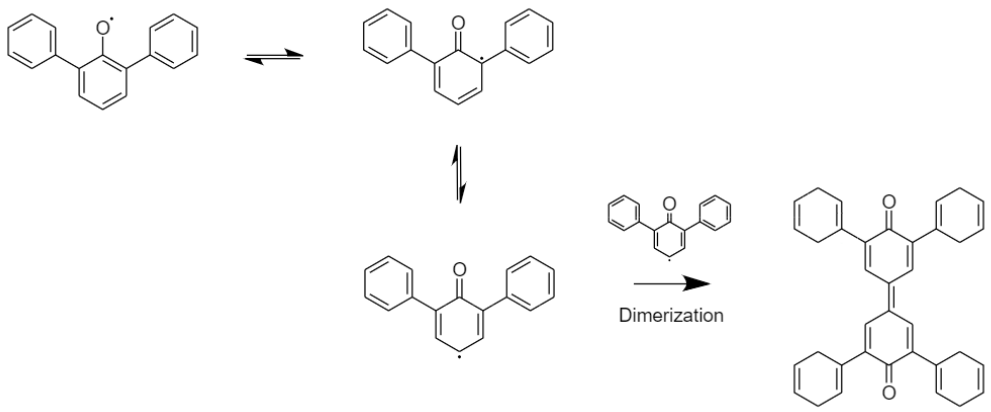

Figure 2.10. Proposed DPP radical formation, resonance contributors and oxidative dimerization pathway of DPP radical to produce a homodimer.

The overpotential (η) for a hydrogen evolution reaction (HER) for the GCE and Pt electrode materials are -1.13 V and -0.27 V, respectively. The overpotential for oxygen evolution reaction (OER) is only likely at Pt surface and is 1.11 V. Therefore, when a positive potential is applied the OER reaction is likely taking place as well as the oxidation of phenol at the Pt electrode. However, such an event is unlikely at the GCE surface. When a negative potential is applied, the oxidation of the phenolate anion at the GCE and Pt takes place; however, so does the HER at both surfaces.

By carrying out anodic oxidation of DPP, the reaction selectivity and yields largely depend on anode materials[58,88]. It has been previously reported that the products,

mechanism and kinetics of electrode reaction may be highly dependent on the composition of the electrode material[88]. For example oxidative decarboxylation on Pt anode produced more products-from-radicals than products-from-cations, compared to the GCE electrode[89]. It was found that carbon anodes were more efficient than Pt anodes at removing a second electron to form a cation (with a proton loss)[27,58,73]. Hence, small differences may be extremely significant in determining the outcome of the reaction. If the anodic material is intimately involved in the reaction that takes place, then the following processes need to be considered. A reactant needs to adsorb onto the electrode surface, undergo electron transfer reaction/electrocatalysis and subsequently desorb off the surface back into the solution. Given the proximity of reactant with the electrode surface, it is also likely that reactant or intermediates may experience double layer effects. The organic radicals have a greater tendency to adsorb onto carbon surface compared to Pt surface due to the presence of paramagnetic centers in the material. It is then likely when the DPP radical is formed on the carbon electrode to undergo more efficient carbon-carbon oxidative dimerization. In addition, when the DPP radical is formed at the carbon electrode surface, it is also possible for further oxidation into a carbocation which is repelled from the surface, but perfectly suited to react with nucleophiles such as water molecules. In this case, the DPP carbocation may react with water to form 2,6-DPPQ. In addition, this would explain the formation of TPBD (Figure 2.11A), which is further oxidized during CV cycling into the corresponding quinone analogue (TPDQ). The water addition onto the phenoxyl radical is well known[90]. Being an electrophilic radical, the OH radical preferentially adds to the ortho-position on phenoxyl radical (~50%) or the *para*-position of phenoxyl radical (~40%). In the case of

the DPP phenoxyl radical, due to substitution at the ortho site, OH would likely add to the *para* site. In the presence of dioxygen, the 1,4-dihydroxycyclohexadienyl formed would likely react with oxygen to form hydroquinone analogues and ultimately 2,6-DPPQ[60].

By contrast, DPP radical formed on Pt surface are easily desorbed and participate in radical reactions readily, such as C-C dimerization to form TPBQ. The over-oxidations of DPP may lead to the formation of oligomers and polymers. However, if the electrode is only minimally involved in the reaction and serves solely as an electron sink or source (transferred *via* outer-sphere mechanisms) to the substrate, then the mechanisms of products formed, and selectivity should be independent of the electrode material. The stability of substrate, such as DPP, or its intermediates produced on the electrode is important for ensuring selectivity and high yields.

The nature of counter electrode may also influence reaction selectivity and yields. The oxidation of a substrate (carboxylic acid) at the anode was taking place during the cathodic generation of a base (which was critical for the deprotonation of carboxylic acid)[45]. Since the electrogenerated based was required for reaction, the Pt cathodic material (counter electrode) provided greatest yield than the GCE electrode, due to the lowest overpotential of Pt for proton reduction compared to GCE. Hence, lower potential difference between anode and cathode was necessary with Pt under constant current electrolysis conditions for synthesis of vinyl sulfones from cinnamic acid[45]. By keeping the potential difference small, the competing reduction process was minimized. In a similar fashion, the switch from carbon to Pt counter electrode in an electrochemical Hofmann rearrangement, produce more readily methoxide on the cathode and improved the yield[91]. Hence, by comparing the working/counter electrodes tested, the potential

difference between anodic oxidation event, such as phenol oxidation and overpotential of each electrode, it can be determined that the smaller potential difference is likely with Pt as a counter electrode compared to GCE as a counter electrode. Hence, when Pt was a CE, from the pro-base (residual water), electrogenerated hydroxyl anion (base) was generated which participated in the reaction with DPP radical or DPP cation to produce 2,6-DPPQ. It is also possible that an electrochemically generated base (hydroxyl anion) deprotonated DPP forms a DPP phenolate, which is further oxidized to a phenoxyl radical and undergoes C-C dimerization. At GCE, the oxidation process may produce a high density of surface carboxyl groups, and arene radicals readily combine with the graphitic electrodes[76,92].

During CV measurements, the potential is applied to an electrode in solution, which results in ordering process to form a structure of oppositely charged ions and solvent molecules at the surface, which is known as the Helmholtz double layer. This layer determined the potential distribution close to the surface and the uniformity of current. This layer also influences the local driving force for electron transfer reactions, which determine the kinetics of electron transfer. If radical and cation formation occurs within the Helmholtz double layer, product selectivity can be enhanced. Upon applied potential, the solvent, and protons are allowed to form on the surface, and participate in reactions. The solvent molecules, such as residual water molecules, may easily react with a DPP radical or a DPP cation to form undesired products, such as 2,6-DPPQ, rather than TPDQ. Upon applied potential when the double layer is formed, the solvent (such as water) may be excluded, and reactions to form 2,6-DPPQ is minimized, while allowing for radical dimerization to form TPDQ in greater yield. If the DPP radical cation is

formed then the water will attack at the 4-position, resulting in the minor product (and ultimately 2,6-DPPQ). Upon electrooxidation, the phenoxy radicals are produced and may undergo several reaction pathways. Firstly, radicals may polymerize into a passivating film on the electrode surface[93]. The polymeric products are formed *via* C–C coupling or ether linkages between phenoxyl radicals, and the polymerization process is usually influenced by the substituent type and number[91]. The second possible reaction pathway is formation of the hydroquinone-liked substances, such as hydroquinone and 1,4-benzoquinone[62,68,94]. Examples of using various anode materials in the cross-coupling reactions have been reported, such as oxidation of phenols and arenes[36]. When a carbon electrode was used for phenol oxidation, only homo-coupled product was observed and not cross-coupled. However, Pt and BDD resulted in a major formation of cross-coupled products compared to GCE[33,55].

The formation of TPDQ in solution is driven by the oxidation of OH functional groups into a phenolate anion. It is likely that the negative potential range favours the formation of the phenolate anion indicated by the E_{pa} at ~-0.5 V[23]. The formation of non-coordinate phenolate anion has been successfully characterized *via* cyclic voltammetry, and was shown to be redox active between -1.25 V to 1.25 V. This suggests that the phenoxyl radical was more likely to be formed from the deprotonation of the phenolate anion in the negative range[24].

Several factors can reduce DPP dimerization, such as irreversible binding and decomposition on the surface, both of which reduce mass balance and yields. If the substrate undergoes adsorption onto electrode, and electrode fouling or grafting takes place, the film formation is likely. Hence, the reagents, intermediates or products will not

desorb off the surface and go back into the solution. If any organics passivate the electrode surface it will result in the formation of an insulating layer and in turn decreased electrode activity and yield. The electrode passivation can be detected by CV and observing the current decrease with each cycle. The electrode passivation is likely at oxide films on metals when high anodic potentials are applied. The formation of insoluble oxidation products may also lead to electrode passivation. The electropolymerization deposited on electrode surface due to anodic oxidation of phenol and *m*-cresol will also lead to electrode fouling[66]. There are several ways to mitigate negative effects of fouling which include electrode material modifications, pulse electrolysis, sonication, alternating the polarity of the electrode, additives, or use of mediators to shuttle redox active species from the bulk phase to electrode surface.

In summary, electrochemical oxidation of DPP yielded two products and 3,3',5,5'-tetraphenyldiphenoquinone (Figure 2.11) depending on the applied potential and electrode surface used, and that TPDQ converts over time into TPBD. By contrast, chemical oxidation produced a major product and a minor product. While the higher yields were observed with chemical oxidation for the dimer, electrochemical oxidation allowed for selectivity of product formation.

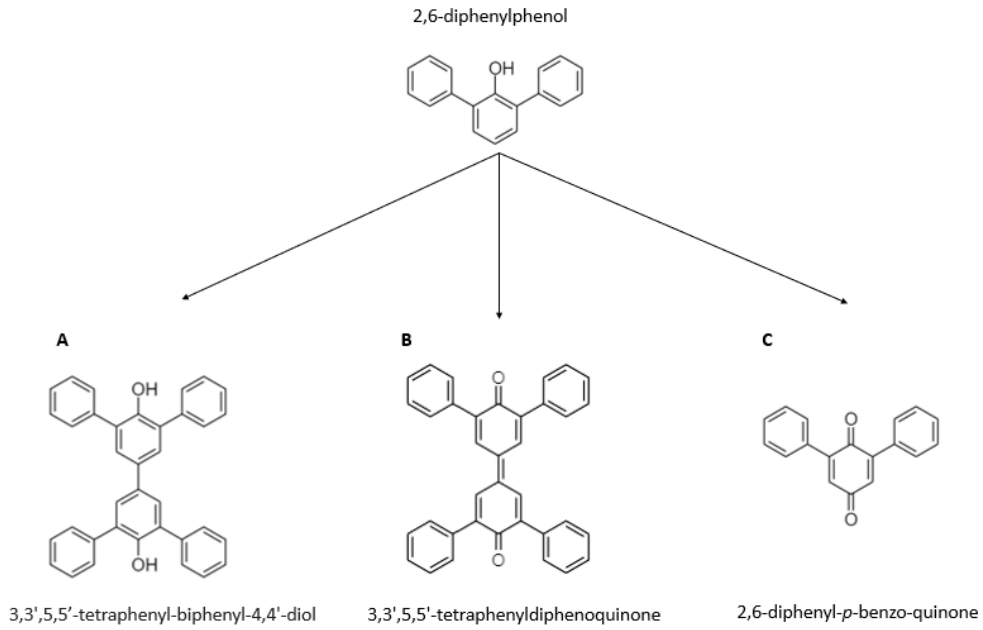

Figure 2.11. Structure of DPP and the proposed DPP-based C-C dimers and other products.

2.4. Conclusions

Electrochemical oxidation and chemical oxidation of 2,6-diphenylphenol (DPP) were achieved. Electrooxidation of DPP exhibited product selectivity and high reaction yield of TPDQ depending on the electrode pair and potential range selected. GCE/GCE electrode pair exhibited the highest yield. While chemical oxidation resulted in a higher dimer yield, it did not allow for selectivity and lack of reaction diversity. The negative potential range always produced TDPQ regardless of electrode materials as it likely favours the formation of the phenolate anion in the reaction pathway. Products formed at 390 nm are likely a crude mixture of 2,6-DPPQ and TPBD. The chemical oxidation of DPP yielded a TPDQ crystal product that was successfully characterized using single molecule XRD, NMR, and UV-vis spectroscopy. With an absorbance at 480 nm, isolated

TPDQ was able to serve as a standard compound in all UV-vis experiments. This chapter indicates that electrochemical methodologies may be used for the formation of *para,para* C-C homodimerization of substituted phenols, and on demand reaction selectivity, compared to chemical oxidation.

Chapter 3 – Electrochemical versus chemical oxidation of 2,2-dihydroxybiphenol

3.1. Introduction

2,2-dihyroxybipheneol (DHBP) is a compound that is one of three isomers of biphenol. Industrially, it serves as a precursor material for the formation of diphosphite ligands, which participates in hydroformylation with a rhodium catalyst[95].This compound has been mainly analyzed for its polymeric potential through chemical oxidation as well as electrooxidation due to the nucleophilic groups on either side of the structure. To optimize the reaction and to yield a longer polymer, copper(II) complexes based on the Schiff base monomer/polymer have been used as a catalyst and hydrogen peroxide as the oxidant for the oxidative polymerization of DHBP[15]. The reaction can yield either a polymer with repeating units on the oxygen through ether linkage, or at the *meta* position (Figure 3.1). Furthermore, optimal reaction conditions were dependent on the reaction time, pH, temperature, and the amount of catalyst and oxidant. The precipitated polymer was determined to be a black amorphous material, a characteristic that can be beneficial in morphology analysis.

Synthesis of tin(II) derivatives containing substituted aromatic 1,2-diols, and of 2,2'-dihydroxybiphenol has been reported using anodic oxidation[96]. In addition, electrooxidation of the isomer, 4,4-biphenol has been reported to form 4,4′-diphenoquinone in a two-electron process[97]. It is of interest given the synthetic benefits of this methodology compared to traditional organic synthesis.

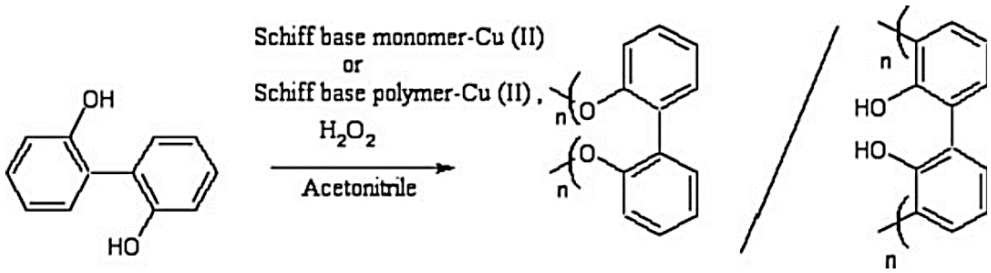

Figure 3.1. Scheme of the chemical polymerization of DHBP[15].

This chapter will focus on the electrochemical oxidation and chemical reaction oxidation of DHBP. Products formed from both reaction types will be monitored and characterized using UV-vis spectroscopy and gas chromatography-mass spectrometry. Based on the literature, it can be expected that through both techniques, polymerization will occur, rather than C-C dimerization given the structure of DHBP.

3.2. Materials and Reagents

DHBP (99%) and tetrabutylammonium perchlorate were from Alfa Aesar and HPLC-grade acetonitrile solvent was from Honeywell at 99.9% purity. Copper perchlorate was purchased from Alfa Aesar for chemical oxidation experiments.

3.3. Electrochemical Measurements

Electrochemical measurements were performed using Autolab PGSTAT302N potentionstat by Metrohm AG. The solutions containing 10 mM DHBP and 0.1 M TBAP in 3 mL acetonitrile were prepared for all reactions unless stated otherwise. The working electrode was the GCE, the reference electrode was an Ag/Ag_+ 10 mM silver nitrate

($Ag/AgNO_3$), and the counter was a platinum wire unless otherwise mentioned. Cyclic voltammetry was performed at 100 mV/s scan rate, unless otherwise specified, and potential ranges: -3 to 3 V, -3 to 0 V, and 0 to 3 V. For each CV, 10 scans were performed.

UV-vis Spectroscopy

Spectroscopic measurements were performed using the Agilent Cary 60 UV-vis spectrophotometer, 1 cm quartz cuvette and 200 - 800 nm wavelength range.

FTIR

The FT-IR instrument used was the ThermoScientific Nicolet 380 spectrophotometer.

GC-MS

The Agilent 7890B GC with the HP-5MS UI column and a 5977A MSD was used for reaction monitoring (method parameters can be found in Appx II 2.32)

TEM Imaging

The Hitachi TEM H7500 MegaView III was used for all TEM images (in collaboration with Meera Patel and Dr. Ruby Sullan at the University of Toronto Scarborough). Formvar coated copper grids were used, and samples were diluted with MilliQ water.

3.4. Results and Discussion

3.4.1. Electrochemical characterization of DHBP

The electrochemical characterization of DHBP was performed as a function of CV cycling (1 CV (reaction time = 10 min) or 20 CVs (reaction time = ~7 h); each CV with 10 scans). The CV of DHBP (Figure 3.2A) displayed two oxidation peaks and one reduction peak. The observed anodic peaks at 0.3 V and ~1.5 V, indicated irreversible oxidation of a DHBP phenolate and phenol, respectively, and cathodic peak at -1.0 V was highly stable, with minimal electrochemical change even after 20 CV (Figure 3.2B). The lack of CV change indicated no electropolymerization on the GCE surface. Typical electropolymerization of phenolic compounds on the electrode surface is characterized by an increase in CV upon scanning.

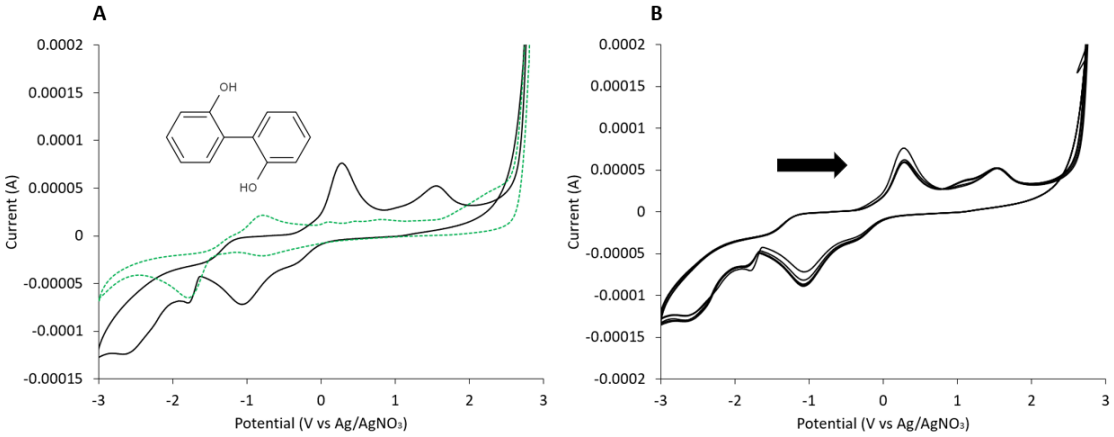

Figure 3.2. Cyclic voltammograms of DHBP as a function of CV ([DPP] = 20 mM, [TBAP] = 0.1 M, ACN, 10 scans per CV). (A) Initial scan at 1st CV (1 CV) overlaid with ACN blank with TBAP only (green-dotted) and (B) all 1-20 CVs. Scan direction indicated by arrow.

E_{pa} of 0.3 V can be attributed to the oxidation of the hydroxyl groups of DHBP. Oxidation of the isomer 4,4'-biphenol yield an E_{pa} of ~0.3 V, associated with oxidation of 4,4'-biphenol to 4,4'-diphenoquinone[97]. This process can be described as a two-electron/two proton oxidation and deprotonation[98]. In addition, the electrooxidation of poly(2,2-dihydroxybiphenol) (PDHBP) with tetrabutylammonium hexafluorophosphate as the electrolyte (i.e. NBu_4PF_6) had undergone cyclic voltammetry, proposing that product undergoes the mechanism shown in Figure 3.3[15]. PHDBP polymer undergoes a two-electron/two proton oxidation and deprotonation to form ketone functional groups, further oxidation would yield a coupling between the oxidized PDHBP and a radical anion complex (Figure 3.3). The one-electron reduction potential of the phenoxyl radicals of DHBP were determined to be 1.00 V vs NHE[99]. Similarly, the E_{pa} at 0.3 V can be ascribed to the phenoxyl radical potential.

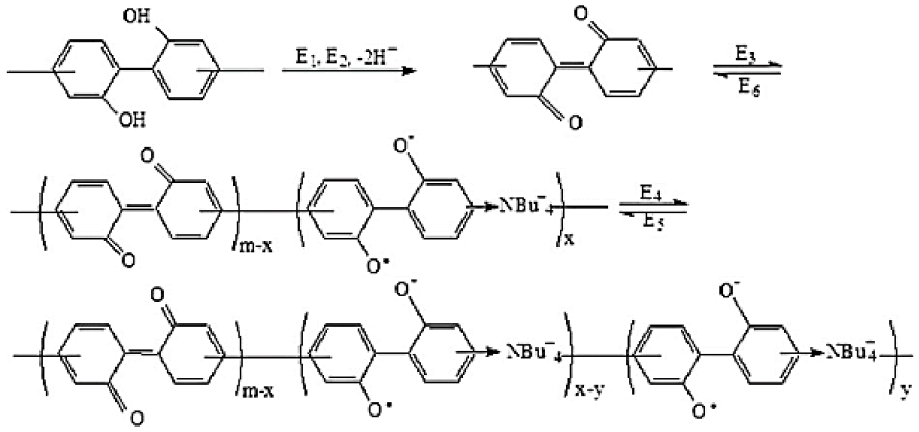

Figure 3.3. Scheme of the electrooxidation of PDHBP[15].

Furthermore, the cycling of DHBP during electrochemical experiments resulted in a dark yellow film that formed on the surface of the GCE. It has been reported that the oxidation of phenol on a stainless-steel electrode exhibited a yellow-brown film after the first CV scan that was due to polyphenol formation[100]. The higher the concentration of DHBP, the visibly thicker the film. Film formation of chlorophenols has been previously recorded as the adsorption of product or analyte on the GCE surface[101]. Exceeding the solubility of the polymer may cause it to adsorb onto the surface, leading to passivation[18]. Also known as electrode fouling, an impermeable layer is formed on the surface of the electrode due to a fouling species. Previous work has indicated that passivation is more likely to occur with substituted phenols rather than non-substituted phenols[66]. An increase in phenol concentration was observed to cause faster deactivation of the electrode surface due to phenol radicals involved in electro polymerization processes[102]. Moreover, electrode fouling by the phenolic oxidation products is more susceptible at higher concentrations. Hence, decrease in UV-vis absorbance at higher concentrations of DHBP likely due to increased electrode fouling.

The electrooxidation of 4,4-biphenol to form 4,4′-diphenoquinone resulted in a quasi-reversible reaction, which was attributed to the adsorption onto the GCE surface[97]. the electrocatalytic oxidation of glutathione and N-acetylcysteine was also carried out using 4,4′-biphenol as a mediator showing that it has good catalytic behavior towards the oxidation of glutathione and N-acetylcysteine, that can be potentially extended towards other solutions and reactions[98].

3.4.2. Spectroscopic Characterization of DHBP Electrooxidation

The electrochemical oxidation reaction was monitored by UV-vis spectroscopy, due to colour changes. UV-vis spectra were collected after every CV experiment to monitor changes as they are indicative of new product formation and yield. In the 200-800 nm range, DHBP did not absorb. After 5 CV (reaction time = ~50 min), there was a visible colour change from clear and colourless to a pale-yellow solution that absorbs at approximately 390 nm. To improve yield, longer reaction times (up to 20 CV) were performed and exhibited absorbance at ~0.2 a.u. (arbitrary units). An increase in CV scanning exhibited an increase in absorbance (Figure 3.4A), hence a linear relationship. Similarly, a concentration-dependent analysis was also performed to evaluate the effect of concentration on product yield. A 390 nm band was also formed across all concentrations used (0.5, 1, 5, 10, 20 mM at 20 CVs). The notable higher absorbance obtained from using 5 mM DHBP is likely attributed to minimal electrode fouling. An increase in concentration will result in increased passivation of the electrode surface and a decrease in absorbance. Lower concentration of DHBP enables higher solution concentration due to minimal passivation on the surface. Therefore, the accumulation of insoluble product at the GCE surface prevented DHBP molecules from interacting.

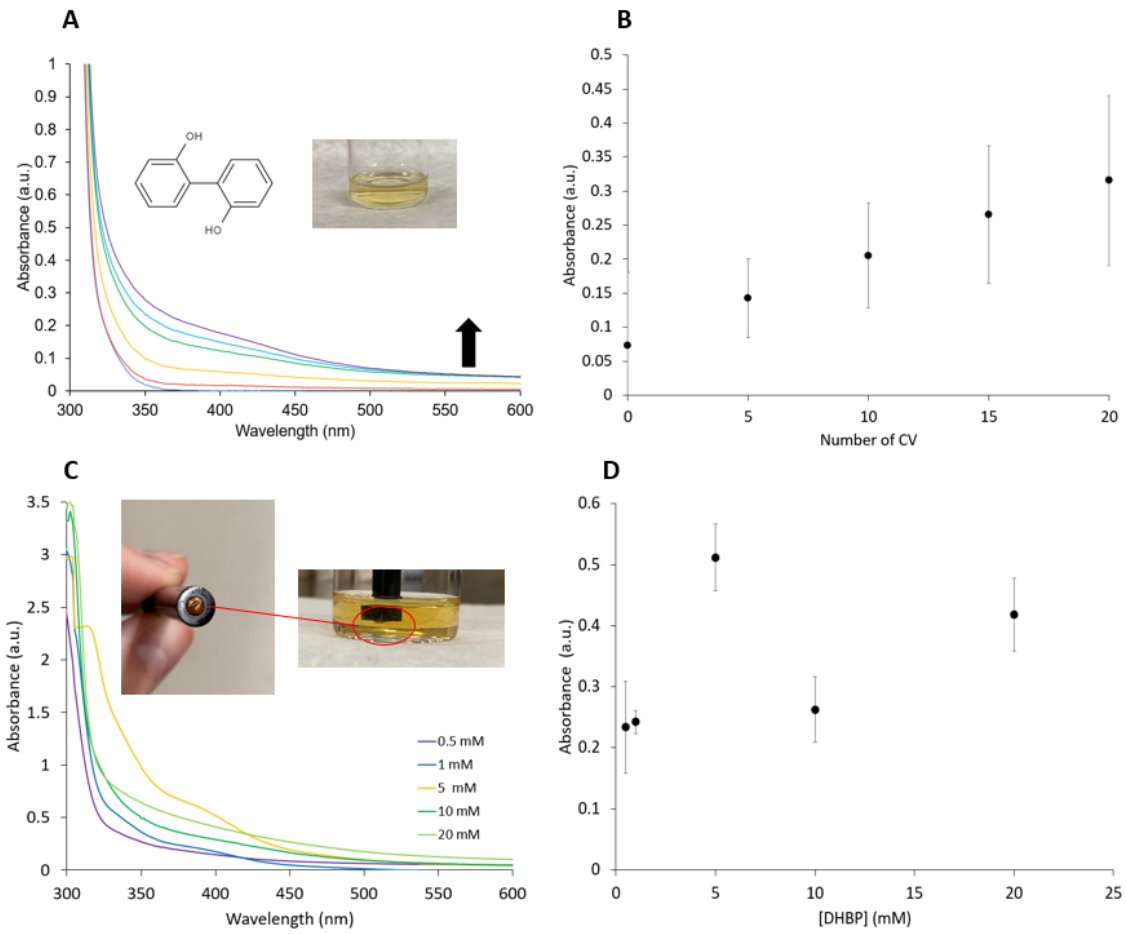

Figure 3.4. (A) UV-vis of CV-dependent analysis of DHBP using electrooxidation at 0, 1, 5, 10, 15 and 20 CVs. [DHBP] = 10 mM, [TBAP] = 0.1 M TBAP, 3 mL ACN (B) triplicates of CV-dependent analysis with standard deviation (C) UV-vis spectra of concentration-dependent analysis of DHBP, [DHBP] = 0.5, 1, 5, 10, 20 mM, [TBAP] = 0.1 M, 3 mL ACN at 20 CVs (D) triplicates of concentration-dependent analysis with standard deviation.

To investigate the effect of potential ranges on DHBP, -3 to 0 V and 0 to 3 V ranges were used. The positive potential range exhibited product reaction at the GCE surface as well as the Pt surface. Both positive and negative potential ranges yielded a shoulder peak at ~390 nm, with yields at ~0.25 a.u. and 0.05 a.u., respectively. The

positive potential range at 20 CVs yielded a product like that of the full range (~0.2 a.u.). The product yield obtained with -3 to 0 V (20 CVs) produced much less product at ~0.05 a.u. compared to product formation at -3 to 3 V and 0 to 3 V.

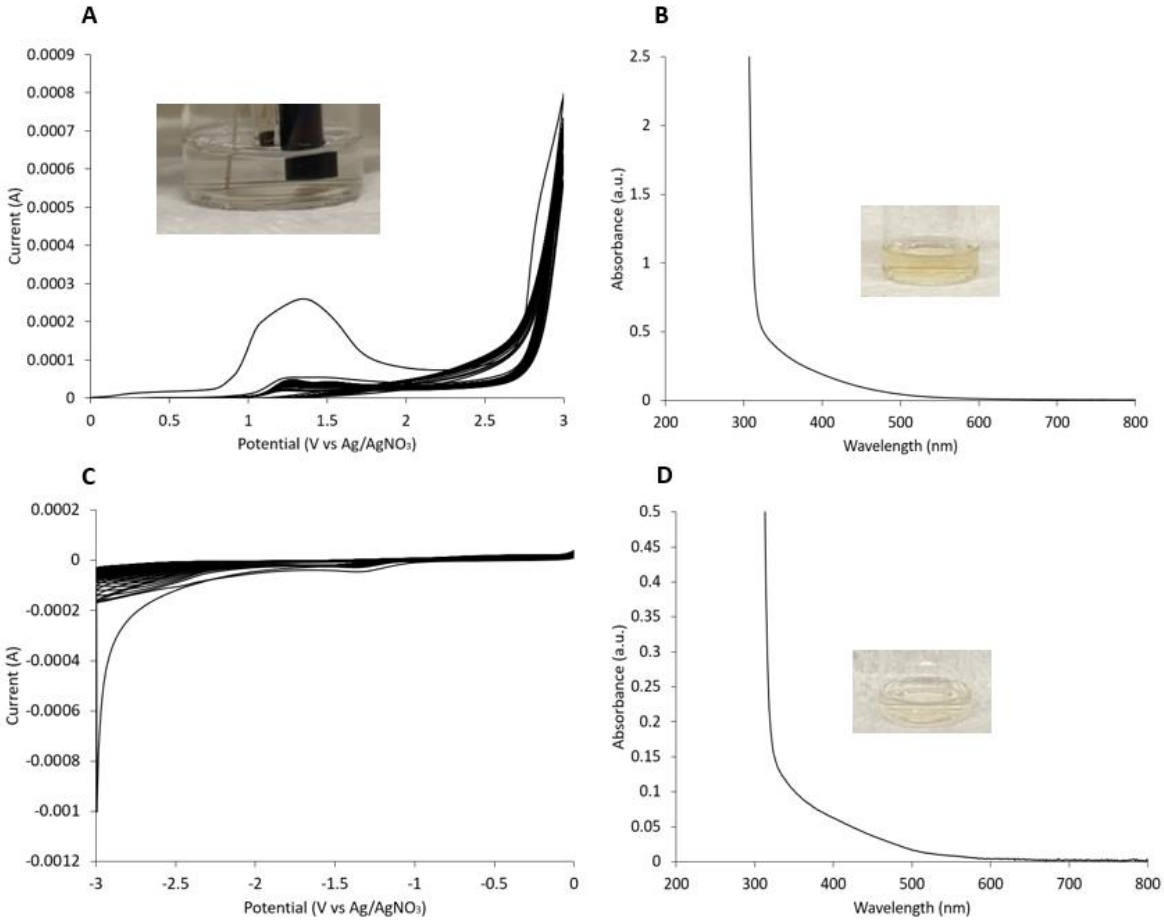

Figure 3.5. 20 CV of 10 mM DHBP and 0.1 M TBAP in ACN at various potential ranges (200 scans = 20 CV) (A) 0 to 3 V (B) UV-vis spectra of non-diluted DHBP post electrochemical reaction at positive range. (C) -3 to 0 V (D) respective UV-vis spectra.

The electrooxidation of DHBP in the positive potential range yields a major E_{pa} peak at ~1.35 V at the first scan, before drastically decreasing in current for subsequent scans. This observation can be attributed to the depletion of DHBP. This behaviour was

also recorded as oxidation of the DHBP units of the PDHBP polymer[15]. Hence, the initial scan can be attributed to the mass oxidation of the OH group of DHBP. It is also possible that decrease in current upon CV scanning may indicate electrode fouling. Electrooxidation *via* the 0 to 3 V range has shown a positive outcome for optimizing the reaction due to the higher yield and drastic shifts in the potential. However, in the negative range, there are no obvious anodic peaks. A small cathodic peak can be seen at ~-1.4 V. Hence, in the absence of phenolate or phenol oxidation, almost no coloured products were formed.

So far, electrochemical oxidation of DHBP resulted in a formation of products, which were soluble in ACN and insoluble in reaction solvent. The insoluble product formed on the electrode surface under experimental conditions used, did not yield enough solid product for additional characterization. However, the suspension (including soluble and insoluble product) after electrooxidation was submitted for analysis by TEM imaging (in collaboration with Dr. Ruby Sullan in University of Toronto Scarborough). The TEM results showed no polymer formation, and the tiny crystal-like structures were due to the TEM grid anomaly, as these were observed in other unrelated TEMs (Figure 3.6). Due to a limited sample amount the dynamic light scattering (DLS) analysis was not possible.

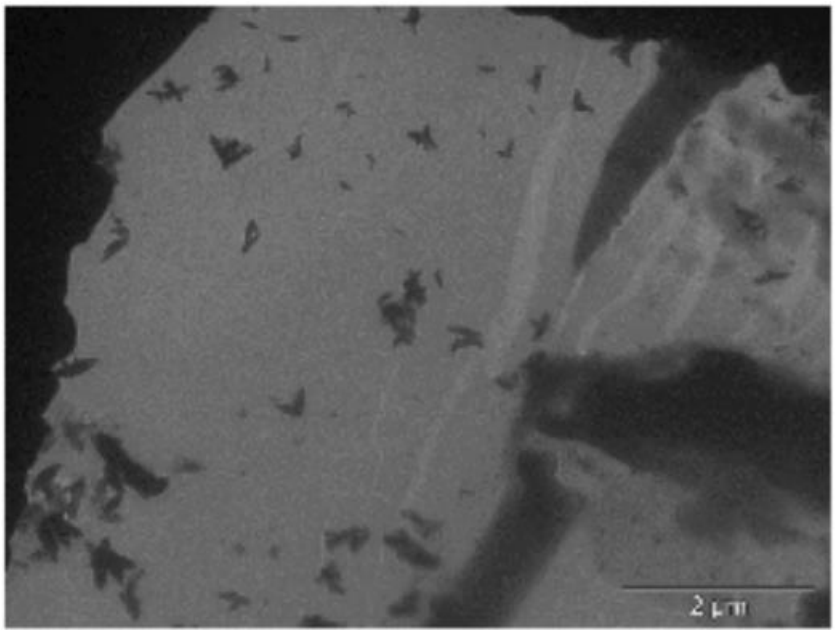

Figure 3.6. TEM image of insoluble film at GCE surface provided by Dr. Ruby Sullan Lab at the University of Toronto Scarborough.

3.4.3. Chemical Oxidation of DHBP

To further understand product formation from electrooxidation of DHBP, the chemical oxidation of 10 mM DHBP with 10 mM copper perchlorate in 3 mL CAN was performed. Upon addition of the oxidizing agent, the solution exhibited a drastic colour change from clear and colourless to a dark brown (Figure 3.7). *Via* chemical oxidation, a clear absorbance band at ~400 nm appeared. This contrasted with electrochemical oxidation which exhibited broad absorbance upon CV cycling. After 24 h, the solution transformed into a clear and light brown solution, with visible brown precipitate in the solution. The supernatant was measured, and an indiscernible broad peak was observed. Non-fluorescent dopamine exhibited no absorbance in water, whereas fluorescent

polydopamine yield broad band absorbance between 340 to 480 nm[103]. The chemical oxidation of DHBP with copper perchlorate was diluted 100x for UV-vis measurement (Figure 3.7) and an absorbance band appears at ~400 nm. Likewise, the electrooxidation of DHBP at the full range (-3 to 3 V) exhibited a shoulder band at ~390 nm. Despite, the identical absorbance, there is a drastic difference in colour, as the chemical oxidation solution yielded a dark brown versus the yellow solution obtained *via* electrooxidation. The coloured insoluble film was also noted to be yellow, in contrast to the dark insoluble product formed during chemical oxidation, which suggests that the two methods yield different products.

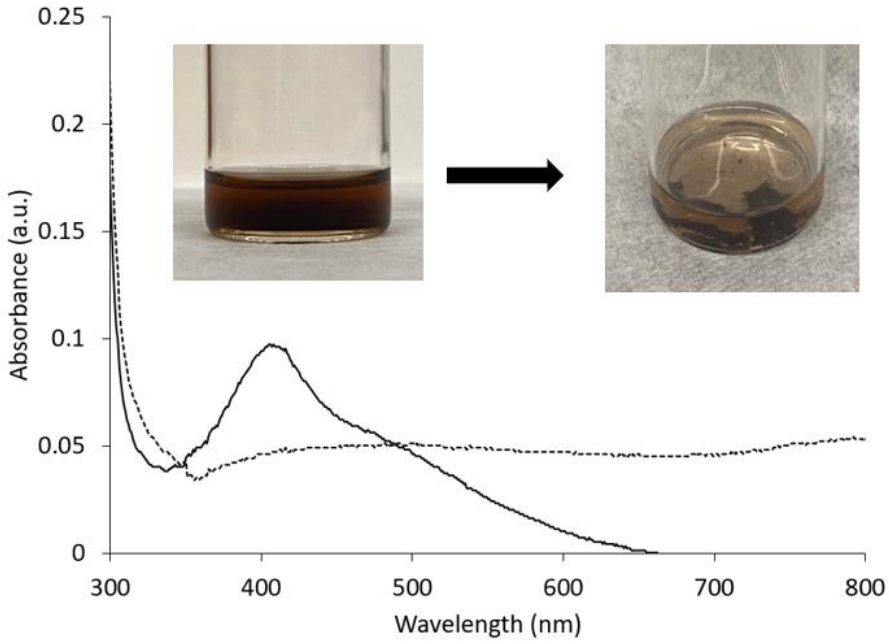

Figure 3.7. UV-vis spectra of the chemical oxidation of 10 mM DHBP and 10 mM copper perchlorate in ACN. Solid line: 100x dilution of the solution, dotted line: 24h after addition of copper perchlorate (measurement of liquid sample only). Inset: Formation of amorphous material after 24 h.

The material was obtained from the chemical oxidation reaction was isolated for FT-IR analysis (Figure 3.8). 24 h after chemical oxidation, a layer of dark product forms at the base of the vial, any physical disturbance or slight agitation to the reaction vessel resulted in clumping. This may be due to the weak interactions between the polymeric units. FT-IR analysis of the brown solid precipitate yields a broad vibrational band at 3551.42 cm^{-1} due to intermolecular bonding, consistent with an O-H stretch. The drastic difference in the IR band at 3351.42 cm^{-1} was due to extensive phenolic content in the polymer and increase in hydrogen bonding in the chain. In contrast to DHBP only, the OH band was significantly less intense (Figure 3.9). 1648 cm^{-1} is likely the C=O stretch from a carbonyl group. The 1095 cm^{-1} band was likely attributed to the C-O stretch from alcohol group during the formation of the polymer. Similarly, PDHBP was also observed to have a broad OH vibrational band at 3259 cm^{-1}, suggesting polymer composing of a mixture of phenylene and oxyphenylene units[15]. Different films produced by chemical oxidation of *p*-cresol, *o,o'*-biphenol and phenol[104]. The increased presence of hydroxyl groups suggests a decrease in the formation of ether linkages and minimal polymer formation[104]. The appearance of an intense carbonyl peak suggests the formation of a new quinone moiety, consistent with the oxidation of an OH group to form a carbonyl and was indicative of polymer formation[66]. Thus, the IR data suggests that a polymeric product was formed and chemical transformation of DHBP (Figure 3.10). It was previously described that the chemical oxidation of DHBP with copper(II) complexes based on Schiff base monomer/polymer as catalysts produced an amorphous black solid, consistent with the dark precipitate obtained experimentally[15]. Various experimental conditions such

as temperature or catalyst concentration (if used) can affect the molecular weight outcome and yield as previously observed[15,105].

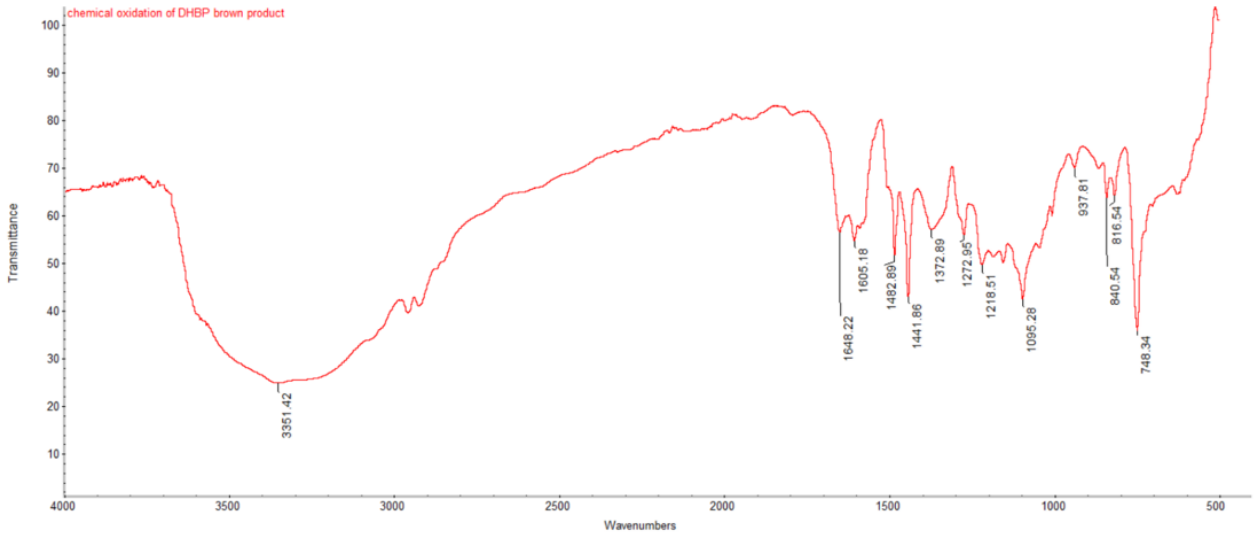

Figure 3.8. FT-IR spectrum of brown precipitate from chemical oxidation DHBP with copper perchlorate in acetonitrile.

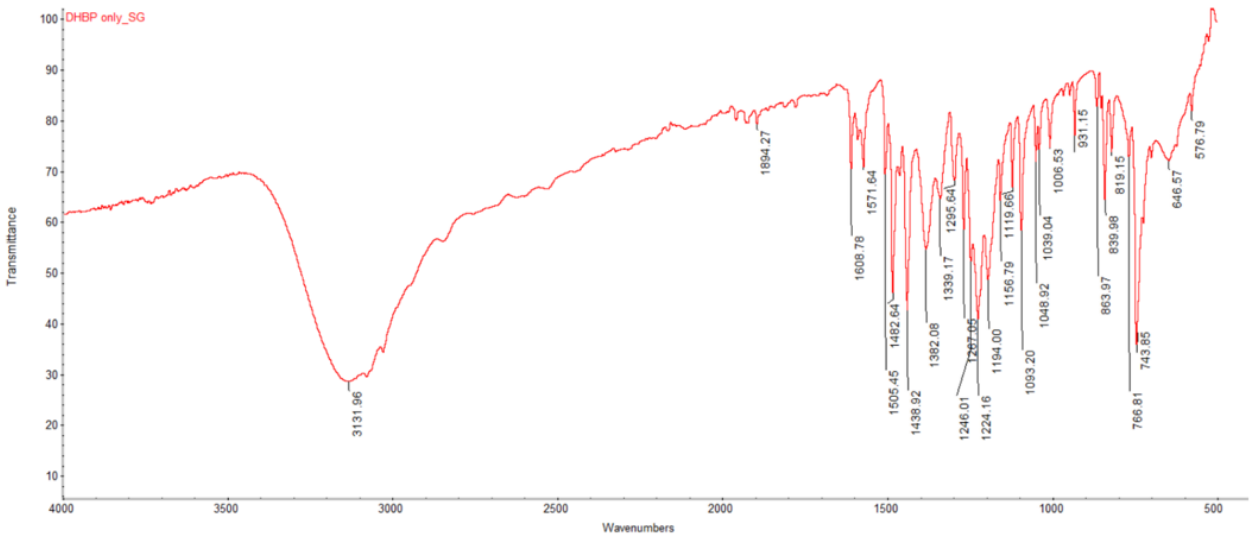

Figure 3.9. FT-IR spectrum of DHBP.

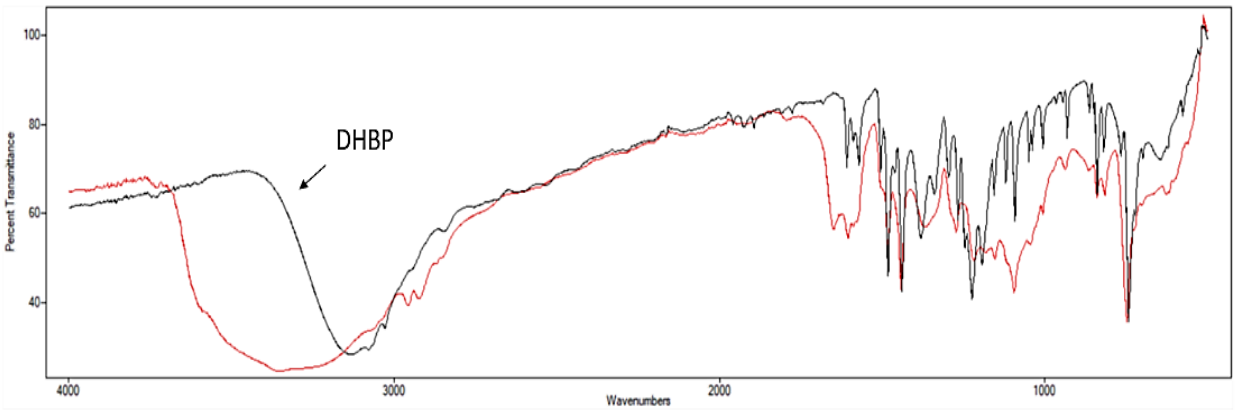

Figure 3.10. Superimposed FTIR spectra of: DHBP (black); brown precipitate obtained from chemical oxidation of DHBP (red).

As mentioned in chapter 2, 2,6-disubstituted phenols are likely to undergo one-electron oxidation and deprotonation (or *vice versa*) to form a hydroxyl radical that undergoes dimerization[22]. Oxidation of DHBP can either generate a dimer from radical-radical coupling and terminate, or further propagate to polymerize due to the two OH sites. Past work has suggested that the reaction favours dimerization due to the lower bond dissociation energy, compared to 4,4-dihydroxyniphenol[106]. The strong substituent effects expressed by 4,4-dihydroxyniphenol expresses a degree of planarity for the radical anion, with planarity being a necessity for resonance stabilization[99]. The stabilizing effect of the intramolecular hydrogen bond found in monoprotonated DHBP can be attributed for the increase in one-electron reduction potential brought on by the OH group in the ortho position[99]. Various oxidizing agents can affect the phenoxyl radical stability as well, such as potassium hydroxide and lead oxide, and can affect its ability to undergo further chemical transformations[8,10]. The oxidation of 2,6-di-*tert*-butyl-4-methylphenol produces a less stable phenoxyl radical, and can generate multiple products[107]. Here, the DHBP phenoxyl radical was likely inhibited from forming a stabilizing planar structure as a result of steric hindrance[99]. Hence the yield of the electrochemical oxidation product, including the type of products formed, can be affected by the type of oxidation method chosen.

The reaction was monitored by GC-MS as well. The electrochemical oxidation reaction of DHBP was also analyzed using GC-MS to ascertain the structures formed (Figure 3.11). The solutions obtained from the electrooxidation of DHBP in the negative range (-3 to 0 V), positive range (0 - 3 V), full range (-3 to 3 V), and the chemical oxidation of DHBP were subject to GC-MS analysis (Figure 3.11) The results exhibited a

large amount of unreacted DHBP in the solution with no major product formation. GC and MS traces can be found in the appendix (Appx III 3.1-8). If polymerization did occur during the reaction, DHBP monomers or polymers would not appear in the chromatogram due to high molecular weight. A small peak can be observed in the DHBP chromatogram and solution obtained at -3 to 0 V and 0 to 3 V range, at ~ 7.6 min. This was likely an impurity of the DHBP solid material due to not being 100% purity and was also observed in a chromatogram containing DHBP only. A small peak can also be observed at ~5.5 min at the 0 to 3 V, -3 to 0 V range that was likely a small oxidation product of DHBP, and hence yellow solution colour. The chemical oxidation solution also exhibited an identical peak at 5.443 min, indicating that chemical oxidation can generate similar small oxidation products. Overall, the yellow solution colour changes upon electrochemical oxidation are likely due to formation of a low yield of a variety of soluble products.

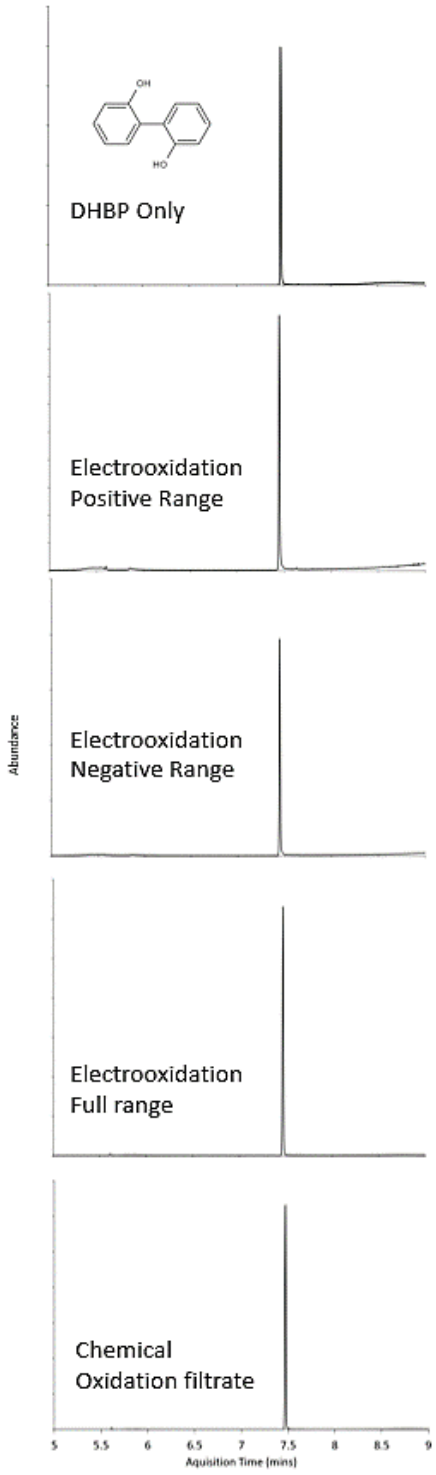

Figure 3.11. Stacked GC-MS spectra of various solutions: DHBP only, electrooxidation (0 to 3 V range), electrooxidation (-3 to 0 V range), electrooxidation (full range) and chemical oxidation of DHBP.

3.4.3.1. Solubility testing

The brown precipitate from the chemical oxidation of DHBP with copper perchlorate was dried and tested with various solvents for solubility characterization.

Out of the solvents tested, the solid was mostly soluble in DMSO and isopropyl alcohol and partially soluble in DMF. There was no direct link between the dielectric constant and the solubility of the product. However, PDHBP has been known to be soluble in DMSO and has been successfully dissolved for characterization using NMR[15]. Given the functional groups of the solid material, as determined *via* IR (OH group, C=O), it was proposed that the polymer was soluble in solvents that can hydrogen bond. Solubility studies show that product was not soluble in methanol and was soluble in isopropyl alcohol.

Table 3.1. Solubility of brown product using various solvents (~ 0.2mg in ~3 mL solvent).

Solvent	**Dielectric constant**	**Solubility**
Water	80.1	No
DMSO	46.68	Yes (cloudy)
Acetonitrile	37.5	Insoluble
DMF	36.71	Partially soluble
Methanol	32.70	No
Isopropyl alcohol	19.92	Yes (cloudy)
Chloroform	4.81	No

The reaction mixture containing insoluble and soluble products were also further analyzed using transmission electron microscopy (TEM) by Meera Patel (in collaboration with Dr. Ruby Sullan Lab at University of Toronto Scarborough). A chemical oxidation solution containing insoluble product was analyzed using TEM imaging (Figure 3.12). The TEM image yielded particle, oligomeric and polymeric structures. Structures similar to DHBP, such as polydopamine, yielded similar spherical and oligomeric properties[103]. The worm-like structures are likely due to strong π-π interactions, as observed with polydopamine[108,109]. Hence, chemical oxidation of DHBP with copper perchlorate formed polymeric structures based on its morphology using TEM imaging. The worm-like

structures were not observed in TEM of the film generated on the electrode surface, suggesting that there was likely no polymer formation, or that concentration was too low for TEM analyses. Dynamic light scattering (DLS) analysis was also performed on insoluble products obtained *via* chemical oxidation and electrooxidation by the Sullan Lab by Meera Patel, but due to limited sample, the obtained molecular weights are not an accurate representation.

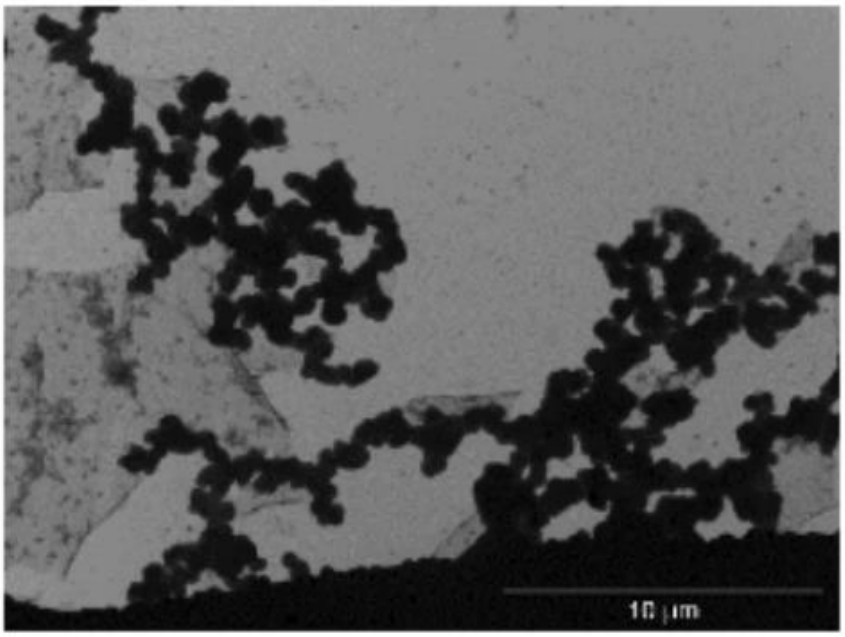

Figure 3.12. TEM image of supernatant obtained from the chemical oxidation of DHBP with copper perchlorate provided by Dr. Ruby Sullan Lab at the University of Toronto Scarborough.

3.5. Conclusion

In this chapter, DHBP was used as the starting material used in chemical oxidation and electrochemical oxidation. Clearly, the reaction products were highly dependent on the oxidation method used, as observed in the reaction color and the insoluble product formed following the reaction. For example, a bright yellow colour solution was observed following electrochemical oxidation compared to the dark brown color obtained in the chemical oxidation. Therefore, the products obtained are dissimilar based on the method used. In addition, the solid products formed by the two different methods, macroscopically, the morphology of the insoluble product obtained electrochemically was formed at the electrode surface as a dark yellow film. This contrasted with the black/brown solid that was formed through chemical oxidation which adopted spheric particle structure, alongside oligomeric and polymeric features.

Chapter 4 – Conclusions and Future Work

4.1. Conclusions

Phenols are used in industry as plastics, resins, and other materials, but are also persistent pollutants in the environment, therefore, there is a necessity to explore mitigation techniques and chemical recycling. One strategy to mitigate phenolic compounds is phenol oxidation, which has been done extensively over the years to understand the mechanism and electron transfer process, typically using strong oxidizing agents. Lack of selectivity, low yields, the use of strong chemicals, and waste production are some issues with the conventional chemical oxidation of phenols. Alternative approaches are therefore appealing, especially those that use greener technologies. The lack of selectivity alongside additional products being made can be a hindrance if there is only one product of interest. Electrochemical methods have been shown to have higher yield and product selectivity. By limiting large conversion of a material to a variety of products, electrochemical techniques can selectivity generate a product that can be isolated for further use, a feature that is normally not observed with traditional oxidation methods. Electrochemical oxidation reduces the need for additional chemicals for the reaction and reduces the number of steps required to obtain a particular reaction.

This thesis explored the products formed *via* chemical oxidation and electrochemical oxidation of bulky phenols: 2,6-diphenylphenol and 2,2-dihydroxybiphenol. DPP contains phenyl rings at the 2 and 6 position and one hydroxyl group, whereas DHBP contains two connected phenyl rings with two hydroxyl groups. The number of hydroxyl groups on a compound, as well as their placement, provides

information on the compounds potential to form a polymeric product upon oxidation. These two compounds were chosen due to their structural properties, such as mono/di-phenol motifs (and in turn their expected differences in reactivity and product formation). DPP and DHBP can be analyzed using known techniques such as cyclic voltammetry, XRD, UV-vis spectroscopy, IR spectroscopy, NMR spectroscopy, TEM imaging, and GC-MS.

In addition, both phenols are industrially relevant, hence appropriate for this study. In chapter 2, we show the chemical oxidation product of DPP was determined to be 3,3',5,5'-tetraphenyldiphenoquinone i.e., TPBQ. Electrooxidation of DPP using varying potential ranges and electrode material generated product selectivity and differing product yield. The negative potential range appeared to favour phenolate formation to form the phenoxyl radical prior to forming TPBQ. The phenoxyl radicals may have a greater tendency to adsorb onto carbon surfaces compared to Pt surfaces due to paramagnetic properties, hence it is more likely that DPP radicals formed on the carbon electrode can undergo more efficient carbon-carbon oxidative dimerization. Other products formed *via* electrochemical oxidation of DPP included 2,6-DPPQ and TPBD (2,6-diphenyl-*p*-benzo-quinone, and 3,3’5,5’-tetraphenyl-biphenyl-4,4-diol). In chapter 2, C-C homo-coupling was achieved from chemical and electrooxidation of DPP. Negligible polymerization was observed when using this phenol under chosen experimental conditions. In contrast to DPP, in chapter 3, DHBP was also electrochemically and chemically oxidized. It is apparent that the two oxidation methods generate obviously different products based on visual characteristics. A yellow and brown solution was made through electrooxidation and chemical oxidation respectively. Electrooxidation of DHBP

generates a pale-yellow solution, indicating that soluble organic products were formed alongside an insoluble film that was formed on the GCE surface. Likely, a polymeric material was made based on the film formation observed on the electrode surface.

Chemical oxidation generated brown-black insoluble products that was analyzed through TEM imaging (courtesy of Meera Patel in collaboration with Dr. Ruby Sullan Lab at University of Toronto Scarborough) and exhibited worm-like structure morphology - an indicator of polymeric products. This product is likely PDHBP – polydihydroxybiphenol, as suggested in literature. This shows that the chemical oxidation of DHBP with copper perchlorate was able to form a polymeric product as shown in the TEM results. In contrast, electrooxidation generated a yellow film on the surface of the glassy carbon electrode and insoluble coloured products in solution. The difference in the solution colour, as well as physical characteristics of the insoluble products, indicated that the oxidation method employed can potentially generate different products.

The data from this thesis indicates that the electrochemical methodologies are valuable tools for selective transformation of phenolics. In addition, the visible differences observed in the insoluble materials formed suggests that a polymeric material of different morphology can be selectively synthesized depending on the oxidation method chosen and can be beneficial for material synthesis. Furthermore, the dependence on electrode material and varying potential ranges allowed product selectivity and reaction flexibility and tunability, which can be useful in industrial syntheses of phenolic analogues and is incomparable by traditional chemical methods. Electrochemical oxidation exhibited more product selectivity and tuning parameters in contrast to

traditional chemical synthesis. This can be beneficial in minimizing waste and biproducts formed in the reaction, in contrast to chemical oxidation.

4.2. Future Research Directions

The work performed for this thesis allowed understanding on the mechanistic pathways that DPP and DHBP undergoes and how electrochemical parameters can influence the product formation. Further exploration into reaction mechanism with the effect of electrode material, temperature, agitation, and potential ranges will be useful in understanding why specific reaction pathways are favoured. In this work, acetonitrile and GCE was used as a solvent and anode material respectively, however, publications indicate that HFIP and the BDD electrode has shown exceptional qualities in minimizing electrode fouling, increasing product selectivity, and increasing product yield[30,73]. BDD has been shown to be effective in minimizing fouling for polymeric compounds. Hence, it may be useful to implement an electrode that can optimize DHBP oxidation while minimizing passivation. In chapter 2, the C-C homo-coupling was achieved by both oxidation methods, however, there is interest in generating asymmetrical dimers from C-C hetero-coupling. For example, DPP and DTBP electrooxidation could yield an asymmetrical dimer to further the synthetic diversity of electrochemically generated products.

Determining product identity is the most important aspect of reaction and product characterization. In chapter 2, two products were identified, however, in chapter 3, the solid precipitates and film were not characterized, therefore future studies should focus on material characterization. TEM imaging of the film will give valuable information on morphological characteristics on the product and if such products are identical to those

formed through chemical oxidation. Additional methods such as mass spectrometry and DLS analysis can be used for molecular weight determination, which can provide information on how reaction parameters influence polymer formation. However, electrooxidation of DHBP to form a polymeric material is ideal because it can be simultaneously isolated from the electrode surface, hence further characterization of the film on the electrode surface is required to understand the product formation under current experimental conditions before expanding to other electrochemical methods and other reaction conditions.

Additional work on DPP would be implementing strategies for scalable product syntheses, specifically exploring the chemical behavior and mechanism the compound undergoes. In this thesis, DPP and DHBP were studied, however, there are other phenolic compounds that are industrially relevant, such as triclosan. They are commonly found in household items and some cosmetics and can end up in our environment as a pollutant. Unlike DPP and DHBP, triclosan has three aryl-chloride bonds, and phenol moieties, which would allow for simultaneous oxidation and reduction upon demand. Toxic compounds can be damaging to the environment and to human health, such as nitrophenols. Nitrophenols are NO_2 group containing phenolic compounds that are commonly used for dyes, insecticides, fungicides and for manufacturing pharmaceuticals. Mono-nitrophenols contain a single NO_2 group and exists in isomers. The OH and NO_2 groups have the potential to oxidize at both sites and degrade to other phenolic compounds. Hence, there is opportunity for studying the remediation of nitrophenols that are present in soil and wastewater.

In summary, electrochemical methodologies offer promising alternatives and complementary strategies towards selective on-demand synthesis.

References

(1) Sojka, S. A.; Wolfe, R. A.; Guenther, G. D. Formation of Phenolic Resins: Mechanism and Time Dependence of the Reaction of Phenol and Hexamethylenetetramine As Studied. *Macromolecules* **1981**, *14*, 1539–1543.

(2) Liu, J.; Chen, R.; Wang, C.; Zhao, Y.; Chu, F. Synthesis and Characterization of Polyethylene Glycol-Phenol- Formaldehyde Based Polyurethane Composite. *Sci. Rep.* **2019**, 1–9. https://doi.org/10.1038/s41598-019-56147-x.

(3) Rochester, J. R.; Bolden, A. L. Review Bisphenol S and F : A Systematic Review and Comparison of the Hormonal Activity of Bisphenol A Substitutes. **2015**, *123* (7), 643–650.

(4) Kahru, A.; Maloverjan, A.; Sillak, H.; Pumaa, L. The Toxicity and Fate of Phenolic Pollutants in the Contaminated Soils Associated with the OibShale Industry. *Environ. Sci. Pollut. Res.* **2002**, *1* (1), 27–33.

(5) Erler, C.; Novak, J. Bisphenol a Exposure: Human Risk and Health Policy. *J. Pediatr. Nurs.* **2010**, *25* (5), 400–407. https://doi.org/10.1016/j.pedn.2009.05.006.

(6) Corrales, J.; Kristofco, L. A.; Baylor Steele, W.; Yates, B. S.; Breed, C. S.; Spencer Williams, E.; Brooks, B. W. Global Assessment of Bisphenol a in the Environment: Review and Analysis of Its Occurrence and Bioaccumulation. *Dose-Response* **2015**, *13* (3), 1–29. https://doi.org/10.1177/1559325815598308.

(7) Michałowicz, J.; Duda, W. Phenols - Sources and Toxicity. *Polish J. Environ. Stud.* **2007**, *16* (3), 347–362.

(8) Cook, C. D. Oxidation of Hindered Phenols. I. Oxidation of and Oxidation Inhibition by 2,6-Di-Tert-Butyl-4-Methylphenol. *J. Chem. Inf. Model.* **1953**, *18*

(3), 261–266.

(9) Cooper, G. D.; Bennett, J. G. Mechanism of Oxidative Polymerization of 2,6-Disubstituted Phenols. Structure of Polymers from Mixed Dimers of 2,6-Dimethylphenol and 2,6-Diphenylphenol. *J. Org. Chem.* **1972**, *37* (3), 441–447. https://doi.org/10.1021/jo00968a025.

(10) Kharasc, M. S.; Joshi, B. S. Reaction of Hindered Phenols. II. Base-Catalyzed Oxidations of Hindered Phenols. *J. Org. Chem.* **1957**, *3179* (November), 1439–1443.

(11) Horswill, E. C.; Howard, J. A.; Ingold, K. U. The Oxidation of Phenols. III. The Stoichiometries for the Oxidation of Some Substituted Phenols with Peroxy Radicals. *Can. J. Chem.* **1966**, *44* (9), 985–991.

(12) Cook, C. D.; Woodworth, R. C. Oxidation of Hindered Phenols. II. The 2,4,6-Tri-t-Butylphenoxy Radical. *J. Am. Chem. Soc.* **1953**, *75* (24), 6242–6244. https://doi.org/10.1021/ja01120a040.

(13) de Jonge, C. R. H. I.; van Dort, H. M.; Vollbracht, L. The Oxidation of Phenols with Leaddioxide. *Tetrahedron Lett.* **1970**, *11* (22), 1881–1884. https://doi.org/10.1016/S0040-4039(01)98108-0.

(14) Harold, B.; Cassis, F. A. Ortho Alkylated Phenols. 2,6-Di-Tert-Butylphenol. *J. Am. Chem. Sociery* **1951**, *73* (7), 3179–3182.

(15) Bilici, A.; Kaya, I.; Dogan, F. Monomer/Polymer Schiff Base Copper(II) Complexes for Catalytic Oxidative Polymerization of 2,2'- Dihydroxybiphenyl. *J. Polym. Sci. Part A Polym. Chem.* **2009**, *47*, 2977–2984. https://doi.org/10.1002/pola.

(16) Kumar, S. S.; Himabindu, V. Materials Science for Energy Technologies Hydrogen Production by PEM Water Electrolysis – A Review. *Mater. Sci. Energy Technol.* **2019**, *2* (3), 442–454. https://doi.org/10.1016/j.mset.2019.03.002.

(17) Elgrishi, N.; Rountree, K. J.; McCarthy, B. D.; Rountree, E. S.; Eisenhart, T. T.; Dempsey, J. L. A Practical Beginner's Guide to Cyclic Voltammetry. *J. Chem. Educ.* **2018**, *95* (2), 197–206. https://doi.org/10.1021/acs.jchemed.7b00361.

(18) Fangmeyer, J.; Behrens, A.; Gleede, B.; Waldvogel, S. R.; Karst, U. Mass-Spectrometric Imaging of Electrode Surfaces — a View on Electrochemical Side Reactions. *Angew. Chemie - Int. Ed.* **2020**, *59*, 20428–20433. https://doi.org/10.1002/anie.202010134.

(19) D., M. B.; Prasad, B. L. V. Selective Electro-Oxidation of Phenol to 1,4-Hydroquinone Employing Carbonaceous Electrodes: Surface Modification Is the Key. *New J. Chem.* **2022**, *46* (5), 2518–2525.

(20) Chan, Y. Y.; Webster, R. D. Electrochemical Oxidation of the Phenolic Benzotriazoles UV-234 and UV-327 in Organic Solvents. *ChemElectroChem* **2018**, *6* (16), 4297–4306. https://doi.org/10.1002/celc.201801375.

(21) Yun, Y.; Yue, Y.; Li, Y.; Webster, R. D. Electrochemical / Chemical Oxidation of Bisphenol A in a Four-Electron / Two-Proton Process in Aprotic Organic Solvents. *Electrochim. Acta* **2013**, *112*, 287–294. https://doi.org/10.1016/j.electacta.2013.08.181.

(22) Zabik, N. L.; Virca, C. N.; McCormick, T. M.; Martic-Milne, S. Selective Electrochemical versus Chemical Oxidation of Bulky Phenol. *J. Phys. Chem. B* **2016**, *120* (34), 8914–8924. https://doi.org/10.1021/acs.jpcb.6b06135.

(23) Foley, L. Pulse Voltammetric Determination of Butylated Hydroxy Toluene in Transformer Oils. **1979**, *51* (7), 818–822.

(24) Weitkamp, R. F.; Neumann, B.; Stammler, H. G.; Hoge, B. Non-Coordinated and Hydrogen Bonded Phenolate Anions as One-Electron Reducing Agents. *Chem. - A Eur. J.* **2021**, *27* (21), 6465–6478. https://doi.org/10.1002/chem.202005123.

(25) Hassanein, M. T.; Gerges, S. S.; Abdo, M. A.; El-Khalafy, S. H. Studies on the Oxidation of 2,6-Di-Tert-Butylphenol by Molecular Oxygen Catalyzed by Cobalt(II) Tetraarylporphyrins Bound to Cationic Latex. *J. Porphyr. Phthalocyanines* **2005**, *9* (9), 621–625. https://doi.org/10.1142/S1088424605000721.

(26) Mutlu, Y. Ç.; Semerci, T. G.; Türk, H. Oxidation of 2,6-Di-Tert-Butylphenol with Tert-Butyl Hydroperoxide Catalyzed by Iron Porphyrin Tetrasulfonate, Iron Porphyrin Tetracarboxylate and Their Supported Analogues in a Water-Methanol Mixture. *J. Hazard. Mater.* **2019**, *371* (November 2018), 280–287. https://doi.org/10.1016/j.jhazmat.2019.03.001.

(27) Kirste, A.; Nieger, M.; Malkowsky, I. M.; Stecker, F.; Fischer, A.; Waldvogel, S. R. Ortho-Selective Phenol-Coupling Reaction by Anodic Treatment on Boron-Doped Diamond Electrode Using Fluorinated Alcohols. *Chem. - A Eur. J.* **2009**, *15* (10), 2273–2277. https://doi.org/10.1002/chem.200802556.

(28) Lips, S.; Wiebe, A.; Elsler, B.; Schollmeyer, D.; Dyballa, K. M.; Franke, R.; Waldvogel, S. R. Synthesis of Meta-Terphenyl-2,2″-Diols by Anodic C−C Cross-Coupling Reactions. *Angew. Chemie - Int. Ed.* **2016**, *55* (36), 10872–10876. https://doi.org/10.1002/anie.201605865.

(29) Wiebe, A.; Lips, S.; Schollmeyer, D.; Franke, R.; Waldvogel, S. R. Single and Twofold Metal- and Reagent-Free Anodic C−C Cross-Coupling of Phenols with Thiophenes. *Angew. Chemie - Int. Ed.* **2017**, *56* (46), 14727–14731. https://doi.org/10.1002/anie.201708946.

(30) Malkowsky, I. M.; Griesbach, U.; Pütter, H.; Waldvogel, S. R. Unexpected Highly Chemoselective Anodic Ortho-Coupling Reaction of 2,4-Dimethylphenol on Boron-Doped Diamond Electrodes. *European J. Org. Chem.* **2006**, No. 20, 4569–4572. https://doi.org/10.1002/ejoc.200600466.

(31) Selt, M.; Franke, R.; Waldvogel, S. R. Supporting-Electrolyte-Free and Scalable Flow Process for the Electrochemical Synthesis of 3,3′,5,5′-Tetramethyl-2,2′-Biphenol. *Org. Process Res. Dev.* **2020**, *24* (10), 2347–2355. https://doi.org/10.1021/acs.oprd.0c00170.

(32) Waldvogel, S. R.; Lips, S.; Selt, M.; Riehl, B.; Kampf, C. J. Electrochemical Arylation Reaction. *Chem. Rev.* **2018**. https://doi.org/10.1021/acs.chemrev.8b00233.

(33) Kirste, A.; Elsler, B.; Schnakenburg, G.; Waldvogel, S. R. Efficient Anodic and Direct Phenol-Arene C,C Cross-Coupling: The Benign Role of Water or Methanol. *J. Am. Chem. Soc.* **2012**, *134*, 3571–3576.

(34) Lucarini, M.; Mugnaini, V.; Pedulli, G. F.; Guerra, M. Hydrogen-Bonding Effects on the Properties of Phenoxyl Radicals. An EPR, Kinetic, and Computational Study. *J. Am. Chem. Soc.* **2003**, *125* (27), 8318–8329. https://doi.org/10.1021/ja034963k.

(35) Loos, G.; Scheers, T.; Eyck, K. Van; Schepdael, A. Van; Adams, E.; Bruggen, B.

Van Der; Cabooter, D.; Dewil, R. Separation and Puri Fi Cation Technology Electrochemical Oxidation of Key Pharmaceuticals Using a Boron Doped Diamond Electrode. *Sep. Purif. Technol.* **2018**, *195* (2018), 184–191. https://doi.org/10.1016/j.seppur.2017.12.009.

(36) Kirste, A.; Schnakenburg, G.; Stecker, F.; Fischer, A.; Waldvogel, S. R. Anodic Phenol – Arene Cross-Coupling Reaction on Boron-Doped. *Angew. Chemie - Int. Ed.* **2010**, *49*, 971–975. https://doi.org/10.1002/anie.200904763.

(37) Fóti, G.; Gandini, D.; Comninellis, C.; Perret, A.; Haenni, W. Oxidation of Organics by Intermediates of Water Discharge on IrO2 and Synthetic Diamond Anodes. *Electrochem. Solid-State Lett.* **1999**, *2* (5), 228–230. https://doi.org/10.1149/1.1390792.

(38) Marselli, B.; Garcia-gomez, J.; Michaud, P.; Rodrigo, M. A.; Mo, M. Electrogeneration of Hydroxyl Radicals on Boron-Doped Diamond Electrodes. **2003**, 79–83. https://doi.org/10.1149/1.1553790.

(39) Zhu, X.; Tong, M.; Shi, S.; Zhao, H.; Ni, J. Essential Explanation of the Strong Mineralization Performance of Boron-Doped Diamond Electrodes. *Environ. Sci. Technol.* **2008**, *42* (13), 4914–4920.

(40) Baroody, H. A.; Kjeang, E.; Soc, J. E.; Baroody, H. A.; Kjeang, E. Predicting Platinum Dissolution and Performance Degradation under Drive Cycle Operation of Polymer Electrolyte Fuel Cells Predicting Platinum Dissolution and Performance Degradation under Drive Cycle Operation of Polymer Electrolyte Fuel Cells. *J. Electrochem. Soc.* **2021**, *168*, 044524. https://doi.org/10.1149/1945-7111/abf5aa.

(41) Gattrell, M.; Kirk, D. W. A Study of the Oxidation of Phenol at Platinum and Preoxidized Platinum Surfaces. *J. Electrochem. Soc.* **1993**, *140* (6), 1534–1540. https://doi.org/10.1149/1.2221598.

(42) Iotov, P. I.; Kalcheva, S. V. Mechanistic Approach to the Oxidation of Phenol at a Platinum/Gold Electrode in an Acid Medium. *J. Electroanal. Chem.* **1998**, *442* (1–2), 19–26. https://doi.org/10.1016/S0022-0728(97)00455-5.

(43) Andreescu, S.; Andreescu, D.; Sadik, O. A. A New Electrocatalytic Mechanism for the Oxidation of Phenols at Platinum Electrodes. *Electrochem. commun.* **2003**, *5* (8), 681–688. https://doi.org/10.1016/S1388-2481(03)00166-8.

(44) Awad, M. I.; Sayqal, A.; Pashameah, R. A.; Hameed, A. M.; Morad, M. Enhanced Paracetamol Oxidation and Its Determination Using Electrochemically Activated Glassy Carbon Electrode HO. **2021**, *16*, 1–15. https://doi.org/10.20964/2021.01.12.

(45) Qian, P.; Bi, M.; Su, J.; Zha, Z.; Wang, Z. Electrosynthesis of (E) - Vinyl Sulfones Directly from Cinnamic Acids and Sodium Sulfinates via Decarboxylative Sulfono Functionalization. *J. Org. Chem.* **2016**, *81*, 4876–4882. https://doi.org/10.1021/acs.joc.6b00661.

(46) Li, X.; Cui, Y.; Feng, Y.; Xie, Z.; Gu, J. Reaction Pathways and Mechanisms of the Electrochemical Degradation of Phenol on Different Electrodes. **2005**, *39*, 1972–1981. https://doi.org/10.1016/j.watres.2005.02.021.

(47) Kiss, L.; Bősz, D.; Kovács, F.; Li, H.; Nagy, G.; Kunsági-Máté, S. Investigation of Phenol Electrooxidation in Aprotic Non-Aqueous Solvents by Using Cyclic and Normal Pulse Voltammetry. *Polym. Bull.* **2019**, *76* (11), 5849–5864.

https://doi.org/10.1007/s00289-019-02678-2.

(48) Demir, H. Ö. A Novel Polyphenol : Synthesis , Characterization and Investigation of Its Thermal and Electrochemical Properties. *Polym. J.* **2012**, *44*, 699–705. https://doi.org/10.1038/pj.2012.17.

(49) Nakamura, Y.; Sato, Y.; Shida, N.; Atobe, M. Electrochemical Trimerization of Catechol to 2,3,6,7,10,11-Hexahydroxytriphenylene Using a Flow Microreactor. *Electrochem. Soc. Japan* **2021**, 13–15. https://doi.org/10.5796/electrochemistry.21-00053.

(50) Röckl, J. L.; Pollok, D.; Franke, R.; Waldvogel, S. R. A Decade of Electrochemical Dehydrogenative C,C-Coupling of Aryls. *Acc. Chem. Res.* **2020**, *53* (1), 45–61. https://doi.org/10.1021/acs.accounts.9b00511.

(51) Francke, R.; Cericola, D.; Kötz, R.; Weingarth, D.; Waldvogel, S. R. Electrochimica Acta Novel Electrolytes for Electrochemical Double Layer Capacitors Based On. *Electrochim. Acta* **2012**, *62*, 372–380. https://doi.org/10.1016/j.electacta.2011.12.050.

(52) Lips, S.; Waldvogel, S. R. Use of Boron-Doped Diamond Electrodes in Electro-Organic Synthesis. *ChemElectroChem* **2018**, *6* (6). https://doi.org/10.1002/celc.201801620.

(53) Eberson, L.; Hartshorn, M. P.; Persson, O. Phenyliodine (III) Bis(Trifluoroacetate) as a Radical Cation Generating Reagent. 1995, pp 640–644.

(54) Ramos-villaseñor, J. M.; Rodríguez-cárdenas, E.; Díaz, C. E. B. Use of 1,1,1,3,3,3-Hexafluoro-2-Propanol (HFIP) Co-Solvent Mixtures in Organic Electrosynthesis. *J. Electrochem. Soc.* **2020**, *167*, 155509. https://doi.org/10.1149/1945-

7111/abb83c.

(55) Elsler, B.; Wiebe, A.; Schollmeyer, D.; Dyballa, K. M.; Franke, R.; Waldvogel, S. R. Source of Selectivity in Oxidative Cross-Coupling of Aryls by Solvent Effect of 1,1,1,3,3,3-Hexafluoropropan-2-Ol. *Chem. Eur. J.* **2015**, *21*, 12321–12325. https://doi.org/10.1002/chem.201501604.

(56) Jiang, G.; Li, F.; Wang, H.; Wu, M.; Qi, S.; Liu, X.; Yang, S.; Ma, J. Perspective on High-Concentration Electrolytes for Lithium Metal Batteries. *Small Struct.* **2021**, *2* (5), 2000122. https://doi.org/10.1002/sstr.202000122.

(57) Bond, A. M. Effect of Temperature and Supporting Electrolyte on the Electrochenical Oxidation of (Benzene)Trlcarbonylchromium and Other π-Hydrocarbon Complexes. *Organometallics* **1986**, *5* (770625), 2553–2555.

(58) Heard, D. M.; Lennox, A. J. J. Electrode Materials in Modern Organic Electrochemistry. *Angew. Chemie - Int. Ed.* **2020**, *59*, 18866–18884. https://doi.org/10.1002/anie.202005745.

(59) Runnels, P. L.; Joseph, J. D.; Logman, M. J.; Wightman, R. M. Effect of PH and Surface Functionalities on the Cyclic Voltammetric Responses of Carbon-Fiber Microelectrodes. *Anal. Chem.* **1999**, *71* (14), 2782–2789.

(60) Colades, J. I.; Daniel, M.; Luna, G. De; Freda, M.; Secondes, N.; Huang, C. Electrochemical In-Situ Hydrogen Peroxide Generation in a Packed-Bed Reactor for Fenton Oxidation of p -Nitrophenol in Aqueous Solution. *Process Saf. Environ. Prot.* **2019**, *123*, 161–168. https://doi.org/10.1016/j.psep.2018.10.014.

(61) Gowda, J. I.; Nandibewoor, S. T. Electrochemical Behavior of Paclitaxel and Its Determination at Glassy Carbon Electrode. *Asian J. Pharm. Sci.* **2014**, *9* (1), 42–

49. https://doi.org/10.1016/j.ajps.2013.11.007.

(62) Boudenne, J. -L.; Cerclier, O.; Bianco, P. Voltammetric Studies of the Behavior of Carbon Black during Phenol Oxidation on Ti/Pt Electrodes. *J. Electrochem. Soc.* **1998**, *145* (8), 2763–2768. https://doi.org/10.1149/1.1838711.

(63) Quell, T.; Hecken, N.; Dyballa, K. M.; Franke, R.; Waldvogel, S. R. Scalable and Selective Preparation of 3,3',5,5'-Tetramethyl-2,2'-Biphenol. *Org. Process Res. Dev.* **2017**, *21* (1), 79–84. https://doi.org/10.1021/acs.oprd.6b00356.

(64) Ezerskis, Z.; Jusys, Z. Electropolymerization of Chlorinated Phenols on a Pt Electrode in Alkaline Solution . Part IV : A Gas Chromatography Mass Spectrometry Study. *J. Appl. Electrochem.* **2002**, *32*, 543–550.

(65) Malkowsky, I. M.; Rommel, C. E.; Wedeking, K.; Fröhlich, R.; Bergander, K.; Nieger, M.; Quaiser, C.; Griesbach, U.; Pütter, H.; Waldvogel, S. R. Facile and Highly Diastereoselective Formation of a Novel Pentacyclic Scaffold by Direct Anodic Oxidation of 2 ,4-Dimethylphenol. *European J. Org. Chem.* **2006**, 241–245. https://doi.org/10.1002/ejoc.200500517.

(66) Ferreira, M.; Varela, H.; Torresi, R. M.; Tremiliosi-filho, G. Electrode Passivation Caused by Polymerization of Different Phenolic Compounds. *Electrochem. Acta* **2006**, *52*, 434–442. https://doi.org/10.1016/j.electacta.2006.05.025.

(67) Berkessel, A.; Adrio, J. A.; Hu, D.; Neudo, M. Unveiling the " Booster Effect " of Fluorinated Alcohol Solvents : Aggregation-Induced Conformational Changes and Cooperatively Enhanced H-Bonding. *J. Am. Chem. Soc.* **2006**, No. 7, 8421–8426.

(68) Hossain, M. A.; Akiyama, K.; Goto, K.; Sugiura, K. I. Thermal Reductive Disproportionation of 3,3′,5,5′-Tetraphenyldiphenoquinone with Drastic Color

Change: Potential Prototype of Data Storage Advanced Materials. *ChemistrySelect* **2016**, *1* (13), 3784–3790. https://doi.org/10.1002/slct.201600437.

(69) Mijangos, F.; Varona, F. Changes in Solution Color During Phenol Oxidation by Fenton Reagent. **2006**, *40* (17), 5538–5543.

(70) Melby, L. R.; Harder, R. J.; Hertler, W. R.; Mahler, W.; Benson, R. E.; Mochel, W. E. Substituted Quinondimethans. II. Anion-Radical Derivatives and Complexes of 7,7,8,8-Tetracyanoquinodimethan. *J. Am. Chem. Soc.* **1962**, *84* (17), 3374–3387.

(71) Goodenough, J. B. Electrochemical Energy Storage in a Sustainable Modern Society. *Energy Environ. Sci.* **2014**, *7* (1), 14–18. https://doi.org/10.1039/c3ee42613k.

(72) Akhmadullin, R.; Gatiyatullin, D.; Verizhnikov, L.; Mukmeneva, N.; Lapteva, L.; Ovchinnikov, V. Research Journal of Pharmaceutical , Biological and Chemical Sciences The Heterogeneous Catalyzed Oxidation in the Liquid Alkaline Medium Of. *5* (494), 494–502.

(73) Röckl, J. L.; Schollmeyer, D.; Franke, R.; Waldvogel, S. R. Dehydrogenative Anodic C-C Coupling of Phenols Bearing Electron- Withdrawing Groups. *Angew. Chemie - Int. Ed.* **2020**, *59*, 315–319. https://doi.org/10.1002/anie.201910077.

(74) Jouny, M.; Lv, J.; Cheng, T.; Ko, B. H.; Zhu, J.; Iii, W. A. G.; Jiao, F. Formation of Carbon–Nitrogen Bonds in Carbon Monoxide. *Nat. Chem.* **2019**, *11*, 846–851. https://doi.org/10.1038/s41557-019-0312-z.

(75) Beil, S. B.; Muller, T.; Sillart, S. B.; Franzmann, P.; Bomm, A.; Holtkamp, M.; Uwe, K.; Wolfgag, S.; Waldovgel, S. R. Novel Active Molybdenum-Based Anode

for Dehydrogenative Coupling Reactions. *Angew. Chemie - Int. Ed.* **2018**, *57* (9), 2450–2454. https://doi.org/10.1002/anie.201712718.

(76) Via, G. G.; Shugart, C. L.; Melnyk, S. L.; Hupman, S. R. One-Step Solvent-Free Synthesis and Grafting of Diazonium Ions at Glassy Carbon Electrodes. *Electroanalysis* **2018**, No. 30, 1–7. https://doi.org/10.1002/elan.201800407.

(77) Labaye, D. E.; Jérôme, C.; Geskin, V. M.; Louette, P.; Lazzaroni, R.; Martinot, L.; Jérôme, R. Full Electrochemical Synthesis of Conducting Polymer Films Chemically Grafted to Conducting Surfaces. *Langmuir* **2002**, *18* (13), 5222–5230. https://doi.org/10.1021/la011439n.

(78) Kirste, A.; Schnakenburg, G.; Waldvogel, S. R.; Chemistry, O. Anodic Coupling of Guaiacol Derivatives on Boron-Doped Diamond Electrodes. *Org. Lett.* **2011**, *13* (12), 3126–3129.

(79) Xu, Q.; Ã, S. W. Original Paper Electrocatalytic Oxidation and Direct Determination of L-Tyrosine by Square Wave Voltammetry at Multi-Wall Carbon Nanotubes Modified Glassy Carbon Electrodes. **2005**, *52*, 47–52. https://doi.org/10.1007/s00604-005-0408-6.

(80) Molina, A.; Gonzalez., J.; Laborda, E.; Compton, R. G. On the Meaning of the Diffusion Layer Thickness for Slow Electrode Reactions. *Phys. Chem. Chem. Phys.* **2013**, *15*, 2381–2388. https://doi.org/10.1039/c2cp43650g.

(81) Gau, V.; Ma, S.; Wang, H.; Tsukuda, J.; Kibler, J.; Haake, D. A. Electrochemical Molecular Analysis without Nucleic Acid Amplification. *Methods* **2023**, *37* (2005), 73–83. https://doi.org/10.1016/j.ymeth.2005.05.008.

(82) Borsche, W. No Title. *Liebigs Ann.* **1900**, *312* (211).

(83) Barrientos, C.; Squella, J. A.; Nun, L. J. Electrochemical Oxidation of 7-, 8- and 9-Hydroxy-3- Ethoxycarbonyl-2,4-Dimethyl Coumarin[4,3-b]Pyridine Isomers at Glassy Carbon in Dimethylformamide. *J. Electrochem. Soc.* **2011**, *158* (5), 166–172. https://doi.org/10.1149/1.3615933.

(84) Suzuki, M.; Sugiyama, T.; Musashi, E.; Kobiyama, Y.; Kashiwada, A.; Matsuda, K.; Yamada, K. Use of Chitosan for Removal of Bisphenol A and Bisphenol Derivatives Through Tyrosinase-Catalyzed Quinone Oxidation. **2010**, 36–40. https://doi.org/10.1002/app.

(85) Cecil, R.; J.S. Littler. Electron-Transfer Oxidations of Organic Compounds. Part 11.l The Oxidation of Phenol and 2,6-Dimethylphenol by the Hexachloroiridate(Iv) Anion. *J. Chem. Soc. B Phys. Org.* **1968**, No. 0, 1420–1427.

(86) Saito, K.; Tago, T.; Masuyama, T.; Nishide, H. Kei Saito, Takahiro Tago, Toru Masuyama, and Hiroyuki Nishide*. **2004**, 730–733. https://doi.org/10.1002/anie.200352764.

(87) Andis, N. M. Al. A New Method for Synthesis of Poly (2 , 6-Dimethyl-1 , 4-Phenylene Oxide) and Poly (2 , 6-Diphenyl-1 , 4-Phenyl Oxide). **2013**, *2013* (I), 0–4.

(88) Hika, W. A.; Woldu, A. R. The Impact of Anode Materials on the Performance of Electrochemical - CO 2 Reduction to Carbon Monoxide. *SN Appl. Sci.* **2021**, No. July. https://doi.org/10.1007/s42452-021-04796-x.

(89) Ross, S.; Finklestein, M. Anodic Oxidations . V . The Kolbe Oxidation of Phenylacetic Acid and 1-Methylcyclohexaneacetic Acid at Platinum and at Carbon. *J. Org. Chem.* **1969**, *34* (10), 2923–2927.

(90) Mvula, E.; Schuchmann, N.; Sonntag, C. Von. Reactions of Phenol-OH-Adduct Radicals. Phenoxyl Radical Formation by Water Elimination. *J. Chem. Soc. Perkin Trans. 2* **2001**, *2*, 264–268. https://doi.org/10.1039/b008434o.

(91) Li, L.; Xue, M.; Yan, X.; Liu, W.; Xu, K.; Zhang, S. Electrochemical Hofmann Rearrangement Mediated by NaBr: A Practical Access to Bioactive Carbamates. *Org. Biomol. Chem.* **2018**, *16* (25). https://doi.org/10.1039/C8OB01059E.

(92) Paulus, G. L. C.; Wang, Q. H. U. A.; Strano, M. S. Covalent Electron Transfer Chemistry of Graphene with Diazonium Salts. *Acc. Chem. Res.* **2013**, *46* (1), 160–170.

(93) Vargas, R.; Borrás, C.; Mostany, J.; Scharifker, R. Electrochemical Oxygen Transfer Reactions: Electrode Materials, Surface Processes, Kinetic Models, Linear Free Energy Correlations, and Perspectives. *J. Solid State Electrochem.* **2016**, *20*, 875–893. https://doi.org/10.1007/s10008-015-2984-7.

(94) Tessensohn, M. E.; Hirao, H.; Webster, R. D. Electrochemical Properties of Phenols and Quinones in Organic Solvents Are Strongly Influenced by Hydrogen-Bonding with Water. *J. Phys. Chem. C* **2013**, *117* (2), 1081–1090. https://doi.org/10.1021/jp311007m.

(95) Buisman, G. J. H.; Kamer, P. C. J.; Leeuwert, P. W. N. M. Van. Rhodium Catalysed Asymmetric Hydroformylation with Chiral Diphosphite Ligands. *Tetrahedron: Asymmetry* **1993**, *4* (7), 1625–1634.

(96) Mabrouk, H. E.; Tuck, D. G. The Direct Electrochemical Synthesis of Tin (II) Derivatives of Aromatic 1 , 2- Diols , and a Study of Their Oxidative Addition Reactions. *J. Chem. Soc. Dalt. Trans.* **1988**, *4*, 2539–2543.

(97) Shayani, H. Electrochemical Study of Adsorption and Electrooxidation of 4,4 ′ - Biphenol on the Glassy Carbon Electrode : Determination of the Orientation of Adsorbed Molecules. *Monatshefte für Chemie - Chem. Mon.* **2019**, *150* (2), 183–192. https://doi.org/10.1007/s00706-018-2318-4.

(98) Shayani-Jam, H.; Nematollahi, D. Electrochemically Mediated Oxidation of Glutathione and N-Acetylcysteine with 4,4′-Biphenol. *Electrochim. Acta* **2011**, *56* (25), 9311–9316. https://doi.org/10.1016/j.electacta.2011.08.010.

(99) Jonsson, M.; Lind, J.; Merenyi, G. Redox and Acidity Properties of 2,2′ - and 4,4′ - Biphenol and the Corresponding Phenoxyl Radicals. *J. Phys. Chem. A* **2002**, No. 106, 4758–4762.

(100) Bao, L.; Xiong, R.; Wei, G. Electrochimica Acta Electrochemical Polymerization of Phenol on 304 Stainless Steel Anodes and Subsequent Coating Structure Analysis. *Electrochim. Acta* **2010**, *55* (12), 4030–4038. https://doi.org/10.1016/j.electacta.2010.02.052.

(101) Fernandez, F.; Berrios, C.; Garrido-Ramirez, E.; Escalona, N.; Gutierrez, C.; Ureta-Zanartu, M. S. Electrooxidation of 2-Chlorophenol and 2,4,6-Chlorophenol on Glassy Carbon Electrodes Modified with Graphite–Zeolite Mixtures Francisco. *J. Appl. Electrochem.* **2014**, No. 44, 1295–1306. https://doi.org/10.1007/s10800-014-0763-2.

(102) Xavier, J. L. N.; Ortega, E.; Ferreira, J. Z.; Bernardes, A. M.; Pérez-Herranz, V. An Electrochemical Study of Phenol Oxidation in Acidic Medium. *Int. J. Electrochem. Sci.* **2011**, *6* (3), 622–636.

(103) Gu, G. E.; Park, C. S.; Cho, H.; Ha, T. H.; Bae, J.; Seok, O. Fluorescent

Polydopamine Nanoparticles as a Probe for Zebrafish Sensory Hair Cells Targeted in Vivo Imaging. *Sci. Rep.* **2018**, No. March, 1–9. https://doi.org/10.1038/s41598-018-22828-2.

(104) Gatrell, M.; Kirk, D. W. A Fourier Transform Infrared Spectroscopy Study of the Passive Film Produced during Aqueous Acidic Phenol Electro-Oxidation. *J. El* **1992**, *139* (10), 2736–2744.

(105) Ardila-suárez, C.; Rojas-avellaneda, D.; Ramirez-caballero, G. E. Effect of Temperature and Catalyst Concentration on Polyglycerol during Synthesis. *Int. J. Polym. Sci.* **2015**, *2015* (910249).

(106) Murakami, Y.; Ishii, H.; Hoshina, S.; Takada, N.; Ueki, A.; Tanaka, S.; Kadoma, Y.; Ito, S.; Machino, M.; Fujisawa, S. Antioxidant and Cyclooxygenase-2-Inhibiting Activity of 4,4′-Biphenol, 2,2′-Biphenol and Phenol. *Anticancer Res.* **2009**, *29* (6), 2403–2410.

(107) Yohe, G. R.; Dunbar, J. E.; Pedrotti, R. L.; Scheidt, F. M.; Lee, F. G. H.; Smith, E. C. The Oxidation of 2,6-Di-Tert-Butyl-4-Methylphenol. *J. Org. Chem.* **1956**, *21* (11), 1289–1292.

(108) Liu, X.; Cao, J.; Li, H.; Li, J.; Jin, Q.; Ren, K.; Ji, J. Mussel-Inspired Polydopamine : A Biocompatible and Ultrastable Coating for Nanoparticles in Vivo. *ACS Nano* **2013**, *7* (10), 9384–9395.

(109) Kim, B. E.; Liu, Y.; Shi, X.; Yang, X.; Bentley, W. E.; Payne, G. F. Biomimetic Approach to Confer Redox Activity to Thin Chitosan Films. *Adv. Funct. Mater.* **2010**, No. 20, 2683–2694. https://doi.org/10.1002/adfm.200902428.

Appendices

Appendix II

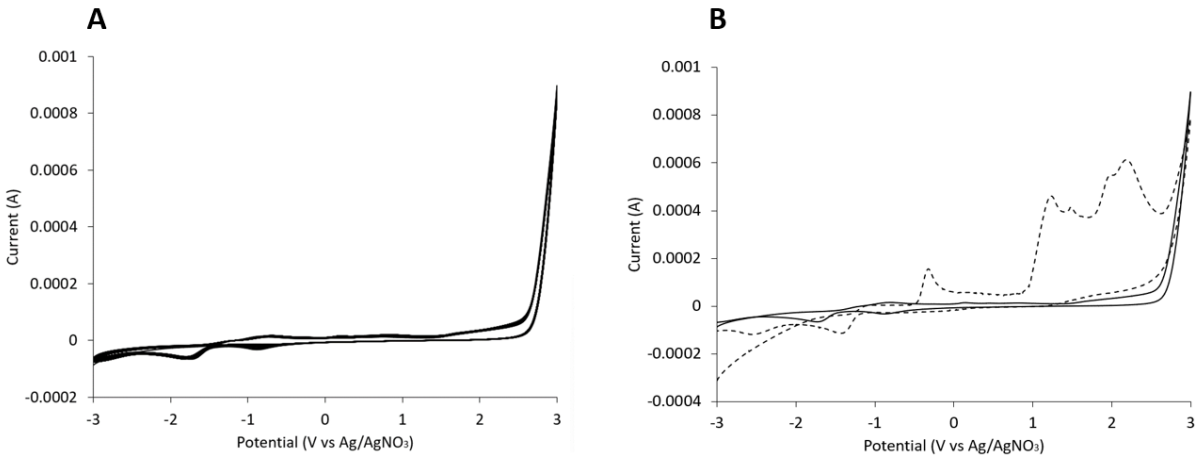

Appx II 2.1. Cyclic voltammogram, 1st scan of 1 CV, scan rate: 100 mV/s. Left to right scan direction. (A) 0.1 M TBAP in 3 mL ACN (B) Dotted line: with 10 mM DPP containing 0.1 TBAP electrooxidized overlaid with blank containing TBAP in ACN only.

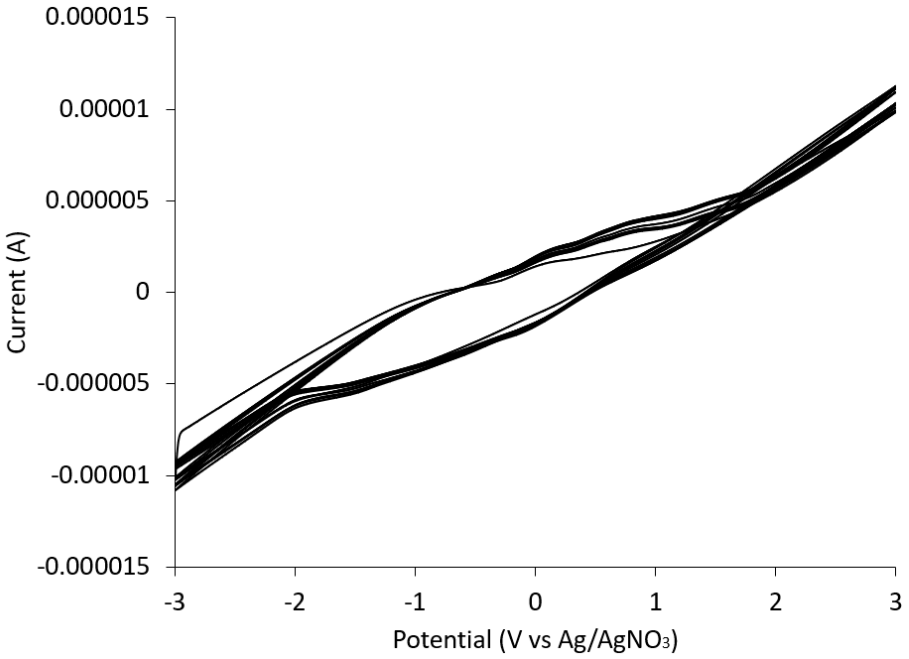

Appx II 2.2. Cyclic voltammogram: 1 CV, scan rate: 100 mV/s. Left to right scan direction. 10 mM DPP in 3 mL ACN.

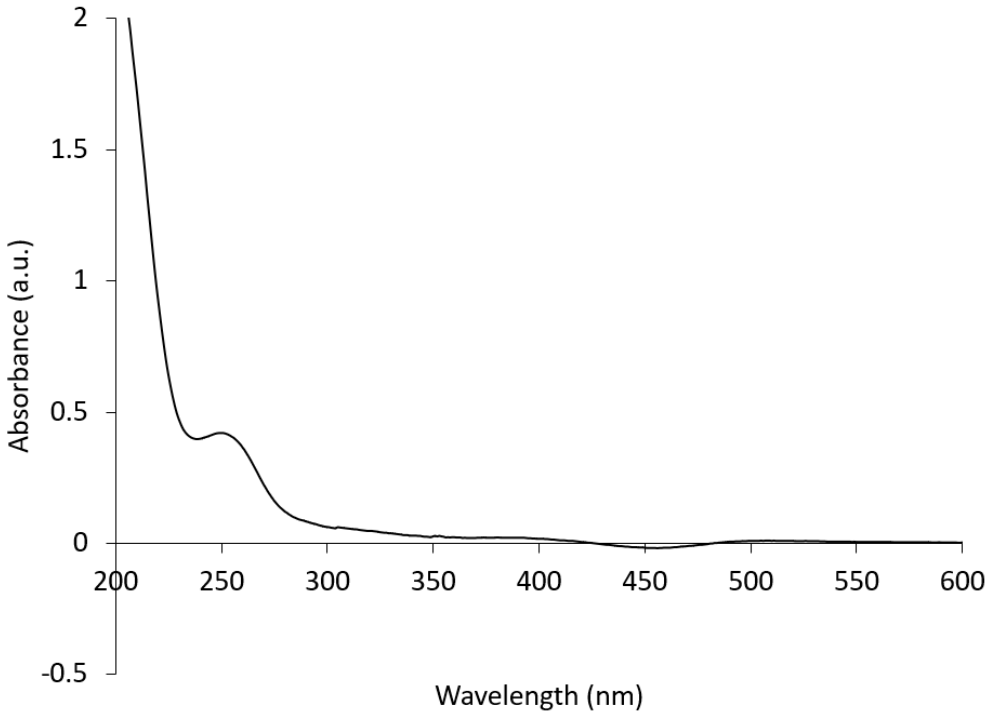

Appx II 2.3. UV-vis spectra of 10 mM DPP with 0.1 M TBAP in 3 mL ACN

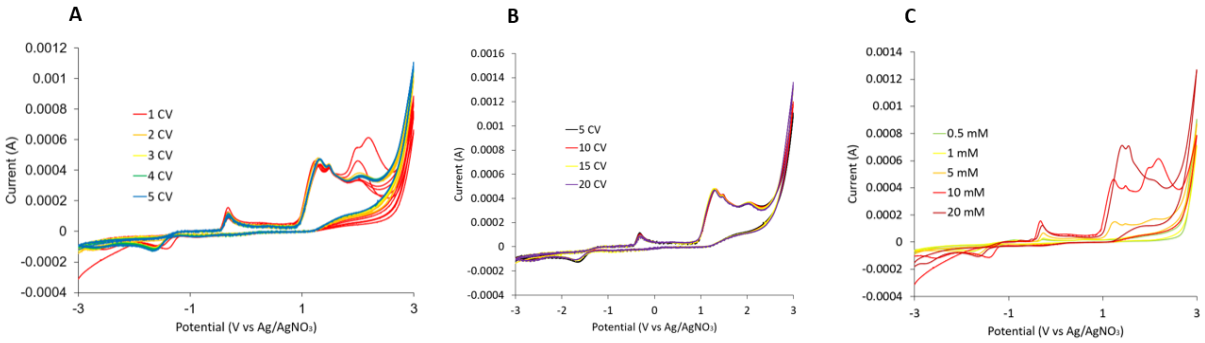

Appx II 2.4. (A) Full scans of CVs 1-5. (B) Full scans for 5 to 20 CV (C) CV as a function of concentration at 1st scan only.

Appx II Table 2.1. Oxidation (anodic) and reduction (cathodic) peak potentials of 10 mM DPP were obtained from cyclic voltammetry measurement (1st full scan). All values are reported against $Ag/AgNO_3$ reference electrode.

Compound	E_{pa} [a,b] (V)	E_{pc} [a,b] (V)
2,6-diphenylphenol	2.11 ± 0.09 1.46 ± 0.05 1.25 ± 0.02 -0.31 ± 0.01	-1.58 ± 0.2

[a] E_{pa} and E_{pc} values were obtained from cyclic voltammetry measurements.
[b] Mean of tripicate measurements ± standard deviation.

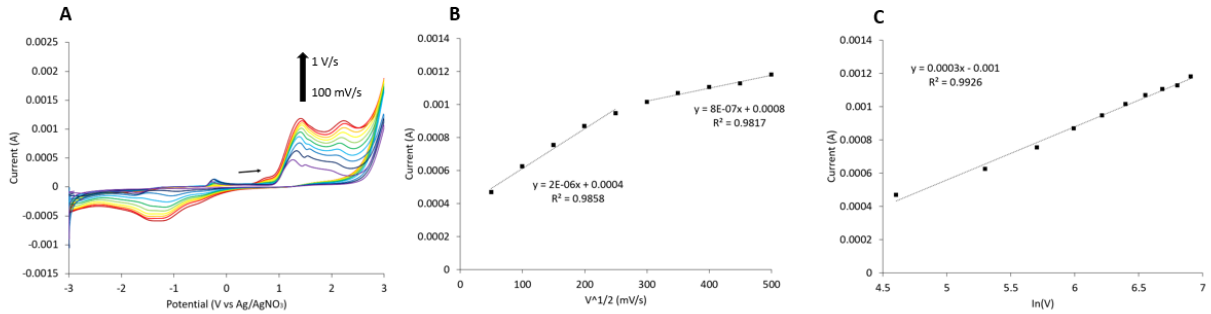

Appx II 2.5. (A) CV scan as a function of scan rates (scan direction is indicated by arrow; 1 CV, [DPP] = 10 mM, [TBAP] = 0.1 M, ACN, 100, 200, 300, 400, 500, 600, 700, 800, 900, 1000 mV/s **(**B) Anodic peak (1.46 V) current as a function of scan rate (C) Square root of scan rate (C) Ln of scan rate.

The Randles-Sevcik equation is used to describe the relationship between the peak current (i_p) and the square root of the scan rate (V s^{-1}), where *n* is the number of electrons transferred in the reaction, A (cm^{-1}) is the surface area of the working electrode, C^o is the concentration of the bulk analyte in solution and D_o is the diffusion coefficient of the oxidized species.

$$i_p = 0.4463\, nFAC\left(\frac{nFvD_o}{RT}\right)^{\frac{1}{2}}$$ Appx II Equation 2.1

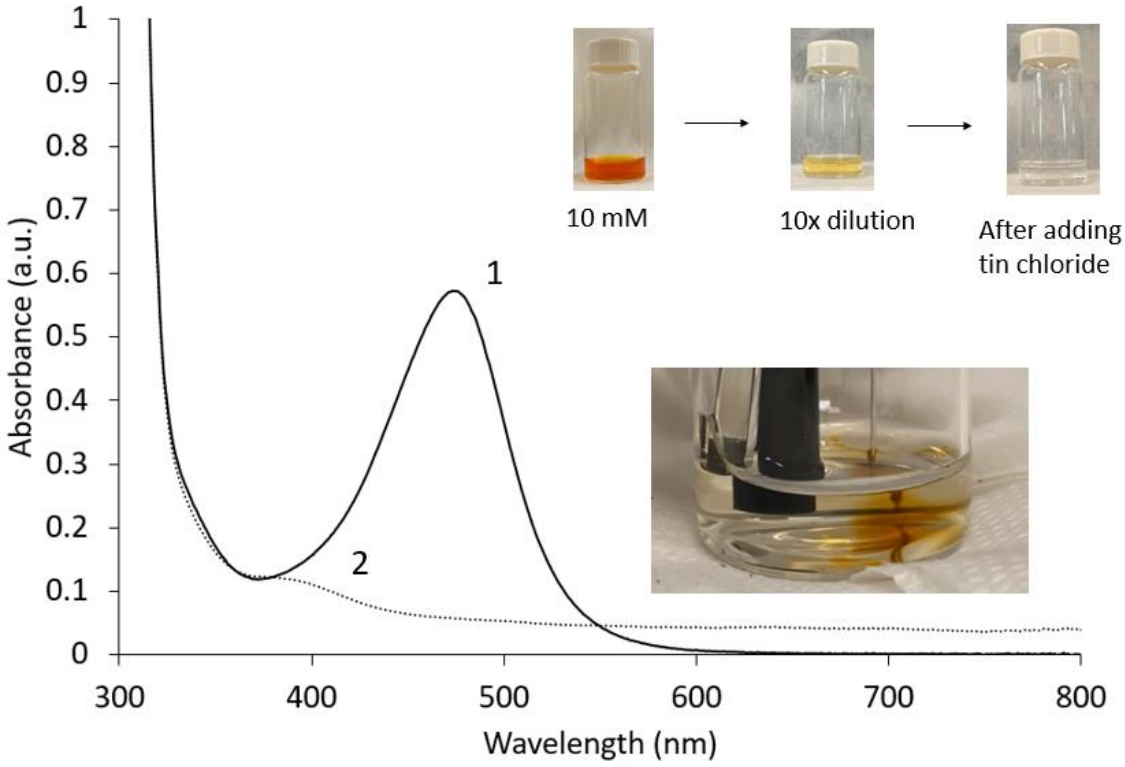

Appx II 2.6. UV-vis spectra of electrooxidation of DPP by using chronoamperometry held at -2 V for 3.5 h. (1) [DPP] = 10 mM, [TBAP] = 0.1 M, 3 mL ACN, 100x diluted (2) after the addition of excess tin chloride.

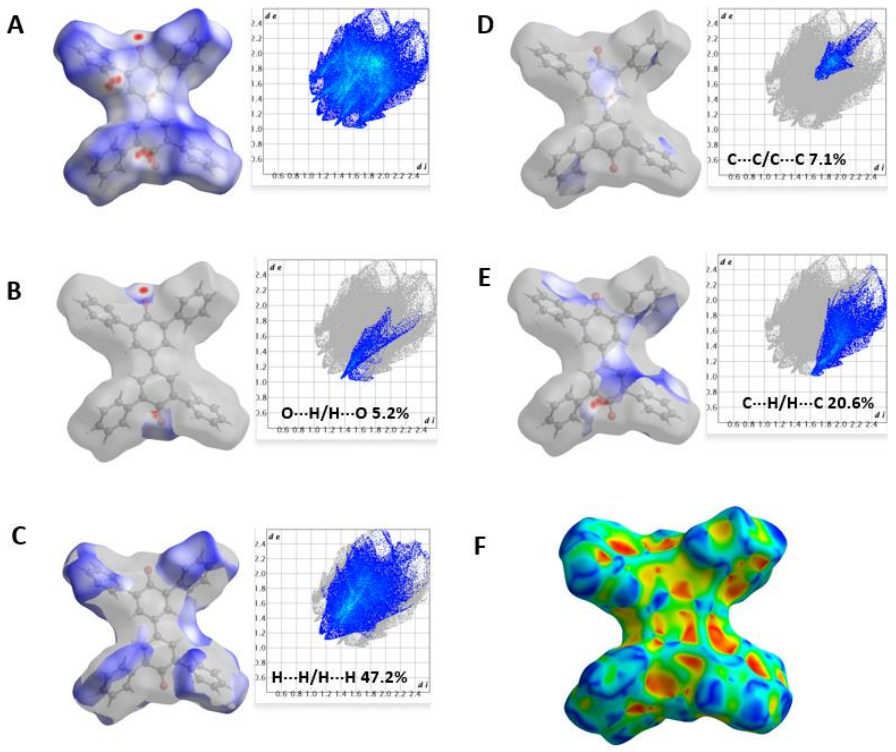

Appx II 2.7. Hirschfeld surface contacts of various atom interactions of TPDQ

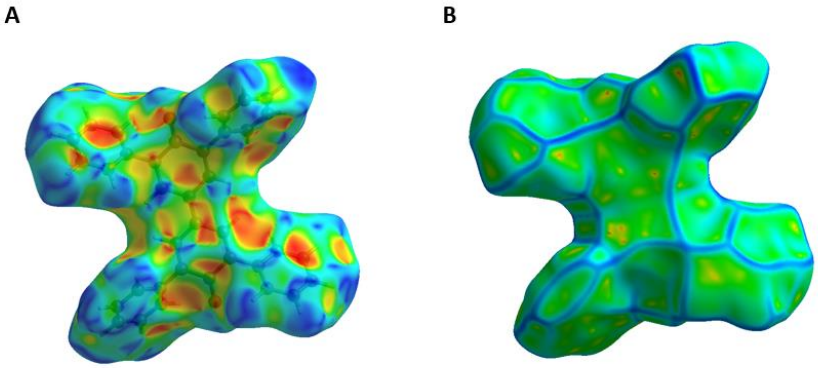

Appx II 2.8. Hirschfeld surface of TPDQ. (A) Shape index format (B) curveness format

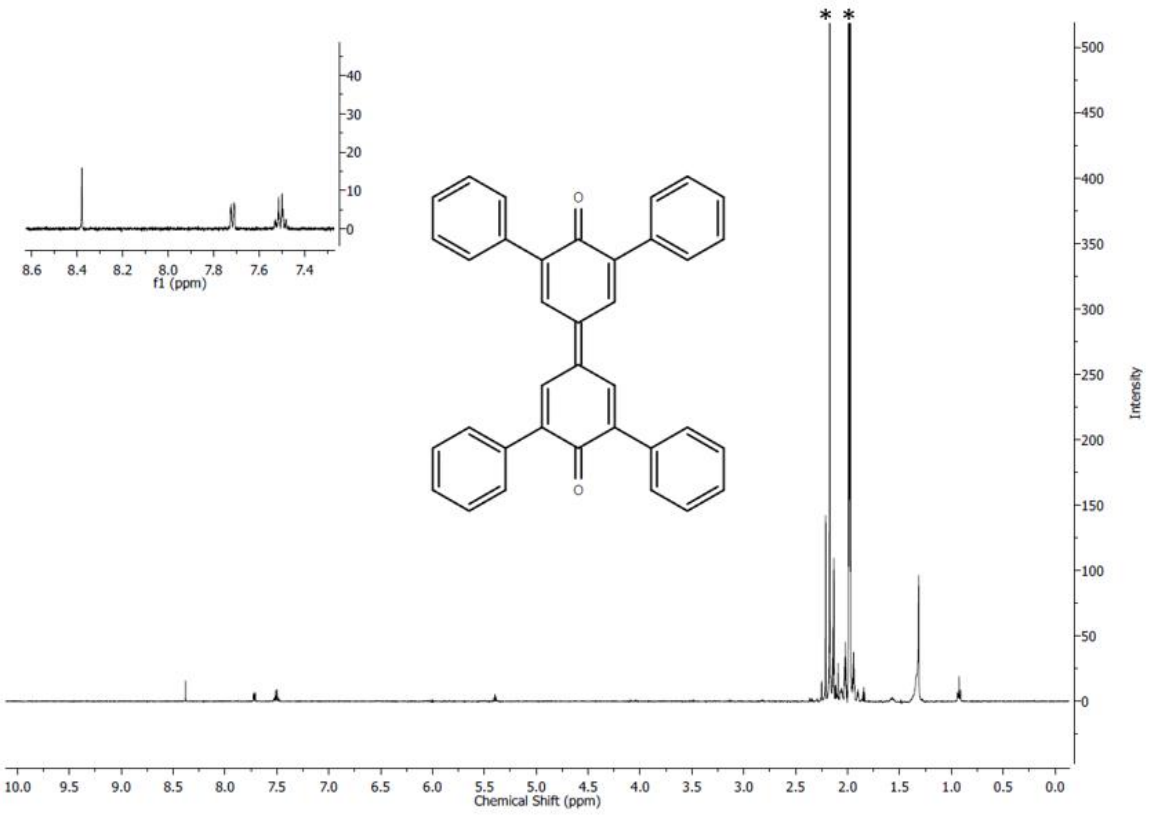

Appx II 2.10. ^{1}H NMR of TPDQ in $CDCI_3$ was obtained from the chemical oxidation of DPP using 10 mM copper perchlorate. *= impurities and solvent peak.

Hydrogen	Chemical Shift (ppm)	Integration
1	7.65; 7.64; ;7.63;7.63	8
2+3	7.51; 7.50; 7.49; 7.49; 7.48; 7.47; 7.46;	12
4	8.14	4

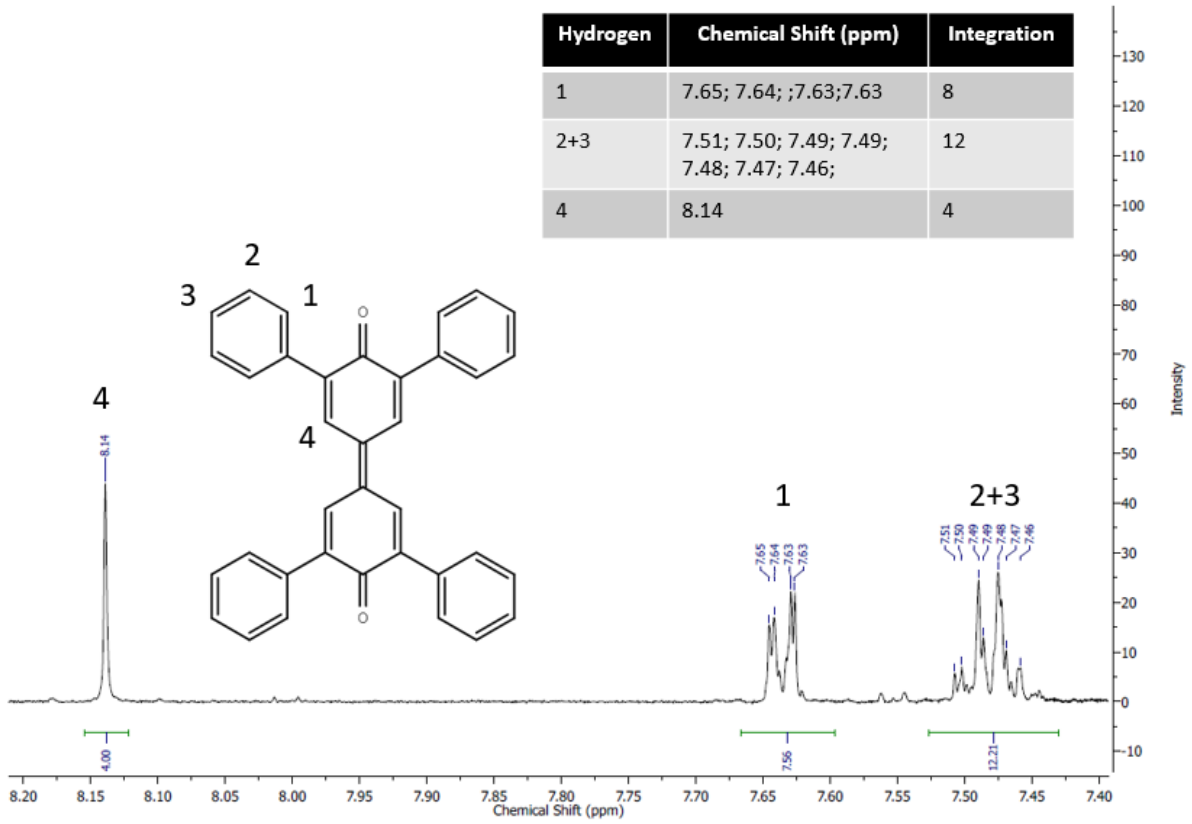

Appx II 2.11. Selected region: ^{1}H NMR of TPDQ in $CDCI_3$ obtained from the chemical oxidation of DPP using 10 mM copper perchlorate.

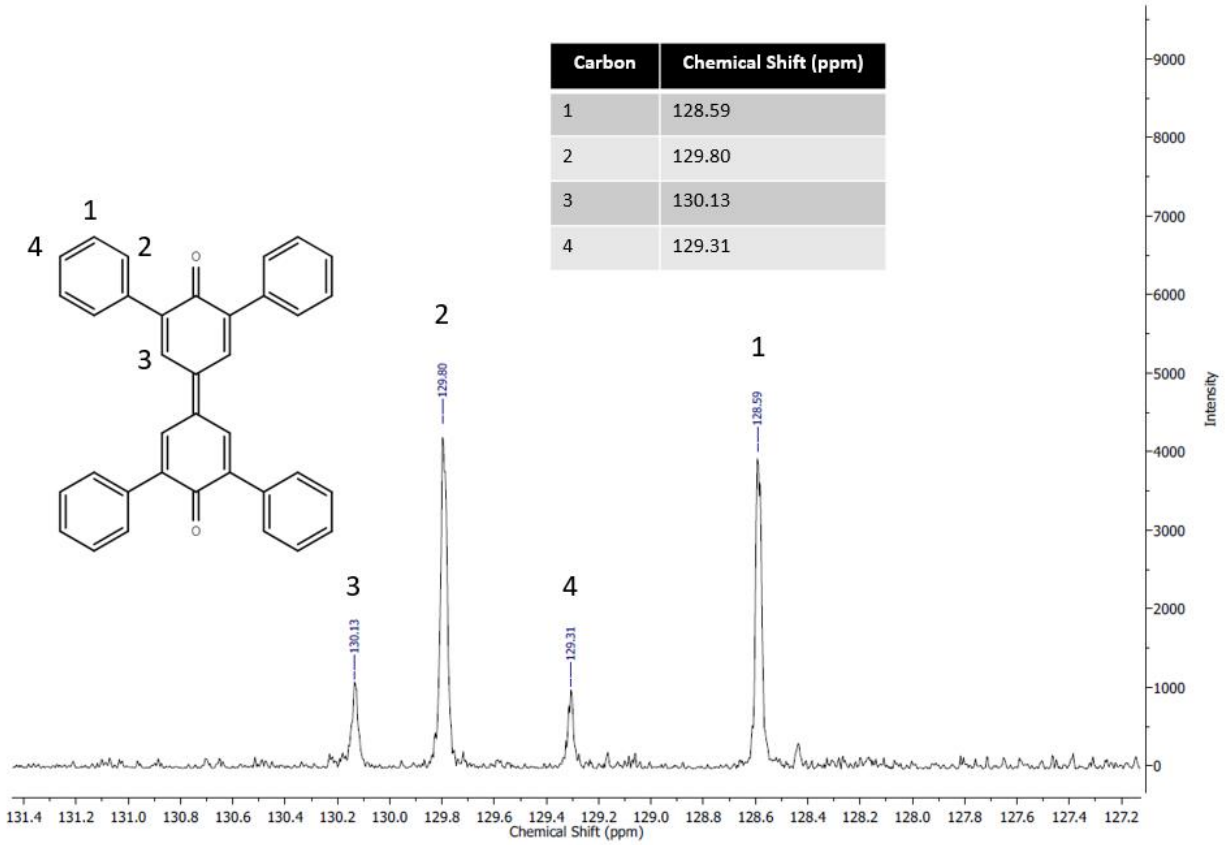

Appx II 2.12. ^{13}C NMR of TPDQ in $CDCI_3$ obtained from chemical oxidation of DPP with 10 mM copper perchlorate.

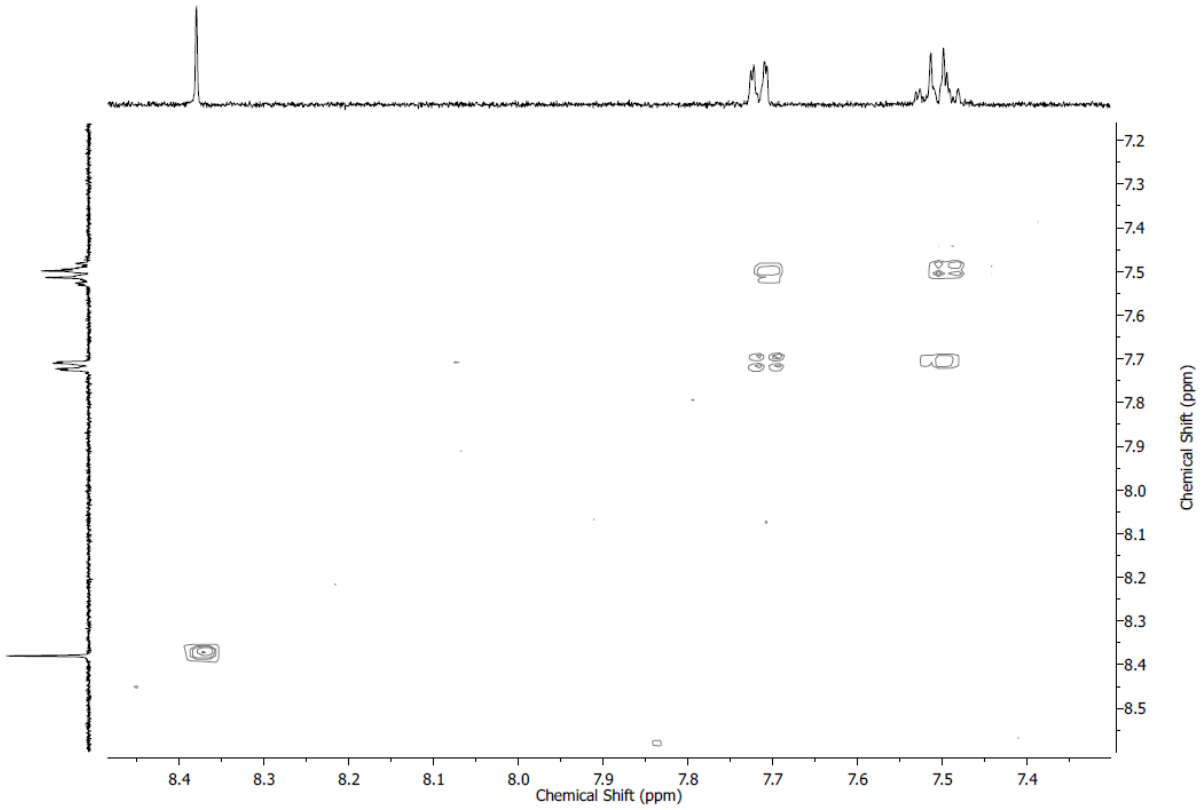

Appx II 2.13. COSY NMR of TPDQ in CD_3CN obtained from chemical oxidation of DPP using 10 mM copper perchlorate.

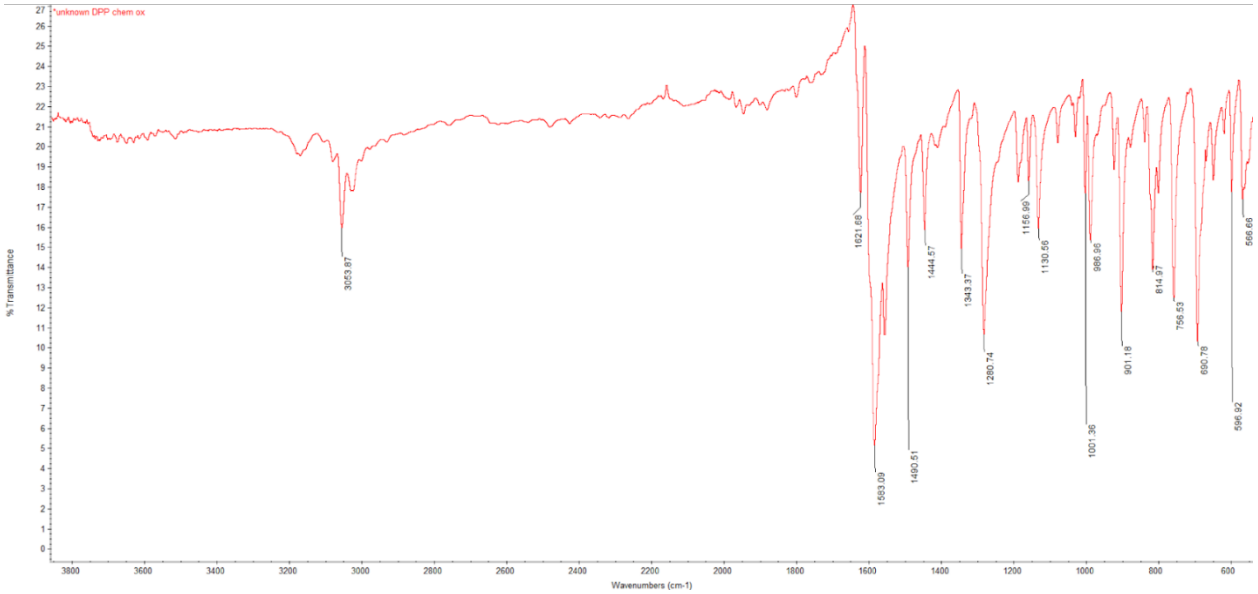

Appx II 2.14. FT-IR spectra of TPDQ filtered from the chemical oxidation of 1:1 10 mM DPP and copper perchlorate.

Hydrogen	Chemical Shift (ppm)	Integration
1	6.16	1
2	7.31; 7.29	2
3	7.11; 7.10; 7.08; 7.08	1
4	7.45; 7.44; 7.42	2
5	7.54; 7.52; 7.52; 7.51	4
6	7.60; 7.59; 7.58; 7.58	4

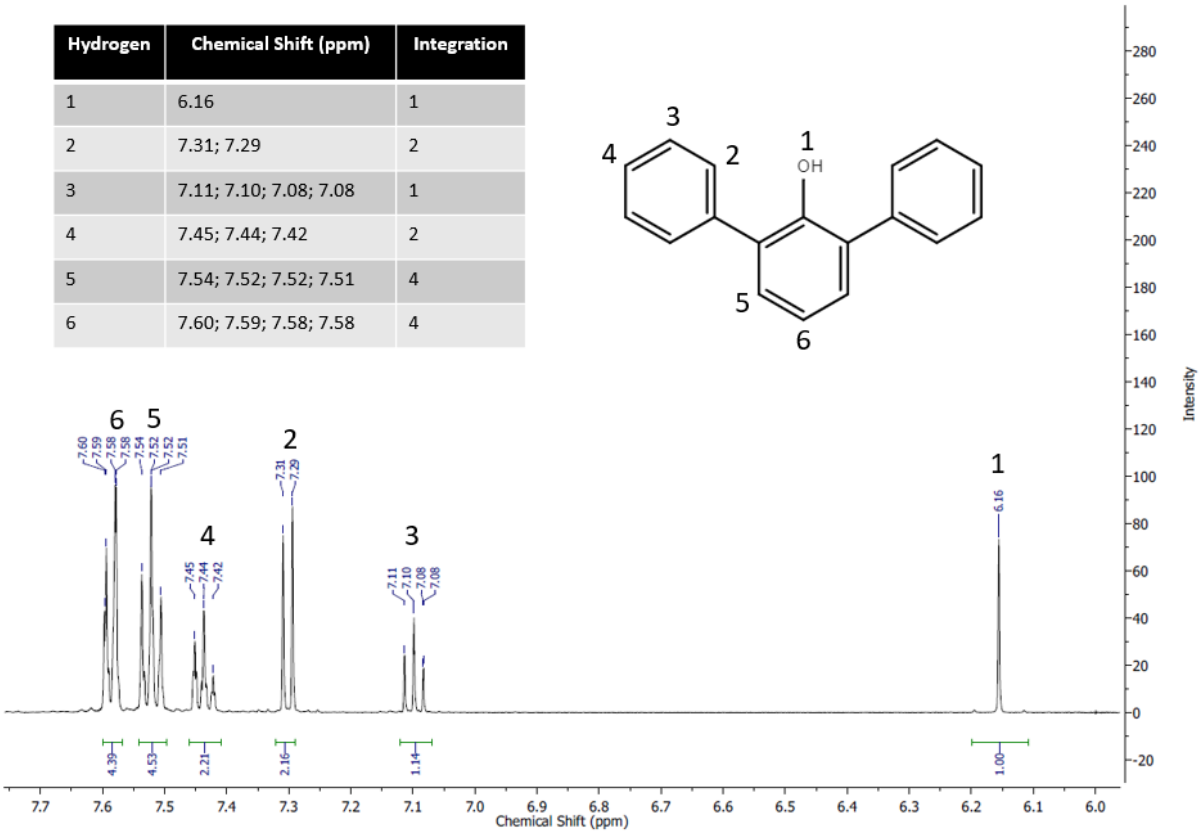

Appx II 2.15. ^{1}H NMR of DPP in CD_3CN.

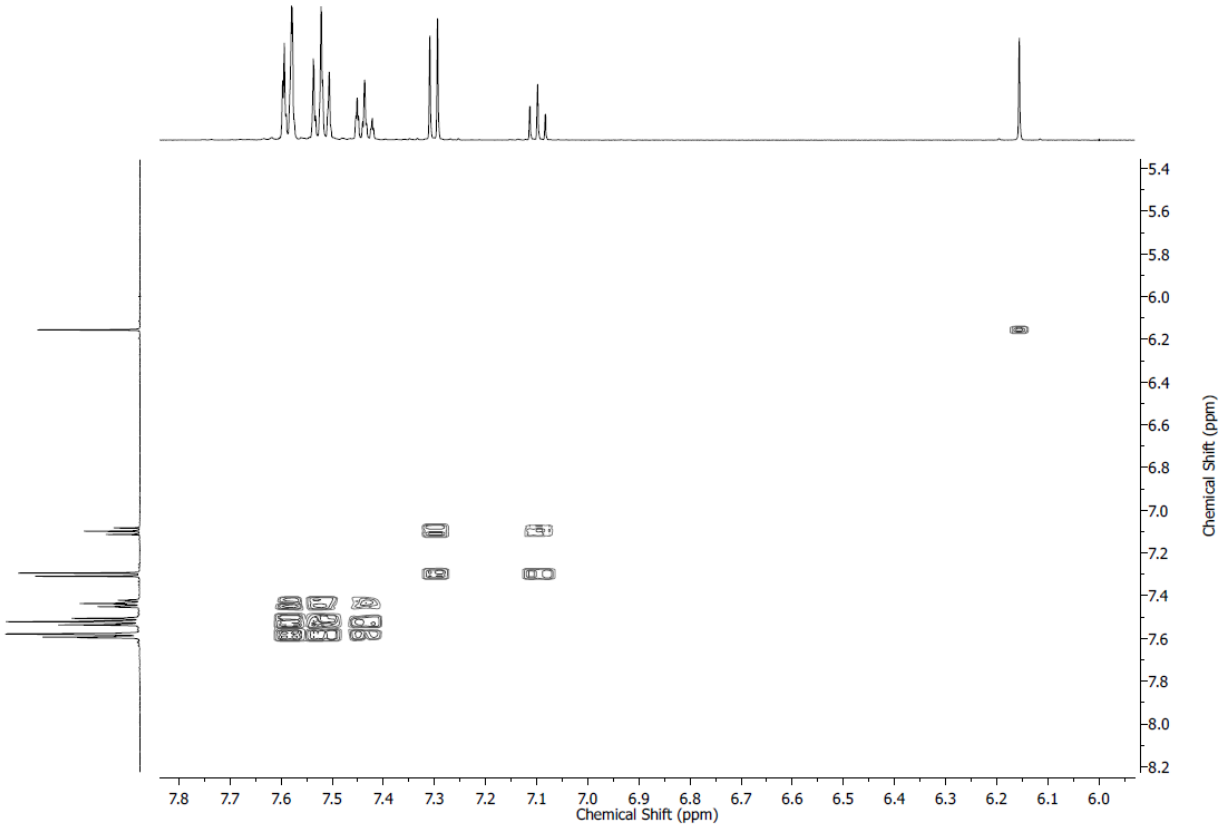

Appx II 2.16. COSY NMR of 10 mM DPP in CD_3CN.

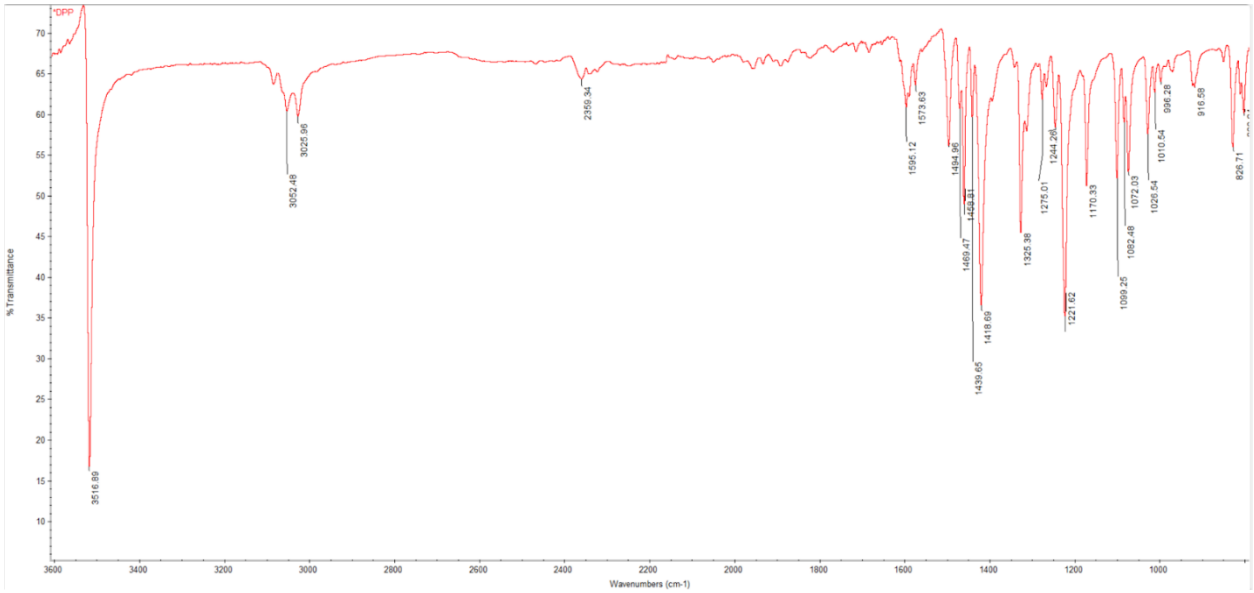

Appx II 2.17. FT-IR spectra of DPP only.

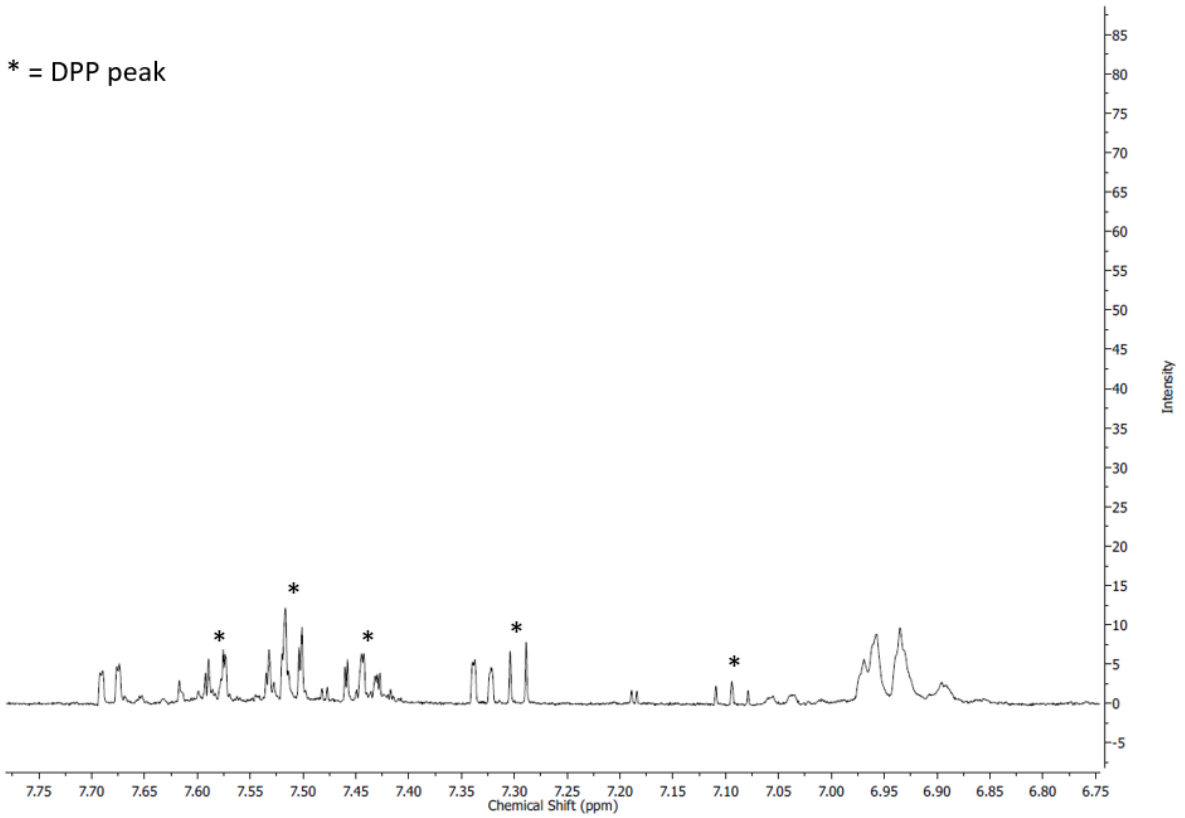

Appx II 2.18. ^{1}H NMR of 10 mM DPP after 800 scans (80 CV) with 0.1 M tetrabutylammonium perchlorate in CD_3CN (stars denote DPP).

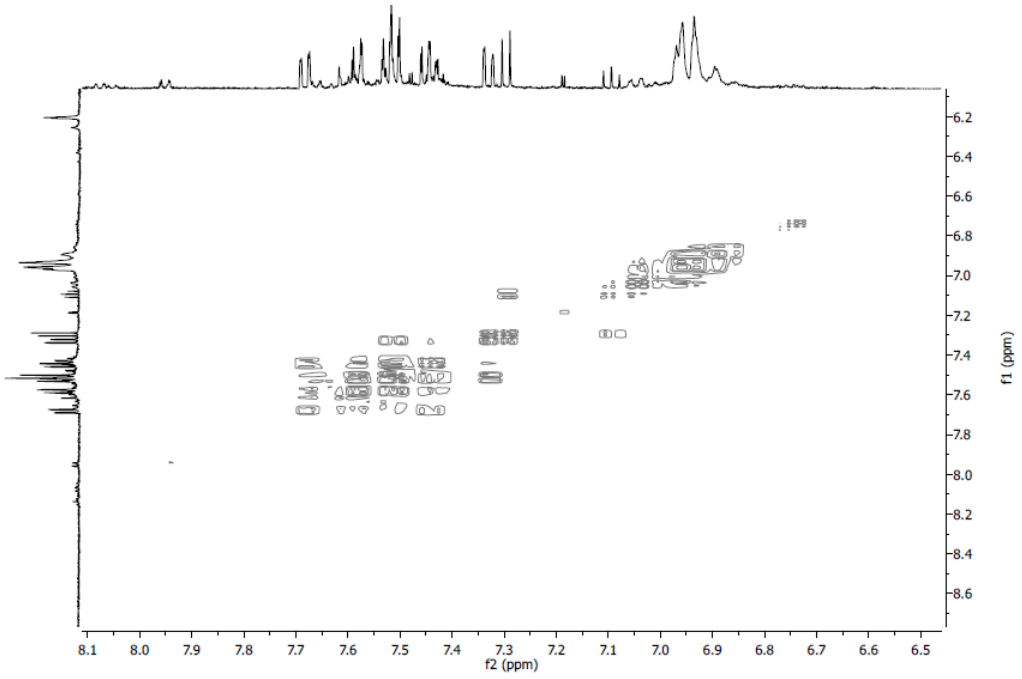

Appx II 2.19. COSY NMR of 10 mM DPP after 800 scans (80 CV) with 0.1 M tetrabutylammonium perchlorate in CD_3CN.

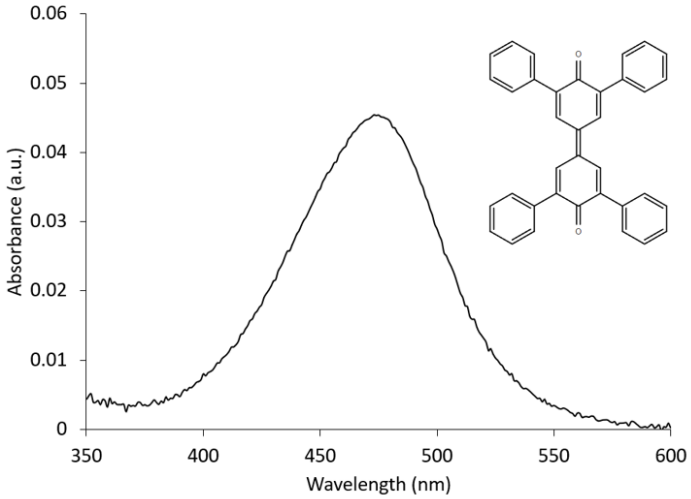

Appx II 2.20. UV-vis spectra of 0.0011mM TPDQ in ACN and $CHCl_3$ (95%/5%). Extinction coefficient used to calculate TPDQ yield: 41263.63 M^{-1} cm^{-1}.

Appx II Table 2.2. Crystal data and structure refinement for 1688_0m.

Identification code	1688_0m	
Empirical formula	C36 H24 O2	
Formula weight	488.55	
Temperature	173(2) K	
Wavelength	0.71073 Å	
Crystal system	Monoclinic	
Space group	$P2_1/n$	
Unit cell dimensions	a = 9.4398(2) Å	α= 90°.
	b = 11.5518(3) Å	β= 111.1240(10)°.
	c = 12.2585(3) Å	γ = 90°.
Volume	1246.92(5) $Å^3$	
Z	2	
Density (calculated)	1.301 Mg/m^3	
Absorption coefficient	0.079 mm^{-1}	
F(000)	512	
Crystal size	0.480 x 0.250 x 0.180 mm^3	
Theta range for data collection	2.943 to 27.532°.	
Index ranges	-12<=h<=12, -15<=k<=14, -15<=l<=15	
Reflections collected	27975	
Independent reflections	2866 [R(int) = 0.0251]	
Completeness to theta = 25.242°	99.9 %	
Absorption correction	Multi-scan	
Refinement method	Full-matrix least-squares on F^2	
Data / restraints / parameters	2866 / 0 / 172	
Goodness-of-fit on F^2	1.058	
Final R indices [I>2sigma(I)]	R1 = 0.0373, wR2 = 0.1017	
R indices (all data)	R1 = 0.0424, wR2 = 0.1060	
Extinction coefficient	n/a	
Largest diff. peak and hole	0.263 and -0.222 $e.Å^{-3}$	

Appx II Table 2.3. Atomic coordinates (x 104) and equivalent isotropic displacement parameters (Å2x 103) for 1688_0m. U(eq) is defined as one-third of the trace of the orthogonalized U_{ij} tensor.

	x	y	z	U(eq)
O(1)	2079(1)	3425(1)	3408(1)	28(1)
C(1)	2846(1)	2559(1)	3825(1)	20(1)
C(2)	3365(1)	2295(1)	5093(1)	19(1)
C(3)	4214(1)	1332(1)	5510(1)	20(1)
C(4)	4575(1)	498(1)	4771(1)	19(1)
C(5)	4031(1)	749(1)	3535(1)	20(1)
C(6)	3272(1)	1733(1)	3074(1)	20(1)
C(7)	2999(1)	3114(1)	5885(1)	20(1)
C(8)	1541(1)	3573(1)	5620(1)	26(1)
C(9)	1246(2)	4340(1)	6383(1)	33(1)
C(10)	2393(2)	4672(1)	7408(1)	35(1)
C(11)	3833(2)	4209(1)	7690(1)	31(1)
C(12)	4132(1)	3430(1)	6940(1)	24(1)
C(13)	2859(1)	1990(1)	1811(1)	21(1)
C(14)	2146(1)	1152(1)	977(1)	26(1)
C(15)	1831(2)	1365(1)	-202(1)	32(1)
C(16)	2242(2)	2407(1)	-558(1)	34(1)
C(17)	2953(2)	3243(1)	267(1)	33(1)
C(18)	3247(1)	3049(1)	1445(1)	27(1)

Appx II Table 2.4. Bond lengths [Å] and angles [°] for 1688_0m.

O(1)-C(1)	1.2328(12)
C(1)-C(6)	1.4778(14)
C(1)-C(2)	1.4830(14)
C(2)-C(3)	1.3578(14)
C(2)-C(7)	1.4838(14)
C(3)-C(4)	1.4452(14)
C(3)-H(3)	0.9500
C(4)-C(4)#1	1.4005(19)
C(4)-C(5)	1.4428(14)
C(5)-C(6)	1.3539(14)
C(5)-H(5)	0.9500
C(6)-C(13)	1.4840(14)
C(7)-C(12)	1.3973(15)
C(7)-C(8)	1.3991(15)
C(8)-C(9)	1.3887(17)
C(8)-H(8)	0.9500
C(9)-C(10)	1.384(2)
C(9)-H(9)	0.9500
C(10)-C(11)	1.3836(18)
C(10)-H(10)	0.9500
C(11)-C(12)	1.3865(16)
C(11)-H(11)	0.9500
C(12)-H(12)	0.9500
C(13)-C(14)	1.3933(16)
C(13)-C(18)	1.3963(16)
C(14)-C(15)	1.3886(16)
C(14)-H(14)	0.9500
C(15)-C(16)	1.3830(19)
C(15)-H(15)	0.9500
C(16)-C(17)	1.3837(19)
C(16)-H(16)	0.9500
C(17)-C(18)	1.3876(16)
C(17)-H(17)	0.9500
C(18)-H(18)	0.9500

O(1)-C(1)-C(6)	121.12(9)
O(1)-C(1)-C(2)	121.58(10)
C(6)-C(1)-C(2)	117.30(9)
C(3)-C(2)-C(1)	119.38(9)
C(3)-C(2)-C(7)	121.36(9)
C(1)-C(2)-C(7)	119.21(9)
C(2)-C(3)-C(4)	123.34(9)
C(2)-C(3)-H(3)	118.3
C(4)-C(3)-H(3)	118.3
C(4)#1-C(4)-C(5)	121.49(12)
C(4)#1-C(4)-C(3)	121.78(12)
C(5)-C(4)-C(3)	116.72(9)
C(6)-C(5)-C(4)	122.76(10)
C(6)-C(5)-H(5)	118.6
C(4)-C(5)-H(5)	118.6
C(5)-C(6)-C(1)	120.25(9)
C(5)-C(6)-C(13)	120.25(10)
C(1)-C(6)-C(13)	119.50(9)
C(12)-C(7)-C(8)	118.48(10)
C(12)-C(7)-C(2)	119.42(9)
C(8)-C(7)-C(2)	122.09(10)
C(9)-C(8)-C(7)	120.31(11)
C(9)-C(8)-H(8)	119.8
C(7)-C(8)-H(8)	119.8
C(10)-C(9)-C(8)	120.43(11)
C(10)-C(9)-H(9)	119.8
C(8)-C(9)-H(9)	119.8
C(11)-C(10)-C(9)	119.84(11)
C(11)-C(10)-H(10)	120.1
C(9)-C(10)-H(10)	120.1
C(10)-C(11)-C(12)	120.05(11)
C(10)-C(11)-H(11)	120.0
C(12)-C(11)-H(11)	120.0
C(11)-C(12)-C(7)	120.85(11)
C(11)-C(12)-H(12)	119.6

C(7)-C(12)-H(12)	119.6
C(14)-C(13)-C(18)	119.11(10)
C(14)-C(13)-C(6)	120.14(10)
C(18)-C(13)-C(6)	120.66(10)
C(15)-C(14)-C(13)	120.44(11)
C(15)-C(14)-H(14)	119.8
C(13)-C(14)-H(14)	119.8
C(16)-C(15)-C(14)	120.19(12)
C(16)-C(15)-H(15)	119.9
C(14)-C(15)-H(15)	119.9
C(15)-C(16)-C(17)	119.66(11)
C(15)-C(16)-H(16)	120.2
C(17)-C(16)-H(16)	120.2
C(16)-C(17)-C(18)	120.69(12)
C(16)-C(17)-H(17)	119.7
C(18)-C(17)-H(17)	119.7
C(17)-C(18)-C(13)	119.89(11)
C(17)-C(18)-H(18)	120.1
C(13)-C(18)-H(18)	120.1

Symmetry transformations used to generate equivalent atoms:

#1 -x+1,-y,-z+1

Appx II Table 2.5. Anisotropic displacement parameters (Å2x 103) for 1688_0m. The anisotropic displacement factor exponent takes the form: -2p2[h2 a*2U11 + ... + 2 h k a* b* U12]

	U^{11}	U^{22}	U^{33}	U^{23}	U^{13}	U^{12}
O(1)	36(1)	20(1)	22(1)	3(1)	4(1)	9(1)
C(1)	20(1)	16(1)	19(1)	2(1)	3(1)	-1(1)
C(2)	18(1)	19(1)	19(1)	1(1)	5(1)	-1(1)
C(3)	22(1)	20(1)	17(1)	3(1)	6(1)	0(1)
C(4)	19(1)	17(1)	19(1)	3(1)	6(1)	0(1)
C(5)	23(1)	19(1)	18(1)	2(1)	6(1)	2(1)
C(6)	20(1)	19(1)	17(1)	2(1)	4(1)	0(1)
C(7)	22(1)	19(1)	20(1)	4(1)	9(1)	2(1)
C(8)	23(1)	28(1)	28(1)	6(1)	10(1)	4(1)
C(9)	33(1)	37(1)	38(1)	12(1)	22(1)	14(1)
C(10)	50(1)	34(1)	30(1)	3(1)	27(1)	11(1)
C(11)	39(1)	37(1)	20(1)	-1(1)	13(1)	2(1)
C(12)	25(1)	30(1)	20(1)	2(1)	9(1)	4(1)
C(13)	22(1)	21(1)	18(1)	4(1)	6(1)	7(1)
C(14)	32(1)	22(1)	23(1)	2(1)	8(1)	7(1)
C(15)	38(1)	34(1)	20(1)	-3(1)	7(1)	11(1)
C(16)	43(1)	42(1)	20(1)	9(1)	13(1)	17(1)
C(17)	40(1)	31(1)	30(1)	13(1)	17(1)	10(1)
C(18)	31(1)	24(1)	24(1)	5(1)	9(1)	4(1)

Appx II Table 2.6. Hydrogen coordinates (x 104) and isotropic displacement parameters (Å2x 10 3) for 1688_0m.

	x	y	z	U(eq)
H(3)	4591	1201	6330	24
H(5)	4213	201	3023	24
H(8)	750	3358	4914	32
H(9)	250	4640	6201	40
H(10)	2192	5215	7915	41
H(11)	4618	4426	8399	38
H(12)	5120	3108	7145	29
H(14)	1873	430	1216	31
H(15)	1332	792	-766	38
H(16)	2036	2549	-1364	41
H(17)	3243	3956	23	39
H(18)	3712	3636	2002	32

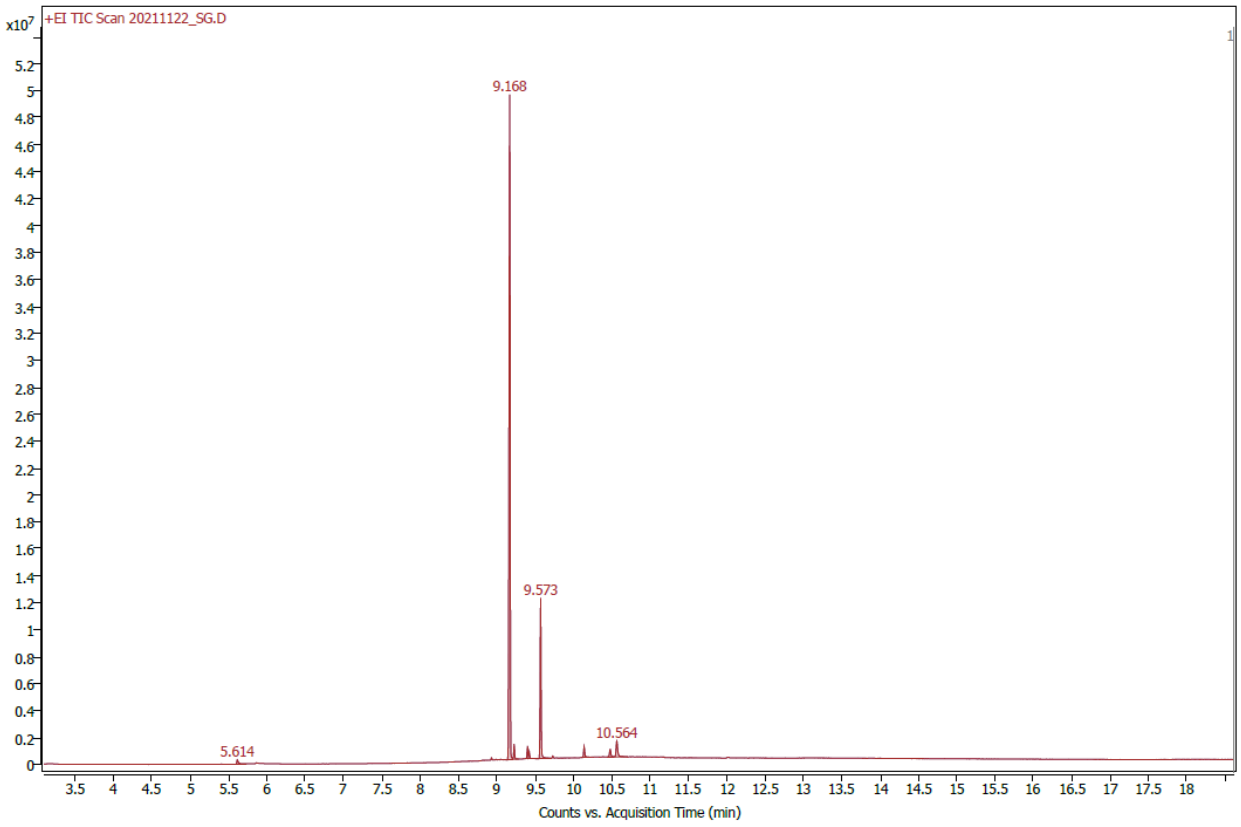

Appx II 2.21. Chromatogram of electrochemical oxidation of DPP from -3 to 3 V (80 CV).

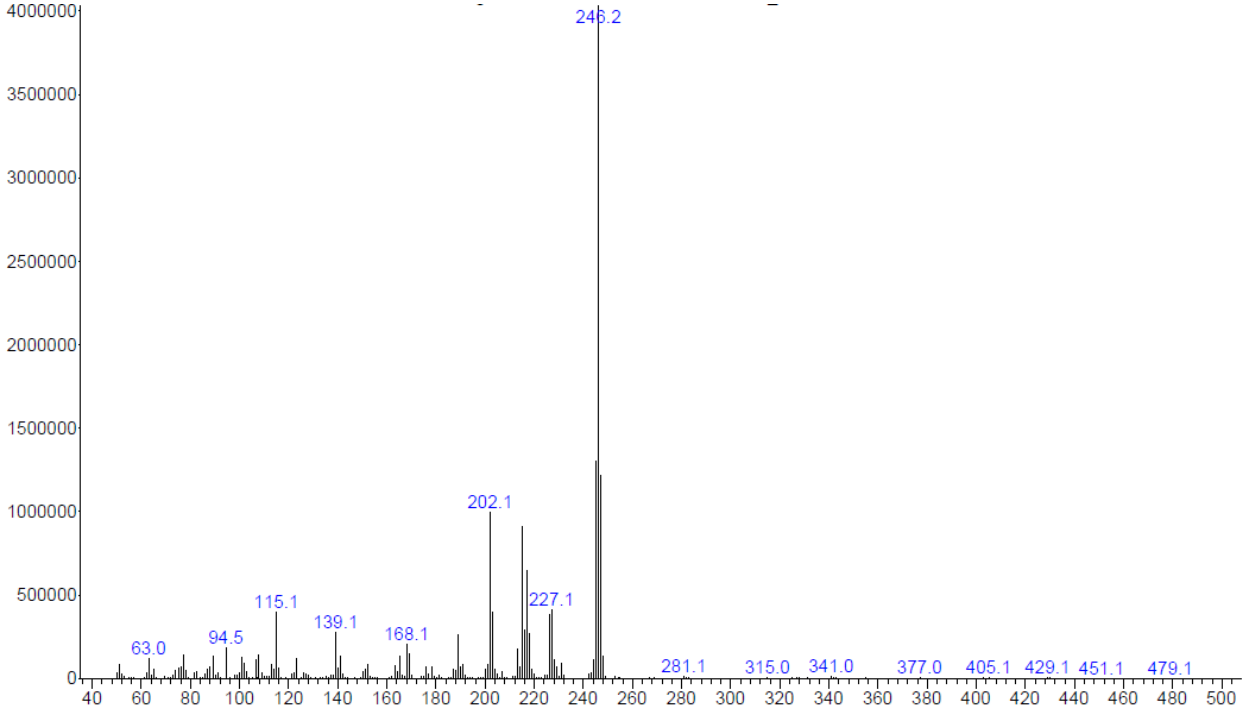

Appx II 2.22. Mass spectra of DPP standard (9.116 - 9.153 min) ([$DPP^{+\bullet}$] = *m/z* 246.1).

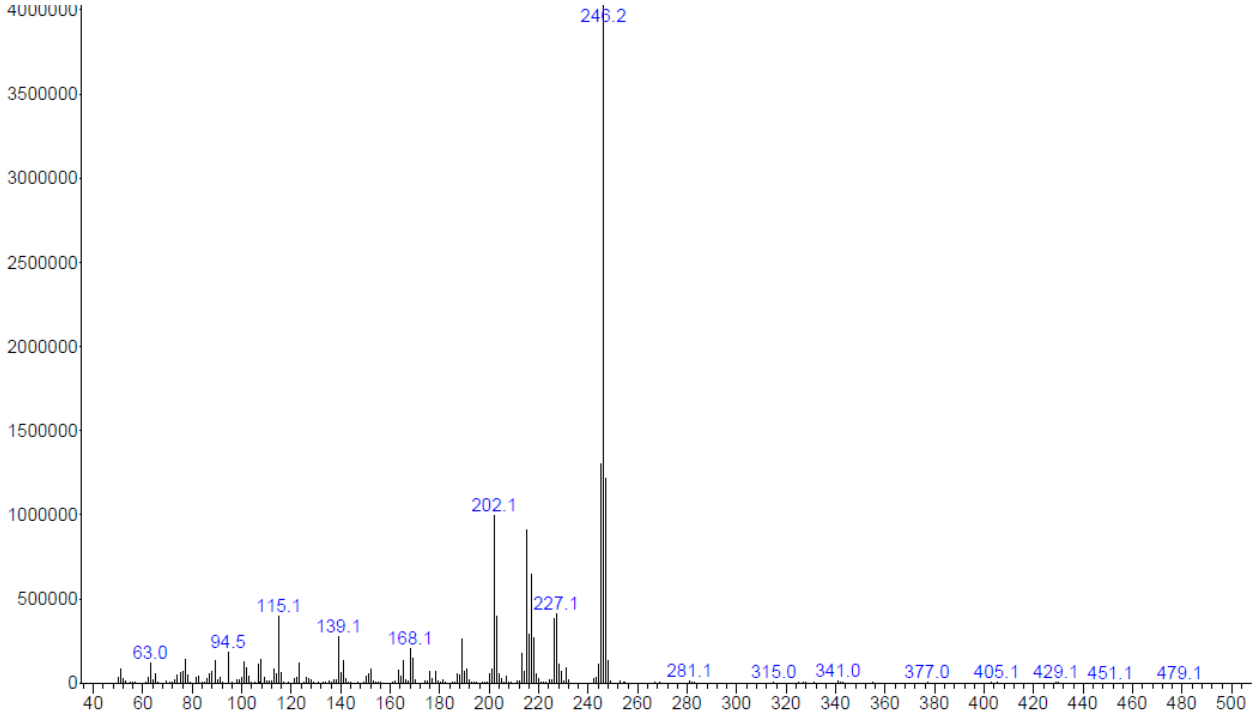

Appx II 2.23. Mass spectra of DPP from -3 to 3 V electrochemical oxidation solution (9.142 - 9.184 min) ([$DPP^{+\bullet}$] = *m/z* 246.2).

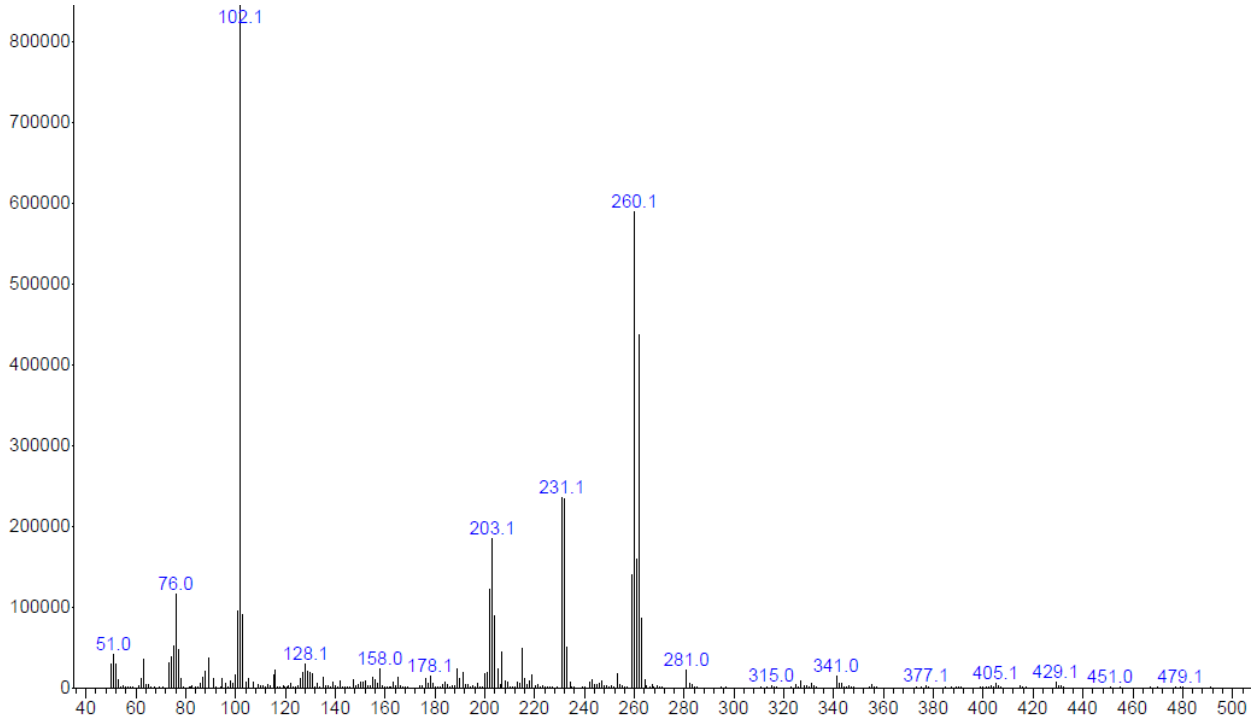

Appx II 2.24. Mass spectra of 2,6-DPPQ from -3 to 3 V electrochemical oxidation solution (RT: 9.557-9.589 min) ([$DPPQ^{+\bullet}$] = *m/*z 260.1).

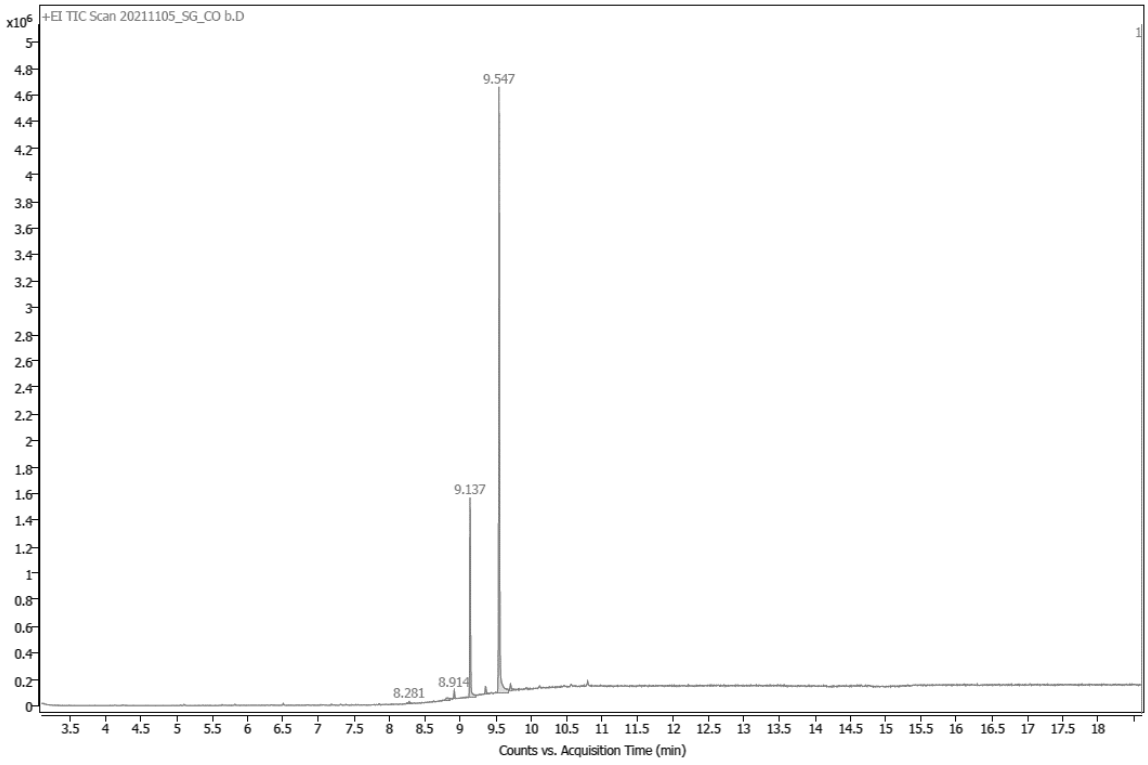

Appx II 2.25. Chromatogram of DPP oxidation with copper perchlorate.

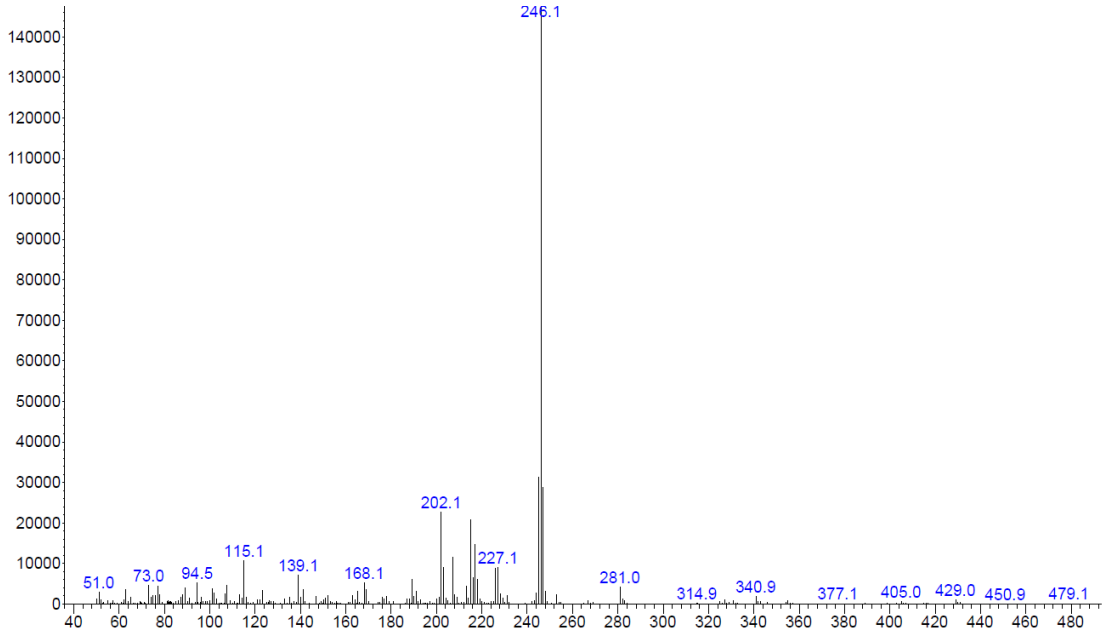

Appx II 2.26. Mass spectra of DPP from chemical oxidation solution (RT 9.122-9.158 min) ([$DPP^{+\bullet}$] = *m/z* 246.1).

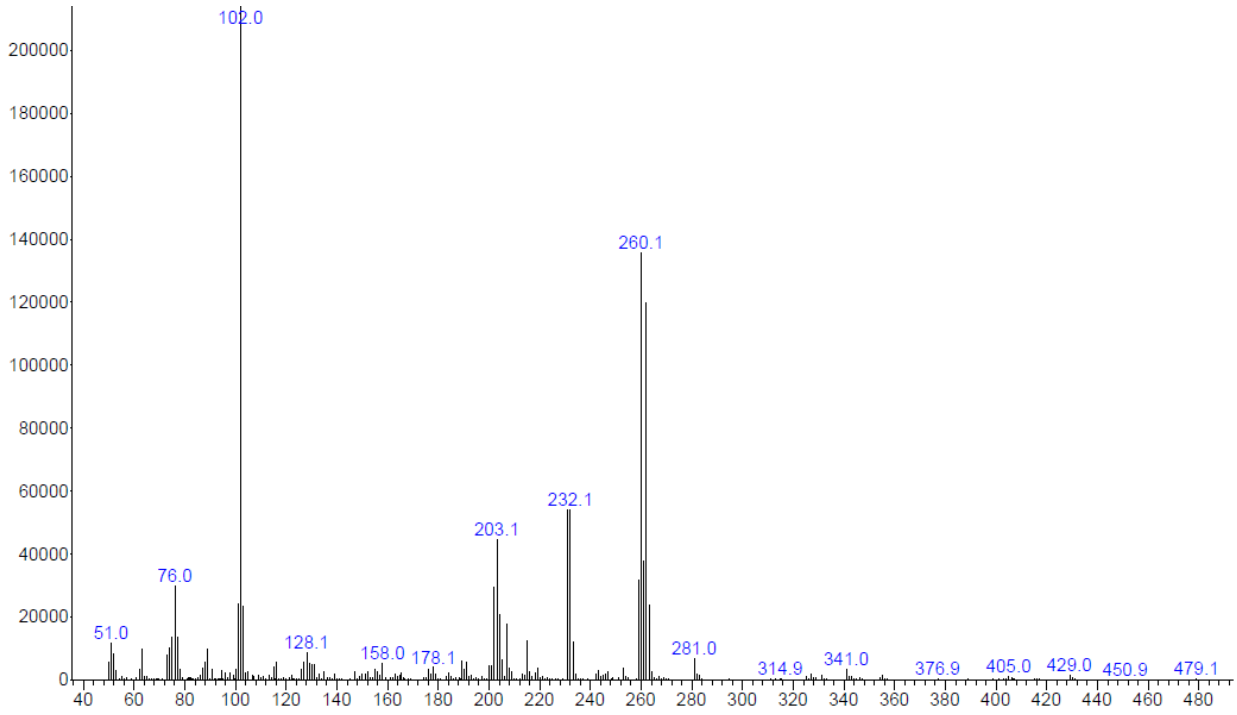

Appx II 2.27. Mass spectra of 2,6-DPPQ from chemical oxidation solution (9.526 - 9.573 min). ([$DPPQ^{+\bullet}$] = *m/z* 260.1)

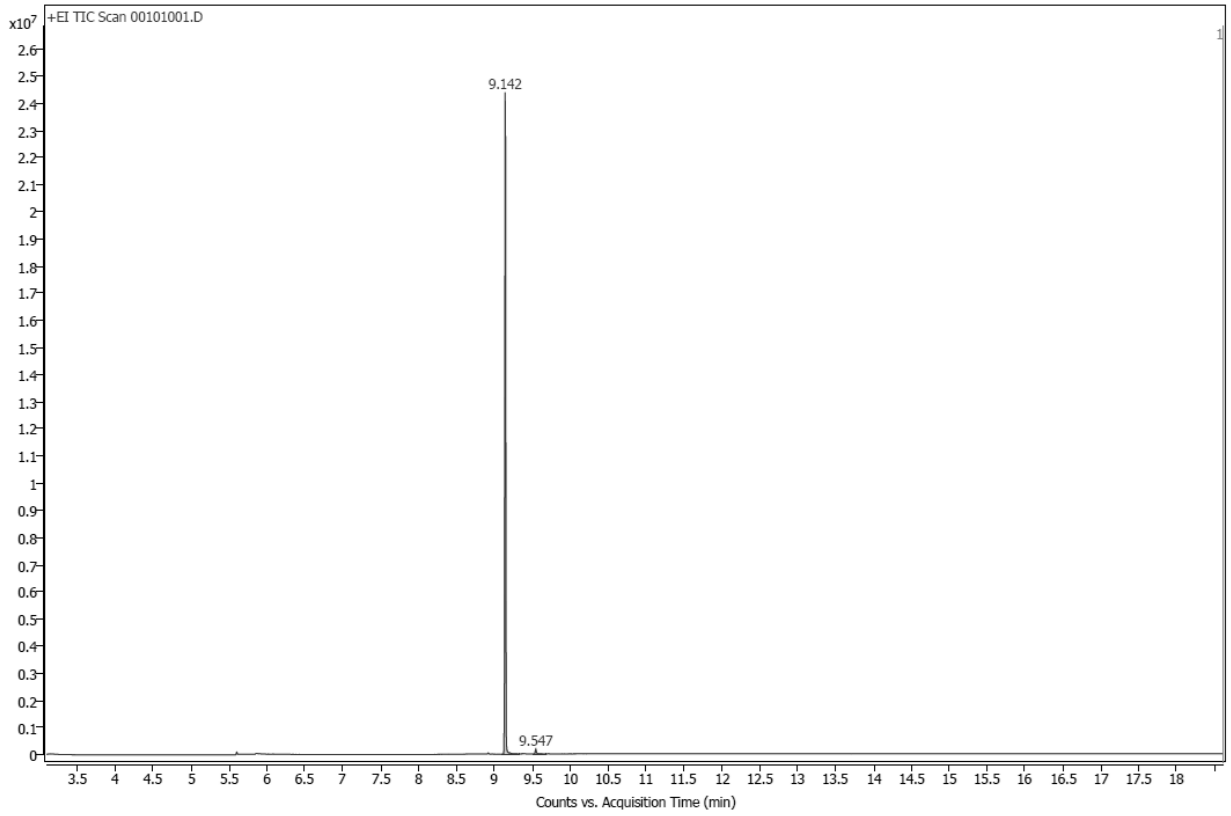

Appx II 2.28. Chromatogram of electrochemical oxidation solution of DPP from -3 to 0 V (20 CV).

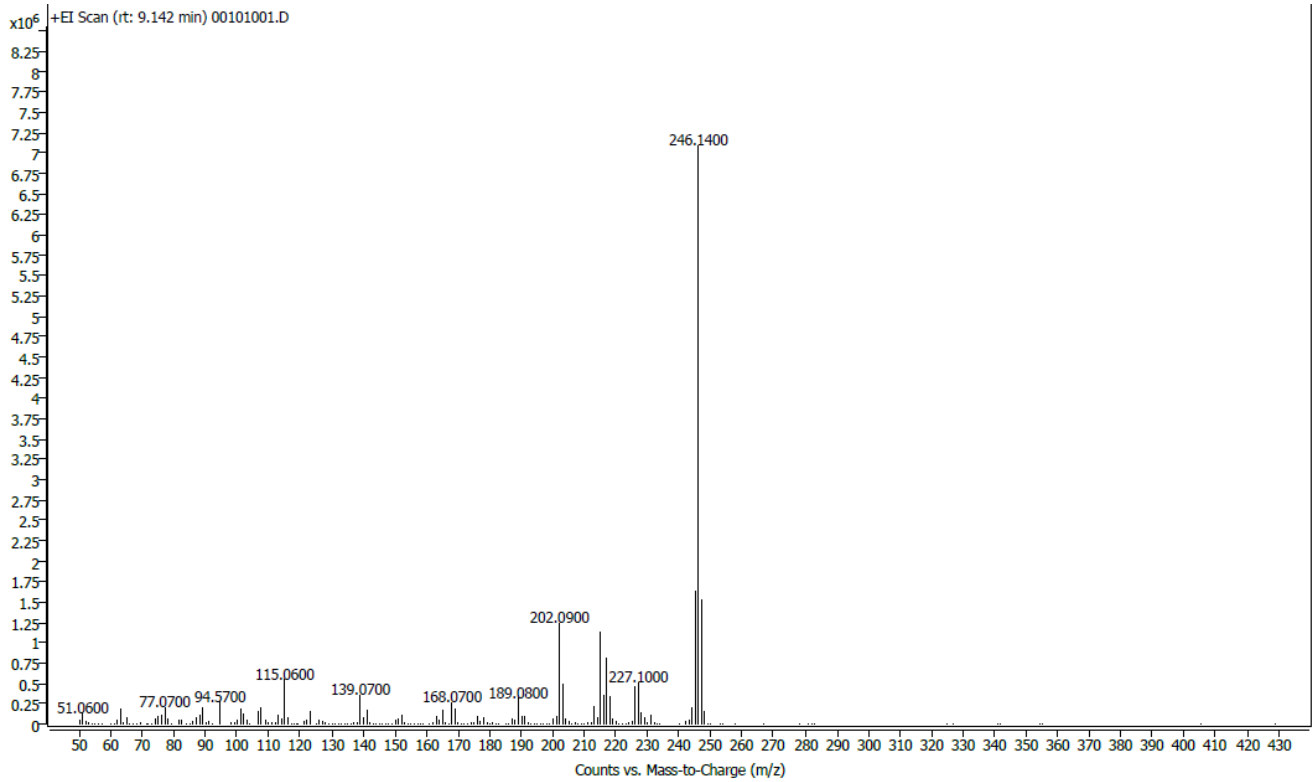

Appx II 2.28. Mass spectra of DPP from electrochemical oxidation solution at -3 to 0 V (RT: 9.142 min) ([$DPP^{+\bullet}$] = *m/z* 246.1).

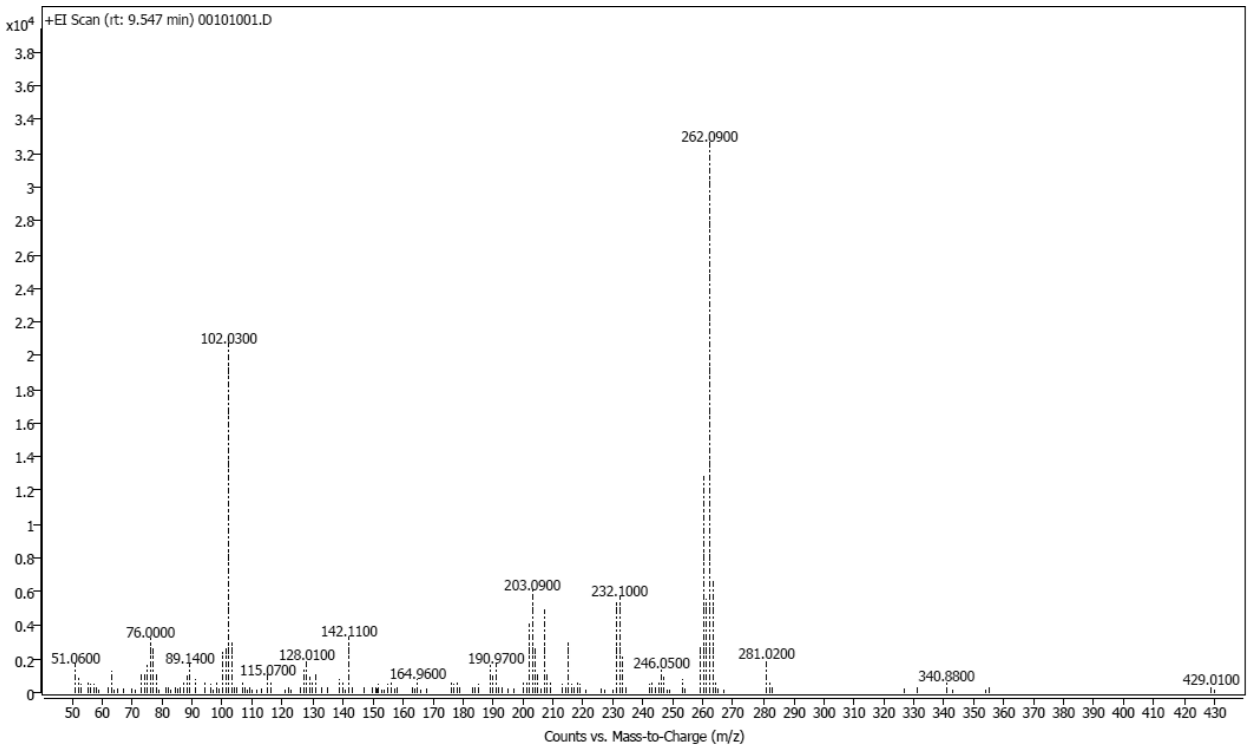

Appx II 2.29. Mass spectra of 2,6-DPPQ from electrochemical oxidation solution at -3 to 0 V (RT: 9.547 min). ([$DPPQ^{+\bullet}$] = *m/*z 260.1)

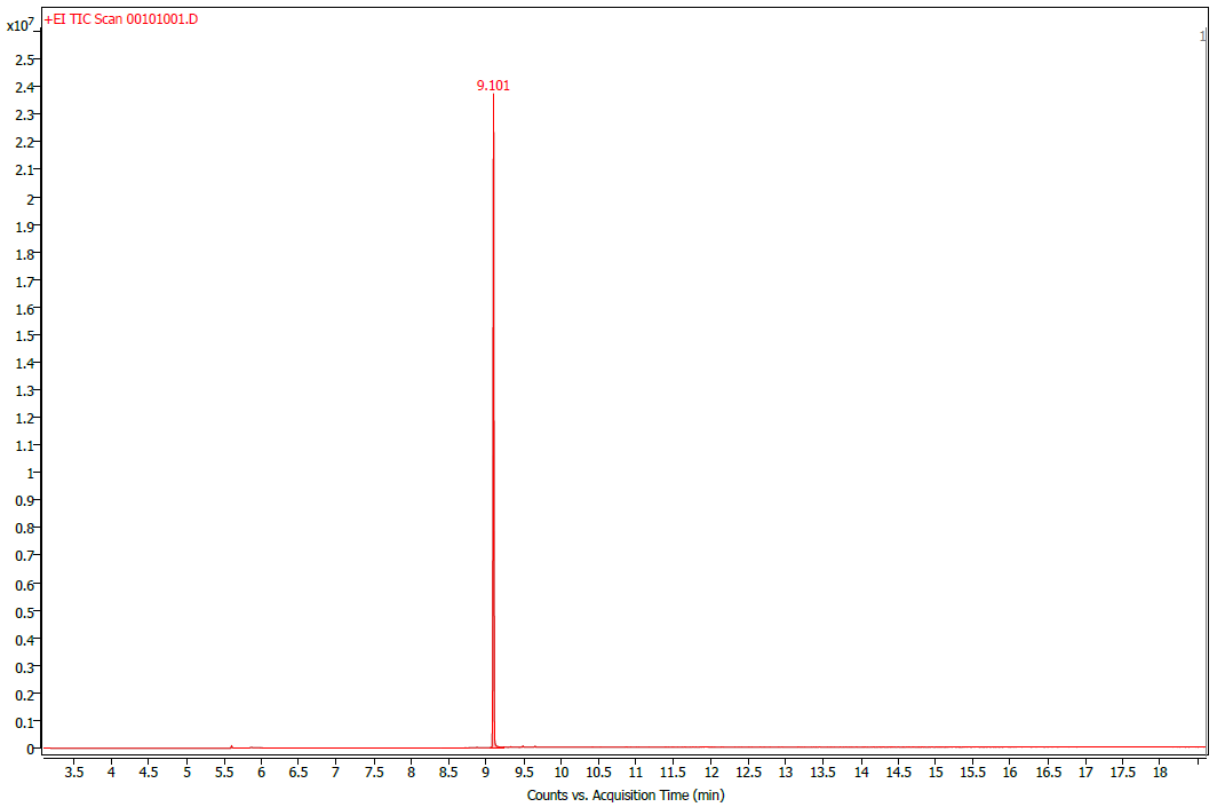

Appx II 2.30. Chromatogram of electrochemical oxidation solution of DPP from 3 to 0 V (20 CV).

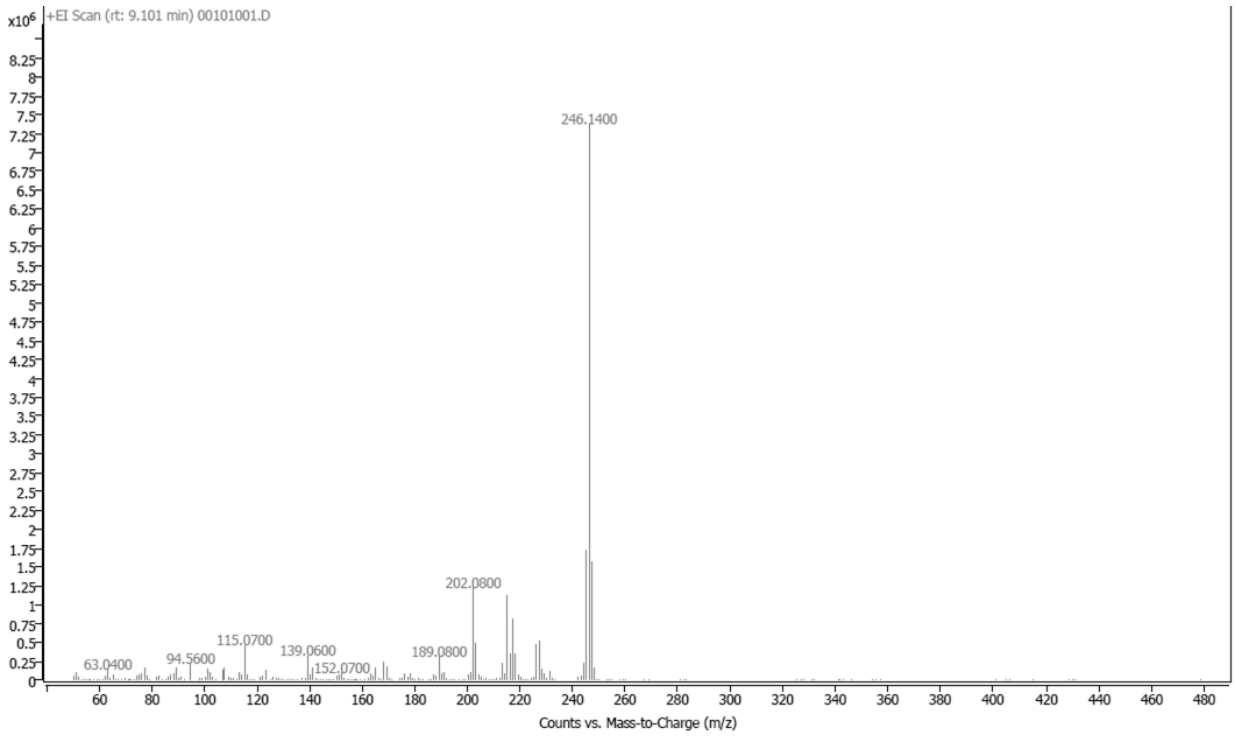

Appx II 2.31. Mass spectra of DPP from electrochemical oxidation solution at 3 to 0 V (RT: 9.101 min) ([$DPP^{+\bullet}$] = *m/z* 246.1).

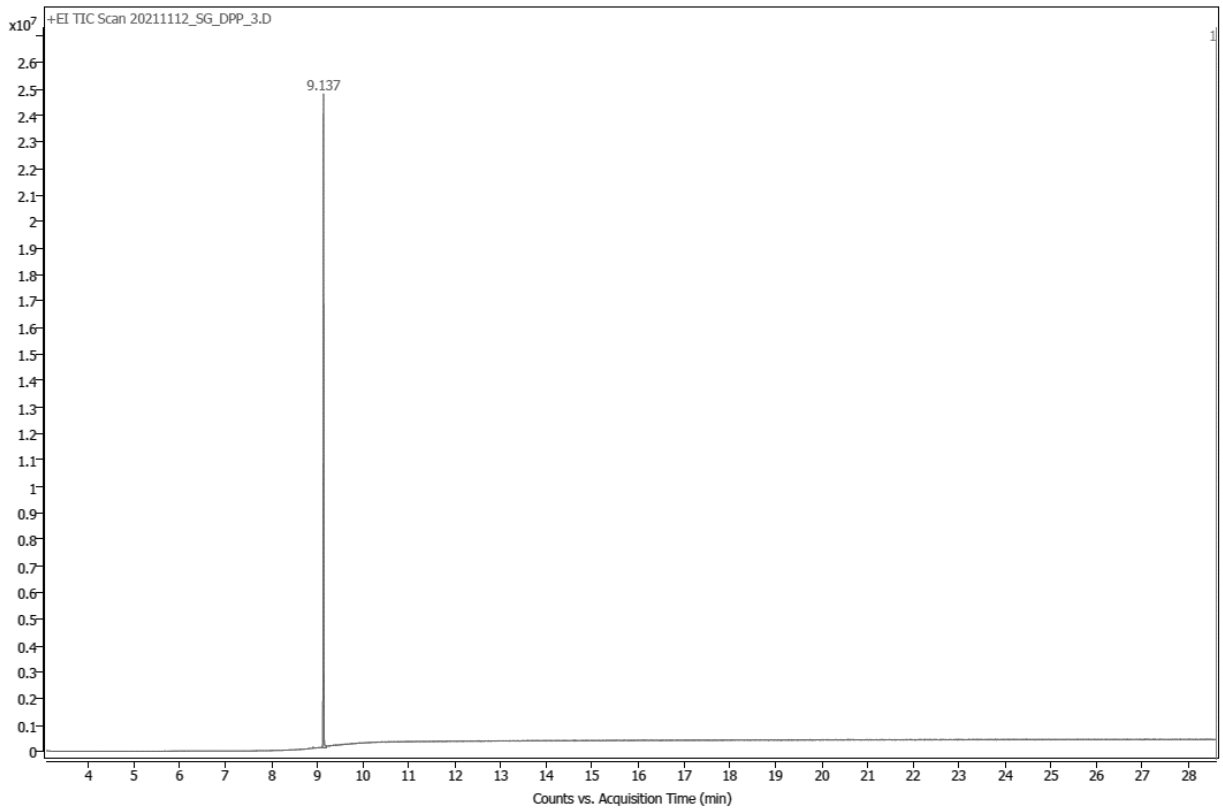

Appx II 2.32. Chromatogram of DPP only (RT: 9.137 min).

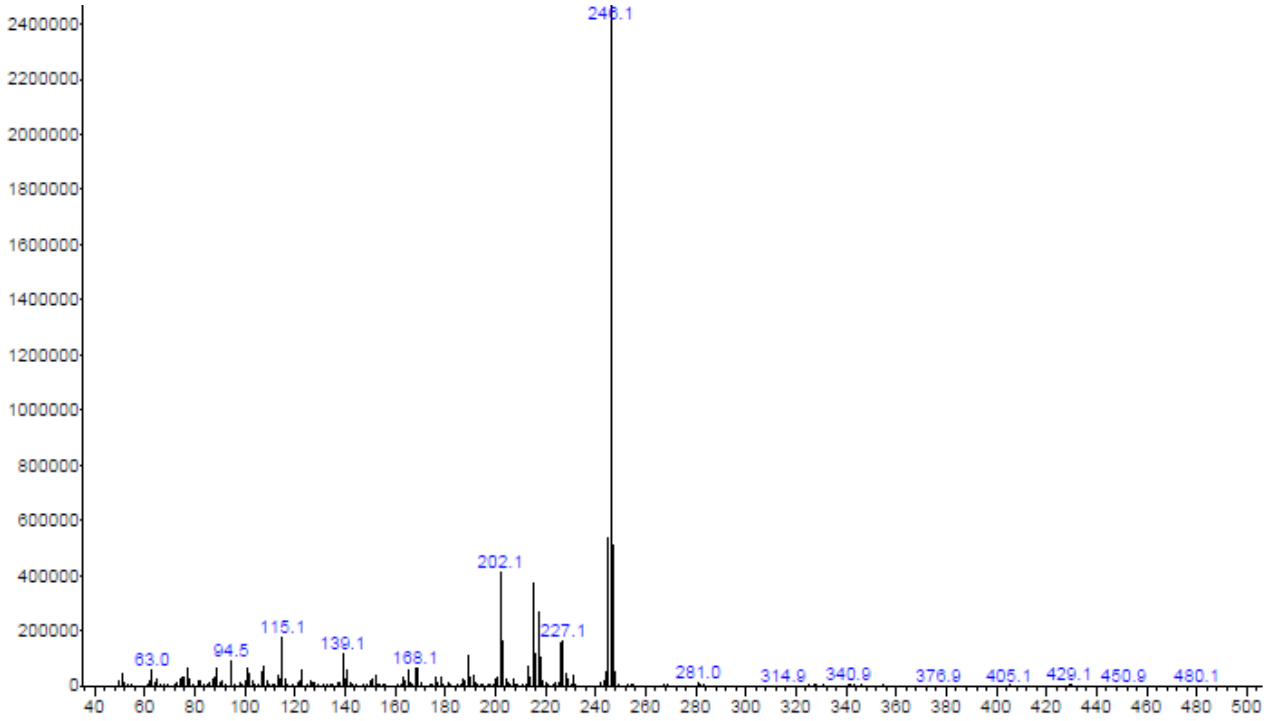

Appx II 2.33. Mass spectra of DPP (RT: 9.137 min) ([$DPP^{+\bullet}$] = *m/z* 246.1).

Appx II 2.34. List of GC-MS parameters.

Solvent A Volume: 8 µL

Solvent B Washes (PreInj): 3

Solvent B Washes (PostInj): 3Run Time: 18.625 min

Oven (Initial: 75 °C

Hold Time: 3 min

Post Run: 100 °C

#1 Rate: °C/min

#1 Value: 300 °C

#1 Hold Time: 10 min

Injection Volume: 1 µL

Solvent A Washes (PreInj): 3

Solvent A Washes (PostInj): 3

Solvent B Volume: 8 μL

Sample Washes: 3

Sample Wash Volume: 3 μL

Sample Pumps: 3

Front SS Inlet He Mode: Split

Split Ratio: 100 :1

Split Flow: 99.997 mL/min

Flow Setpoint: (Initial)0.99997 mL/min

Post Run: 0.75 mL/min

Column Information: Agilent 19091S-433: 93.92873 HP-5MS 5% Phenyl Methyl Silox

MS Information

Acquisition Mode: Scan

Solvent Delay (minutes): 3

MS Source: 230 C maximum 250 C

MS Quad: 150 C maximum 200 C

Appendix III

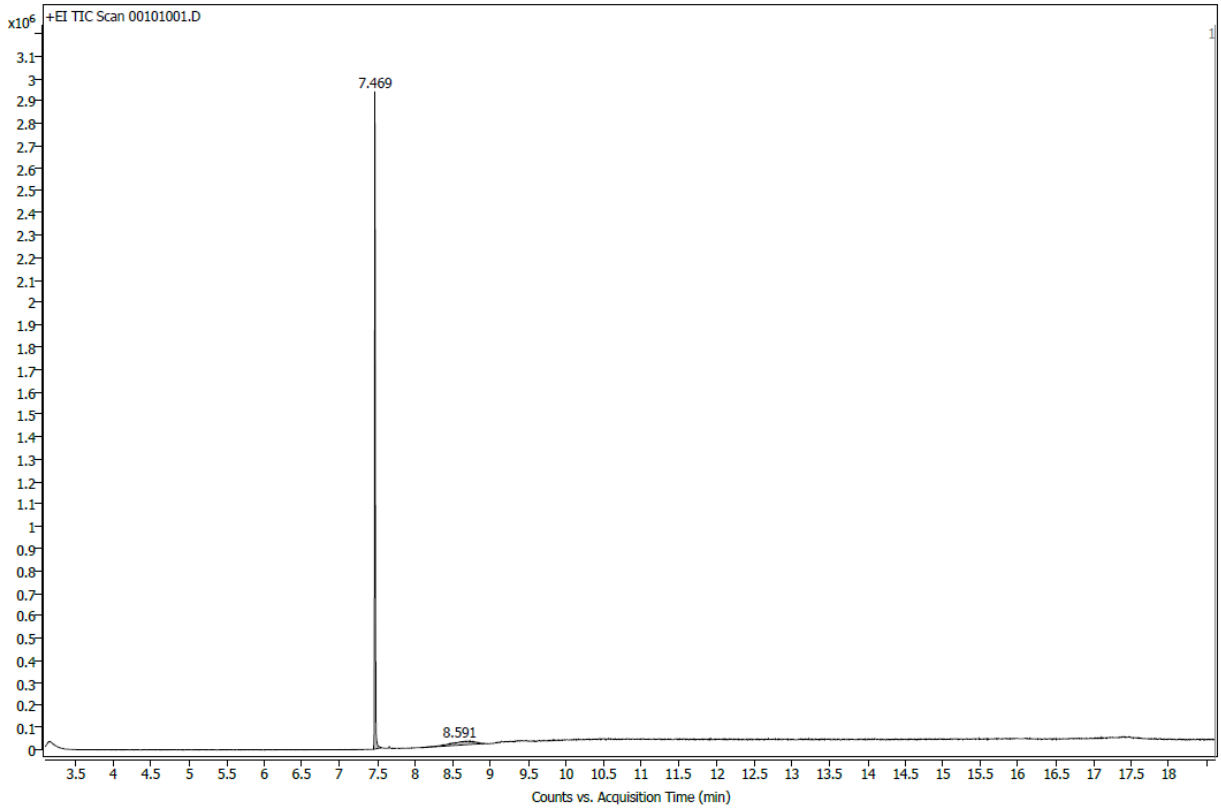

Appx III 3.1. Chromatogram of DHBP only (RT: 7.469 min).

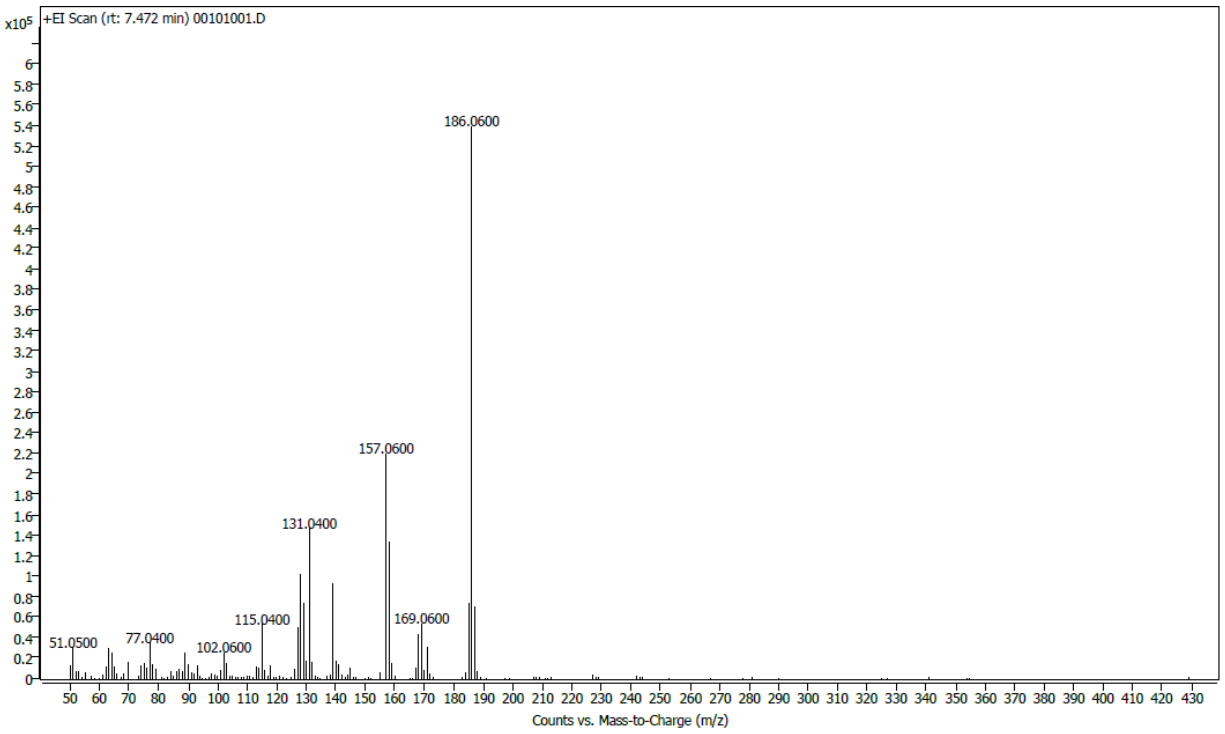

Appx III 3.2. Mass spectrum of DHBP only (RT: 7.469 min) ([DHBP$^{+\bullet}$] = *m/*z 186.1).

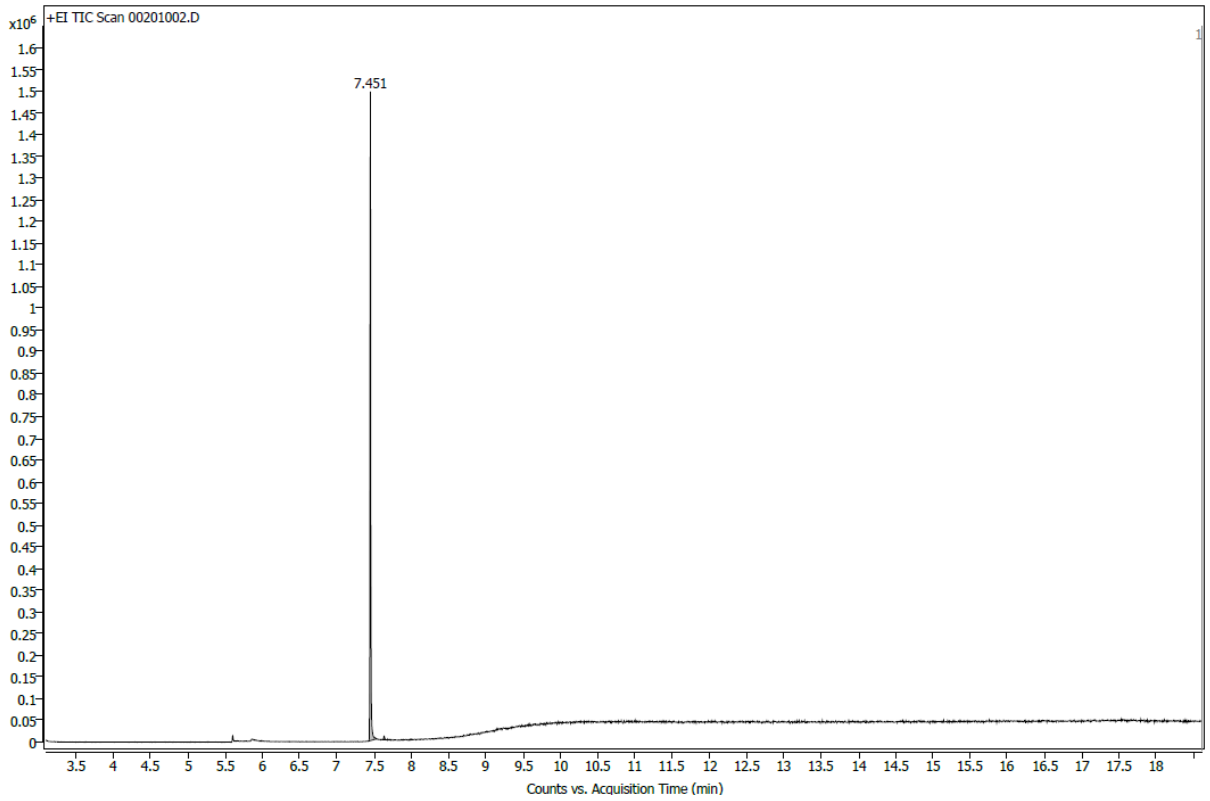

Appx III 3.3. Chromatogram of the electrooxidation of DHBP in 0 to 3 V range (20 CV).

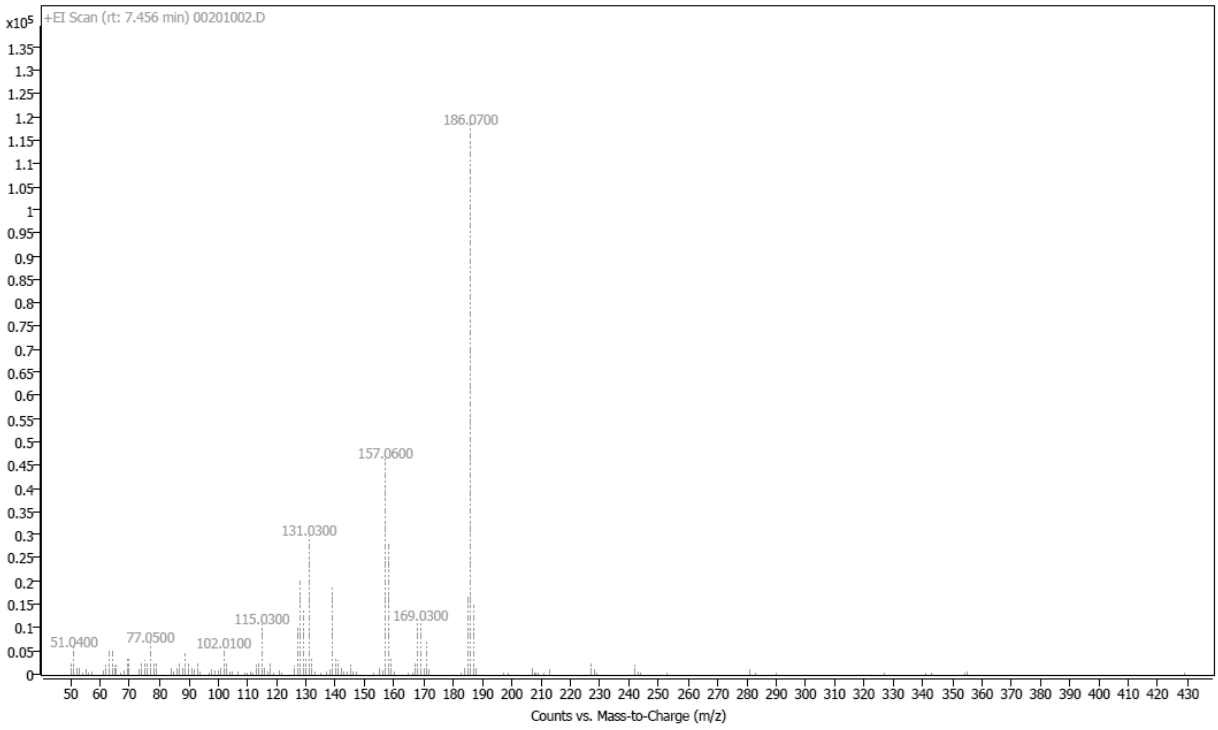

Appx III 3.4. Mass spectrum of DHBP (RT: 7.456 min) ([$DHBP^{+\bullet}$] = *m/*z 186.1).

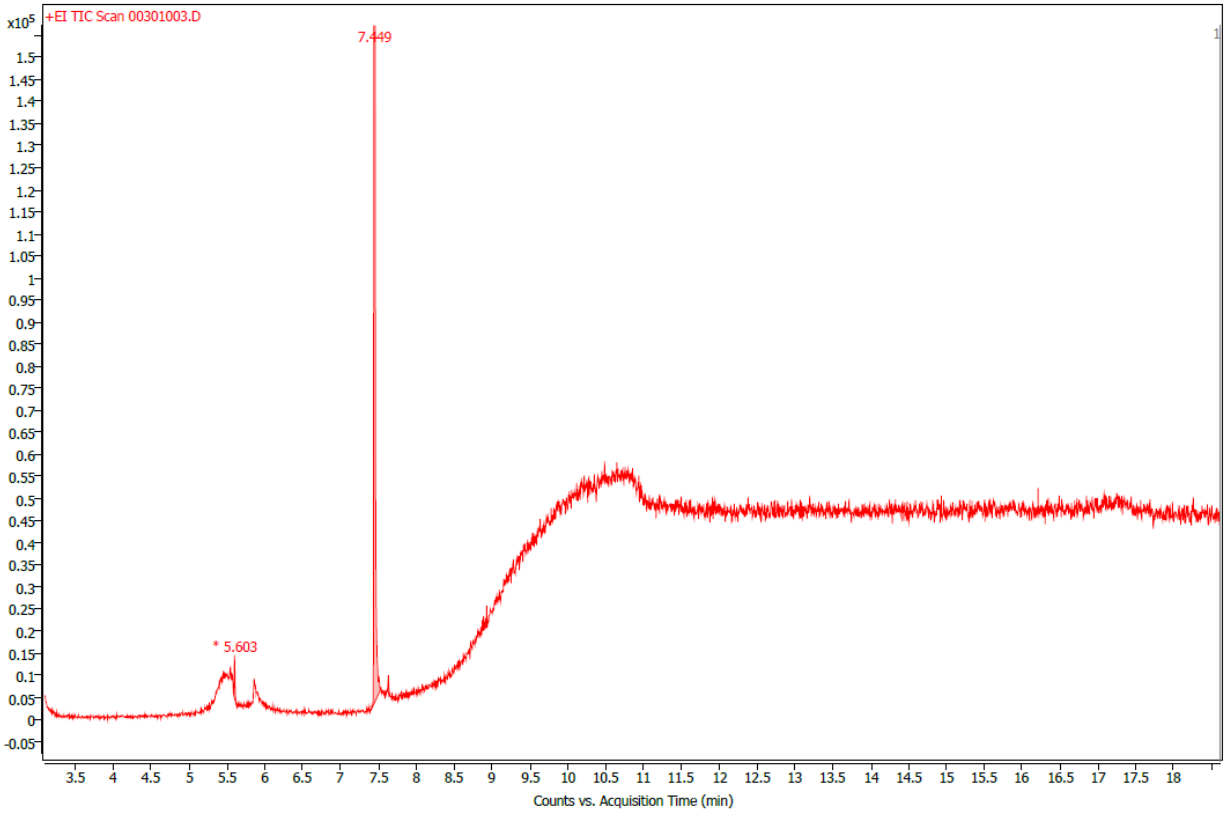

Appx III 3.5. Chromatogram of the electrooxidation of DHBP in -3 to 0 V range (20 CV).

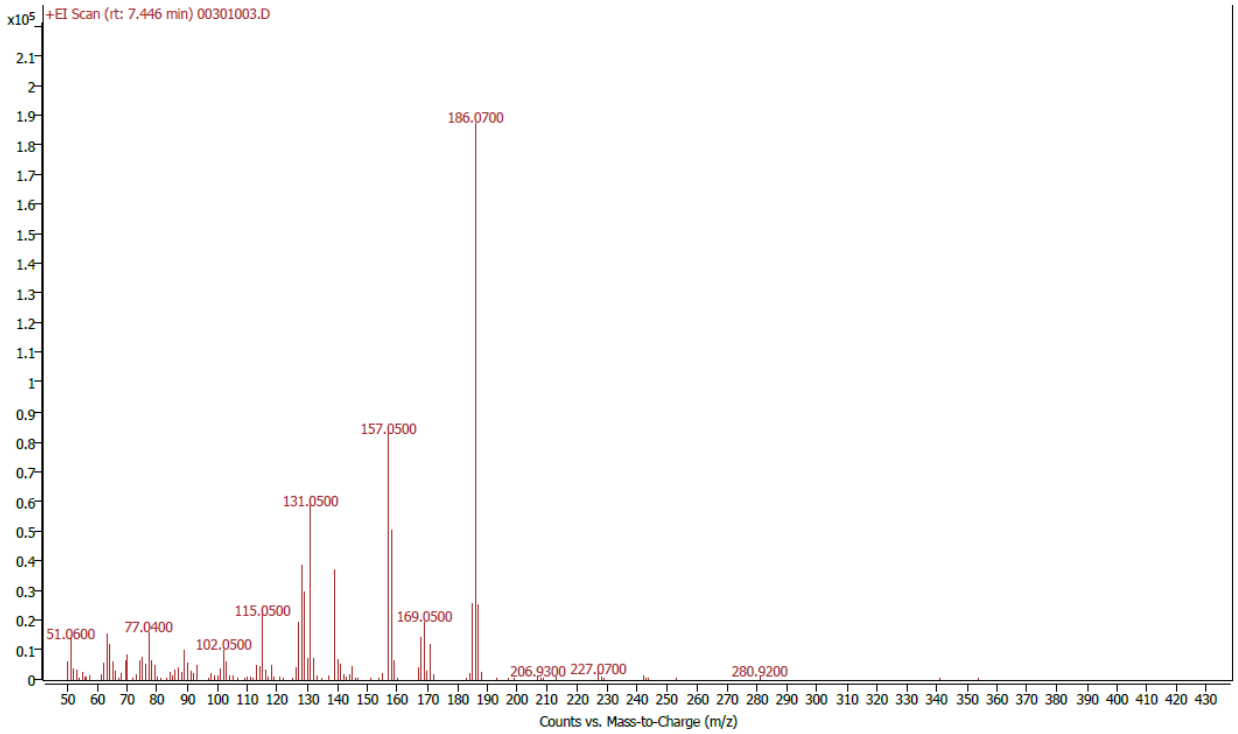

Appx III 3.6. Mass spectrum of DHBP (RT: 7.446 min) ([$DHBP^{+\bullet}$] = *m/z* 186.1)

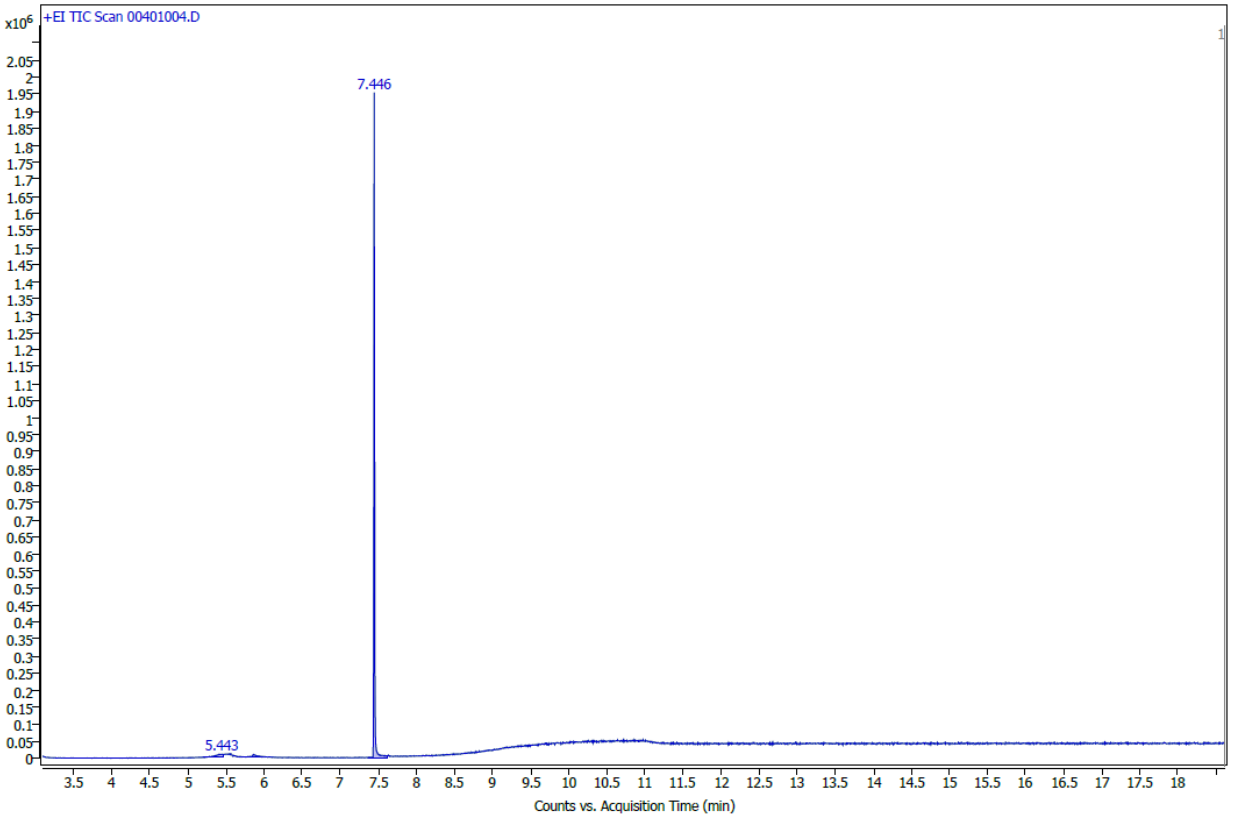

Appx III 3.7. Chromatogram of chemical oxidation solution of DHBP with copper perchlorate; filtrate.

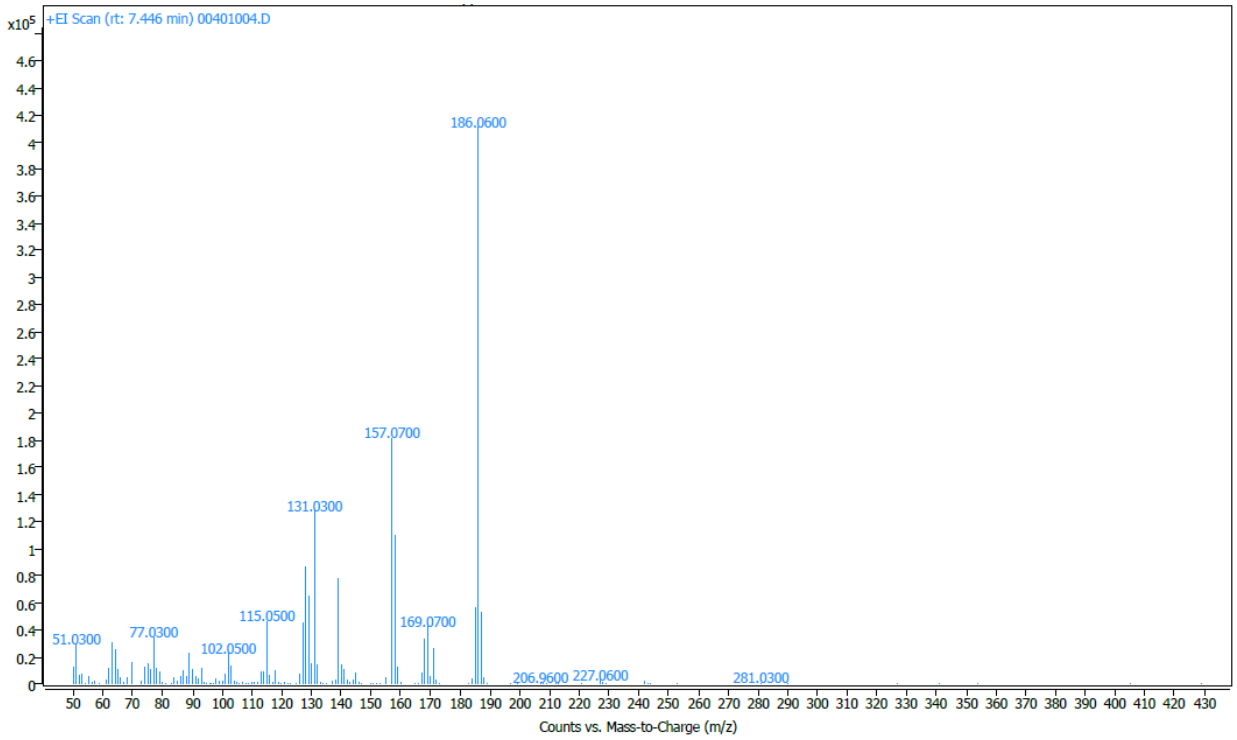

Appx III 3.8. Mass spectrum of DHBP (RT: 7.446 min) ([$DHBP^{+\bullet}$] = *m/z* 186.1)